PARALOG SPECIFIC FUNCTIONS OF THE COPII MACHINERY IN CRANIOFACIAL DEVELOPMENT OF ZEBRAFISH *Danio rerio*

By

David Boyd Melville

Dissertation

Submitted to the Faculty

of the Graduate School of Vanderbilt University

in partial fulfillment of the requirements

for the degree of

DOCTOR OF PHILOSOPHY

in

Cell and Developmental Biology

August 2012

Nashville, Tennessee

Approved:

Chris Wright

Anne Kenworthy

Jason Jessen

Melanie Ohi

For my family

ACKNOWLEDGEMENTS

I thank my mentor Ela Knapik, whose patience, support, trust, and willingness to go to bat on my behalf have made all the difference. I have grown and matured because of her influence, and greatly enjoyed my time in her lab. She gave me the freedom to follow through on unconventional ideas and to think for myself, and involved me in a great breadth of projects. My role in the lab, which she proclaimed as "P.I. in training," has been an inimitable learning experience.

I would like to thank my committee, Chris Wright, Ann Kenworthy, Jason Jessen, and Melanie Ohi for their guidance and support. Their steering of my project and mindset has been invaluable to my growth as a scientist.

I must thank the Cellular, Biochemical and Molecular Sciences Training Program as well as the National Institute of Health for funding my research.

I would like to thank some great collaborators: Antonis Hatzopolous for his brilliant ideas about how to tell our stories and how to make them better; and Jeff Smith, Kevin Bradley, and Joan Breyer for their advice on the large scale and computational side of research, as well as being great fun to work with.

I would also like to thank my labmates, Daniel Levic, Kirill Zavalin, Witold Rybski, Swapnalee Sarmah, Wen-der Wang, Lauren Beihoffer, and Cory Guthrie, who have made the lab a productive, intellectually stimulating, and friendly place to work. I have felt I could rely on my labmates when I needed them, and I will always treasure their friendship.

Lastly, I would like to thank my family, my parents who have always supported me and put up with my eccentricities with good humor, my three boys Preston, Franklin, and

Nathaniel who are a constant source of joy for me, and especially my wife Ya-ping, whose constant support has been essential in everything I do.

TABLE OF CONTENTS

LIST OF TABLES

Table Page

LIST OF FIGURES

Figure Page

LIST OF ABBREVIATIONS

brk: brak mutant

CHIP-seq: Chromatin immunoprecipitation sequencing

Col2α1: Collagen2α1

COPII: Coat Protein Complex Type II

CLSD: Cranio-lenticulo-sutural dysplasia

CDAII: Congenital dyserythropoietic anemia type II

CREB3L2: cyclic AMP response element binding protein 3-like 2

dpf: days post-fertilization

ECM: Extracellular matrix

EndoH: Endoglycosidase H

ER: Endoplasmic Reticulum

ERES: ER exit sites

ERGIC: ER-Golgi intermediate complex

FACS: Fluorescence Activated Cell Sorting

fel: *feelgood* mutant

Fn: fibronectin

GAG: glycosaminoglycan

hpf: hours post-fertilization

MO: Morpholino oligonucleotides

mgt: maggot mutant

OTFBS: Over-represented Transcription Factor Binding Site Prediction Tool

PCR: Polymerase Chain Reaction

PVDF: Polyvinylidene fluoride

rnd: round mutant

S1p: Site-1 protease

S2p: Site-2 protease

SDS-PAGE: Sodium dodecyl sulfate-polyacrylamide gel electrophoresis

stn: strangelove mutant

TEM: Transmission electron microscopy

UPR: Unfolded protein response

WGA: Wheat germ agglutinin

zhi: zhivago mutant

CHAPTER I

INTRODUCTION

Many of the most basic functions of cells, including intercellular communication, organelle formation, and extracellular matrix deposition, are reliant on trafficking of proteins to their required destination. The first and critical step for proteins within the secretory pathway is exit from the endoplasmic reticulum (ER) and transport to the Golgi apparatus. Disruptions in this transport are often detrimental to the cell and result in various human syndromes (Stagg et al., 2008; O'Donnell et al., 2011). The secretory system is often exploited by pathogens such as enterohemorrhagic *Escherichia coli* seeking entry to the machinery, possibly in order to manipulate proteins secreted by or expressed at the plasma membrane of host cells (Kim et al., 2007). The COPII coat proteins and their effectors are the primary mediators of ER-to-Golgi transport. While a requirement for COPII transport is universal among cells, different cell types and tissues have highly divergent requirements for COPII mediated secretion. Understanding how COPII function is regulated across different tissues and for different cargos will help to understand basic cellular mechanisms and allow for development of better approaches to treat numerous diseases.

Protein Transport

Protein transport is a complex process that involves diverse components of the cellular machinery, which must not only transport cargo, but must also allow for proper

recycling of resident proteins back to the compartment of origin. This cellular machinery includes not only vesicular coat proteins, but also diverse molecular components ranging from actin, which maintains membrane structures, to Rab GTPases, which act to target vesicles to correct membranes (Campellone et al., 2008; Bonifacino and Glick, 2004; Gurkan et al., 2007). After their initiation of protein translation, secretory cargos undergo translocation across the ER membrane and insertion into the lumen entering the membrane-enclosed network of outer cellular compartments. Within the ER lumen cargos encounter a vast integrated biological system responsible for forming and maintaining folded proteins, initiating N-linked glycosylation, and identifying and destroying misfolded protein.

After initial processing within the ER lumen, cargos are prepared for export by concentrating them at ribosome-depleted ER exit sites (ERES) (Figure 1.1). Here, the GTPase Sar1 recruits the inner (Sec23-Sec24) and outer (Sec13-Sec31) COPII coat proteins, which help to deform the budding membrane to allow vesicle formation and fission (Figure 1.2). The vesicles are then trafficked along microtubules by the dynactin/dynein machinery, which interact with the inner coat protein Sec23 (Watson et al., 2005). In yeast, these COPII vesicles travel directly to the *cis*-Golgi, but in vertebrate cells they undergo homotypic fusion, which is mediated by Sec23-TRAPP complex interactions (Cai et al., 2007). This homotypic vesicle fusion results in the formation of the ER-Golgi intermediate complex (ERGIC), which serves as a sorting center for COPII and COPI vesicles (Appenzeller-Herzog and Hauri, 2006), although its formation and function are poorly understood.

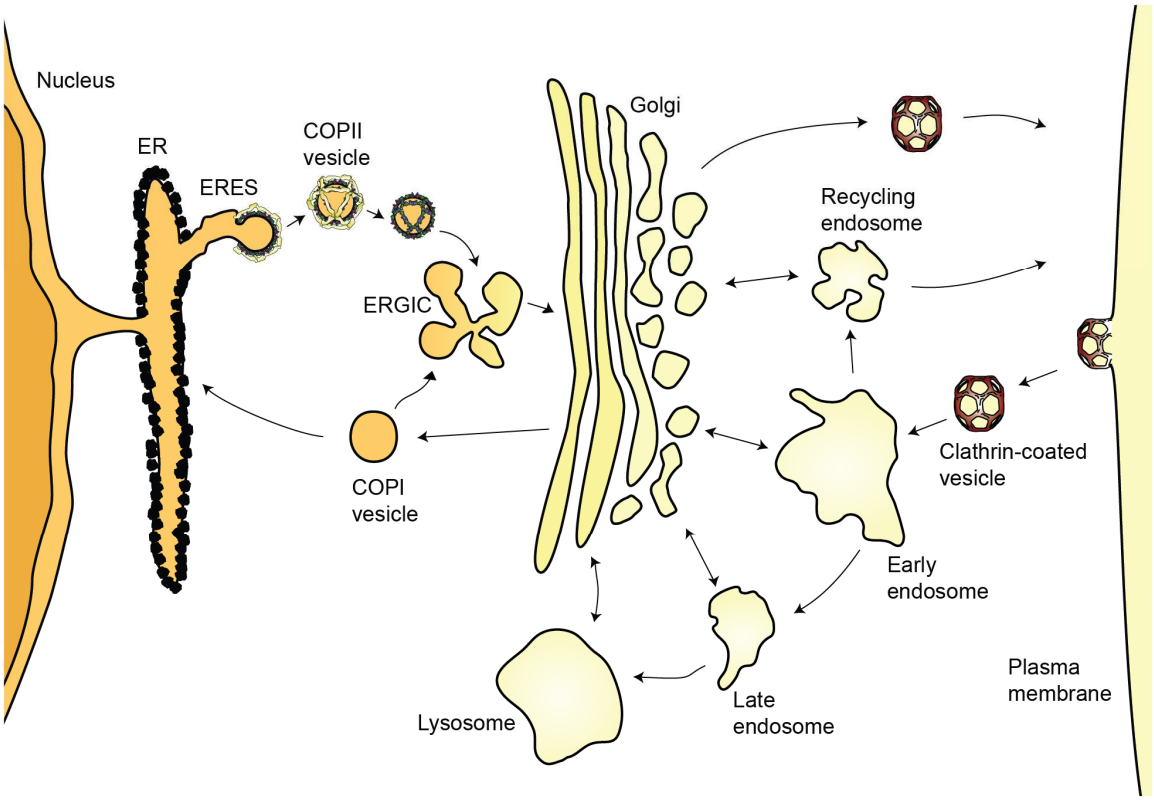

Figure 1.1: The Secretory Pathway. Schematic of the cellular compartments involved in protein trafficking and the directions of transport to/from these compartments, including the structure of two vesicular protein coats (COPII, clathrin).

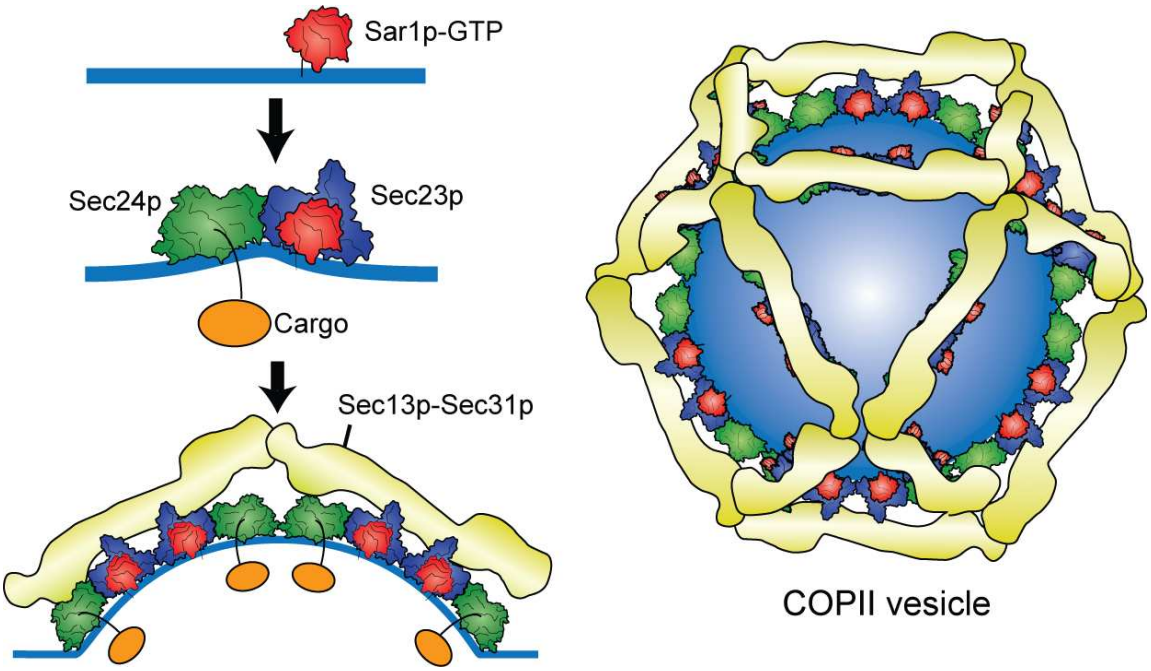

Figure 1.2: The COPII complex. Graphic depicting the process of COPII coat mediated membrane deformation (left), and a complete COPII vesicle (right) (Melville and Knapik, 2011).

From the ERGIC, cargos are sorted to the Golgi, although whether this involves maturation of the ERGIC into a new Golgi stack or vesicular transport in still unclear (Nakano and Luini, 2010). Once in the Golgi, cargo proteins are further processed and exported, while ER-resident proteins are recycled back by COPI-mediated retrograde transport. The ER and Golgi do not act as completely separate entities, but have a highly dynamic relationship, and are dependent on each other for proper function and maintenance of cell homeostasis (Altan-Bonnet et al., 2004; Ward et al., 2001; Pulvirenti et al., 2008).

COPII

The COPII machinery is the primary mediator of ER-to-Golgi transport. COPII vesicle budding is initiated when the small, cytoplasmic GTPase Sar1 undergoes a conformational change upon GTP binding, exposing an amphipathic α-helix that allows Sar1 to associate with the ER membrane (Barlowe et al., 1994; Matsuoka et al., 1998; Huang et al., 2001). Sar1 then recruits the Sec23/Sec24 heterodimer to the ER surface, forming a "pre-budding complex". Sec23 acts as a GTPase-activating protein for Sar1, whereas Sec24 plays a role in protein cargo selection (Miller et al., 2002; Mancias and Goldberg, 2008). These three proteins form the inner coat and are thought to impose the initial ER membrane deformation. Next, the COPII outer coat complex assembles by Sec13 and Sec31 heterotetramers, which form a cage-like structure that encompasses the pre-budding vesicle (Figure 1.2) (Stagg et al., 2006; O'Donnell et al., 2011). The outer coat appears to be primarily responsible for membrane fission (Fath et al., 2007; Stankewich et al., 2006; Fromme et al., 2007).

COPII components are highly conserved throughout the plant and animal kingdoms. The yeast *Saccharomyces cerevisiae* has one Sec23 gene and three Sec24 paralogs (Sec24, Lst1 and Iss), while vertebrate genomes contain four Sec24 (A, B, C and D) and two Sec23 paralogs (A and B) (Paccaud et al., 1996; Tang et al., 1999). Although yeast Sec23 and Sec24 are essential for survival, private variants in genes of COPII components in humans cause a broad spectrum of diseases with clinical manifestations as diverse as skeletal defects, anemia, and lipid malabsorption (Boyadjiev et al., 2006; Bianchi et al., 2009; Schwarz et al., 2009; Jones et al., 2003). The precise molecular and cellular mechanisms that lead to such outcomes are poorly understood, underscoring the importance of animal models to study these organ- and tissue-specific deficits (Schwarz et al., 2009; Lang et al., 2006).

Sec23 and Sec24 paralogs are necessary for skeletal development

Unbiased, forward genetic screens in zebrafish have been particularly useful to uncover the functions of genes that encode various COPII components. For example, the zebrafish *bulldog/sec24d* was recovered in a phenotype-driven screen for craniofacial dysmorphology mutations (Neuhauss et al., 1996; Driever et al., 1996). *bulldog* mutants are characterized by a short, flattened jaw, kinked pectoral fins, and short body length, but overall embryo patterning appears normal (Sarmah et al., 2010). This phenotype suggests that Sec24D activity is critical for the development of skeletal elements in the jaw, fin and notochord. The specificity of the phenotype caused by the loss of such a universal component in a pervasive cellular pathway is striking but not unique. The zebrafish *crusher/sec23a* mutant (Lang et al., 2006) manifests complex skeletal

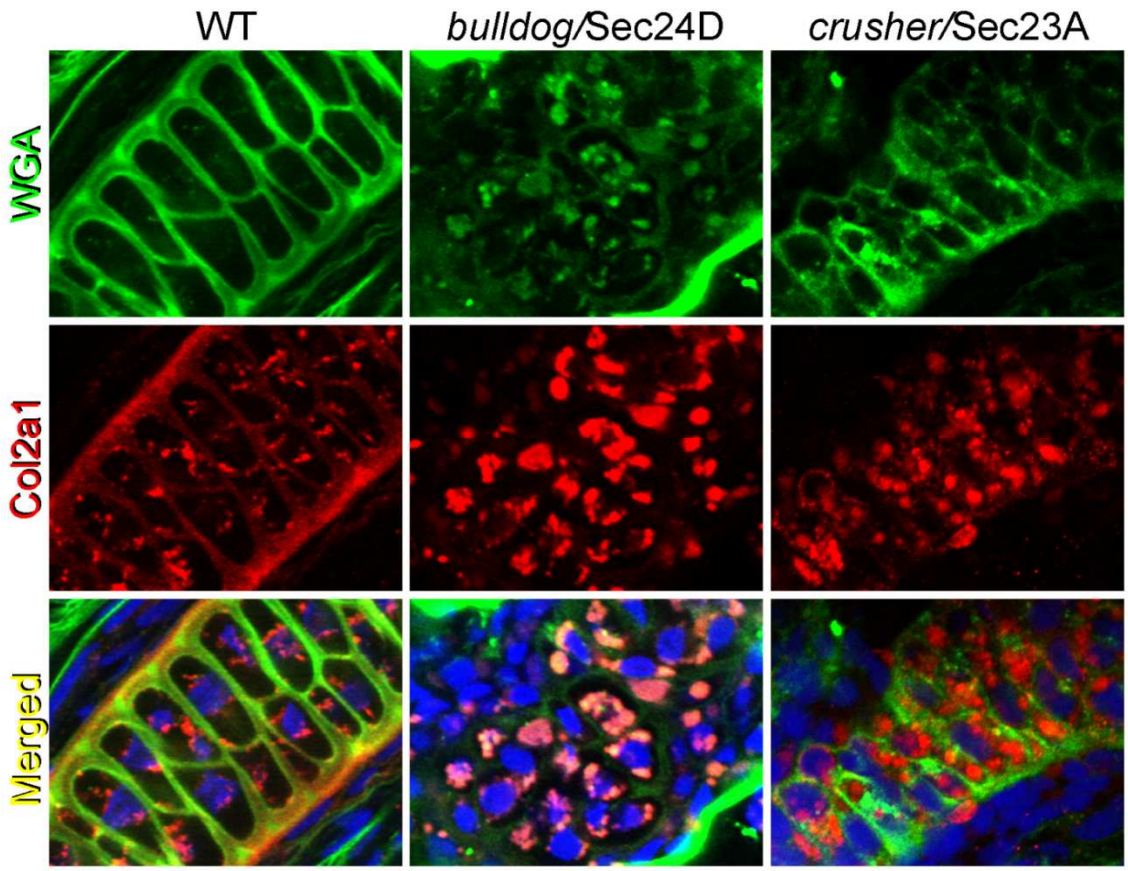

Figure 1.3: COPII mutants *bulldog/sec24d* and *crusher/sec23a* fail to traffic collagen. Immunostaining of WGA (green), which binds N-glycosylated proteins, and Col2α1 (red) in the Meckel's cartilage of 4 dpf *bulldog* and *crusher* embryos. Mutant chondrocytes accumulate intracellular type-II collagen deposits not seen in wild type.

dysmorphology that closely resembles the *bulldog* phenotype. At the cellular level, *bulldog* and *crusher* chondrocytes fail to traffic type-II collagen and other ECM proteins out of the ER (Figure 1.3).

When considering how impairing a seemingly essential function, ER-to-Golgi transport, can lead to a tissue-specific phenotype, an important question to address is whether the *bulldog* and *crusher* mutants represent hypomorphic or null phenotypes affecting only certain proteins in a subset of cell types. The four alleles of *bulldog* lead to progressively longer truncations of the Sec24D protein, yet they all result in an identical phenotype, strongly suggesting that all of the *bulldog* alleles are genetic nulls (Figure 1.4). Similarly, the only identified Sec23A mutant in zebrafish, *crusher,* also results in a premature stop codon, leading to nonsense-mediated decay of the transcript (Figure 1.4). Maternal contributions of proteins or transcripts could theoretically account for the largely normal early development of *bulldog* and *crusher* mutants, as both Sec23A and Sec24D are maternally deposited. However, activation of zygotic transcription in zebrafish occurs concurrently with degradation of maternal mRNAs (during the midblastula transition at 3 hours post-fertilization)(Ferg et al., 2007) making it unlikely that maternal proteins take part in COPII assembly beyond the initial stages of development. Moreover, if maternal contribution was a major factor, then antisense morpholino knockdown targeted to both maternal and zygotic mRNAs would result in a significantly more severe phenotype than either of the mutants present, but this is not the case. Thus, the most probable scenario is that *bulldog* and *crusher* represent genetic nulls. If these are null alleles, then this suggests that the phenotypes of *crusher* and *bulldog* reflect the specific functions of Sec23A and Sec24D in skeletal development.

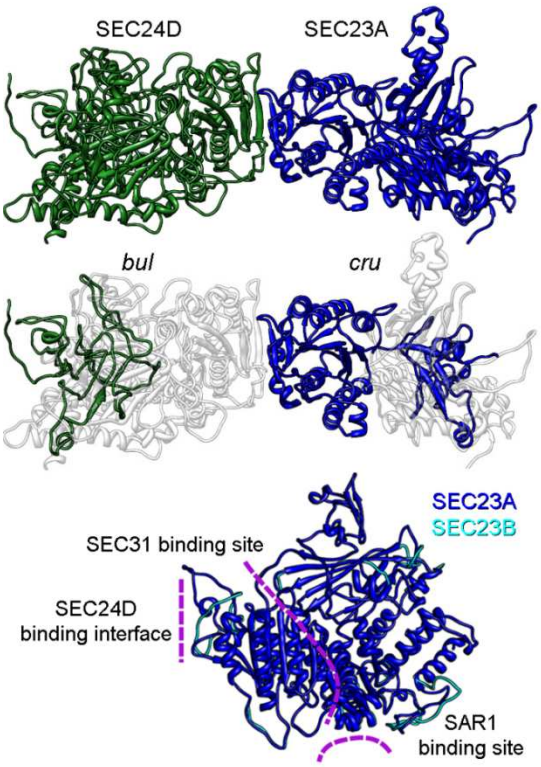

Figure 1.4: *bulldog* and *crusher* encode mutations in the COPII complex. Structure of human SEC24D and SEC23A (Top), and the truncation caused by *bulldog* and *crusher* mutations in zebrafish proteins as projected on human proteins (Middle). Overlay of the structure of human SEC23A and SEC23B. Binding interfaces to other proteins are indicated by purple lines (Bottom).

Further support for this notion comes from the clinical analysis of the Cranio-lenticulo-sutural dysplasia (CLSD), a rare genetic disease with a recessive mode of inheritance caused by a point mutation in the *SEC23A* gene (Boyadjiev et al., 2006). CLSD patients have skeletal dysmorphologies and cellular defects that are very similar to the *crusher* zebrafish variant, also suggesting that at least some of the tissue-specific roles of COPII elements have been conserved during evolution. To date, no human syndromes have been identified that disrupt Sec24D. Thus the zebrafish mutations are the primary tools to study Sec24D function in vertebrates.

Although traditionally the COPII-dependent anterograde protein transport was considered an essential pathway with universal functions in all cells, these recent clinical data and animal studies have challenged this view (Aridor and Hannan, 2002; Zanetti et al., 2012). How, then, is the anterograde protein secretion organized in vertebrates? Do cargo adaptors transport proteins according to developmental stage, type of cargo protein, or cell type? Alternatively, could dynamic regulation allow a combinatorial COPII system to assemble uniquely in various cell types to meet the specific secretory demands during development and adult homeostasis? In support of this notion, ubiquitylation has been shown to alter Sec23 function (Fromme et al., 2008; Jin et al., 2012).

Chondrocyte development

Craniofacial malformations are involved in three-fourths of all congenital birth defects in humans (Chai and Maxson, 2006). Critical to the development of the head is the cranial neural crest. Cranial neural crest gives rise to a variety of different cell types, and is responsible for most of the hard tissues in the head (Kimmel et al., 2001). Neural

crest arises from the lateral margins of the neural plate. Neural crest cells (NCCs) undergo epithelial-mesenchymal transition and migrate throughout the body, giving rise to various cell types such as neurons, pigment cells, and chondrocytes. Migrating NCCs condense and interact dynamically with the local environment to form the pharyngeal arches that later give rise to much of the skeleton and muscle of the head. The initial signals that lead to pharyngeal arch formation come from the craniofacial ectoderm, but afterwards the cranial neural crest cells become the driving factor (Chai and Maxson, 2006). In the formation of pharyngeal arches, NCCs cells differentiate into chondrocytes, the cartilage-producing cells of the body. Chondrocytes secrete large quantities of type-II collagen, which makes up 90% of the ECM produced by chondrocytes. As this ECM is made, chondrocytes lose their cell-cell attachments, and the accumulation of collagen fibrils and other matrix proteins form cartilage. This cartilage is later invaded by osteoblasts to form the bones of the face.

Stage, cargo and cell specific aspects of Sec23 and Sec24 functions

It is possible that distinct cargo adaptors, e.g. Sec24D, function at defined developmental stages and that this results in the tissue-specific phenotypes seen in various COPII mutations. Cranial NCC migration and condensation at the pharyngeal arches requires diverse cell-cell and cell-matrix interactions such as integrin-fibronectin interactions (Strachan and Condic, 2008; Testaz et al., 1999). Similarly, NCC differentiation into chondroblasts, proliferation, and secretion involves high levels of type-II collagen and other ECM proteins (Lang et al., 2006; Sarmah et al., 2010; Hickok et al., 1998).

In *bulldog/sec24d* mutants, NCC migration is not disrupted (Sarmah et al., 2010). Proteins involved in the initial steps of mesenchymal condensations of NCC, cell-cell and cell-matrix interactions (i.e., N-cadherin and its partner β-catenin, Fibronectin, and Integrin β1) are properly localized to the plasma membrane. Additionally, *bulldog* embryos have similar numbers of chondrocytes as wild-types, further suggesting that the early stages of chondrogenesis that involve NCC migration, condensation, differentiation, and proliferation proceed normally. However, *sox9a* down-regulation, which typifies maturing chondrocytes, does not take place in *bulldog* mutants, and chondrocytes fail to become hypertrophic. Collectively, these findings indicate that whereas Sec24D-dependent protein transport is dispensable for the early steps of chondrogenesis, it is required for chondrocyte maturation and hypertrophy. Therefore, we postulate that Sec24D function is required at specific stages of cartilage development.

An alternative explanation for the late skeletal-specific defects could relate to the heavy secretory load in maturing chondrocytes that could overwhelm the available pool of COPII components. It is conceivable that at early developmental stages there is sufficient supply of coat proteins to meet the secretory demand, but as development progresses and the load of transported proteins increases, phenotypes emerge in highly secretory cells such as chondrocytes. This possibility seems unlikely, because collagen is not secreted at earlier stages in the notochord, where the secretory load is significantly lower than in chondrocytes. Furthermore, components of the collagen receptor complex, such as Integrin β1, are transported to the plasma membrane at the stage when ER is already backlogged with ECM proteins. Therefore, it seems improbable that the trafficking defects in *bulldog* chondrocytes are due solely to cargo overload, although

cargo load might contribute to the overall phenotype.

The special problem of collagen

Another possibility is that the nature of transport cargo could demand specialized adaptors for ER exit. For example, large fibrillar collagens (type-I or type-II) fail to exit the ER in *bulldog* mutants. It is conceivable that Sec24D is essential specifically for the transport of type-II collagen. This could help explain the characteristics of the *bulldog* phenotype, because cells of all of the affected tissues (the jaw, fin, and notochord) contain collagens. This special requirement of Sec24D for collagen secretion could reflect unique nature of intracellular collagen transport.

Collagen and other large proteins are transported somewhat differently than other cargos, because of their large size and inflexible shape (Stephens and Pepperkok, 2002; Bonfanti et al., 1998; Canty and Kadler, 2005). While cargo-free self-assembled COPII vesicles are 40-80 nm in diameter, procollagen bundles form stiff 300 nm rods, and other cargos (e.g. lipid droplets) can be 600 nm in size. While various reports have shown that the COPII coat proteins are essential for proper collagen trafficking (Lang et al., 2006; Boyadjiev et al., 2006; Fromme et al., 2008), there is still controversy over their exact role.

Collagen has a profound importance in human biology and disease. It composes ~30% of the body's protein and is the primary source of tensile strength in tissues (Flint et al., 1984). It plays an important role in bone, cartilage, and basement membranes, and different collagen types have been implicated in a myriad of human disorders including fibrosis, osteoarthritis, osteogenesis imperfecta, and porencephaly (Trojanowska et al.,

1998; Goldring and Goldring, 2007; Rauch and Glorieux, 2004; Gould et al., 2005).

Collagen is initially translated as a long peptide with a left-handed helix structure and a globular region at both terminal ends. The C-terminal domain of the peptide is then N-glycosylated, and the individual peptides interact to form a trimer with a right-handed helix. This trimer is further modified and stabilized by several other peptides including the collagen-specific Hsp47, which travels with collagen to the *cis*-Golgi where it is recycled back to the ER.

There are several competing hypotheses for how procollagen bundles are transported to the Golgi (Fromme and Schekman, 2005). One is that COPII core proteins form large vesicles or tubules that can accommodate large ECM proteins. Another is that COPII components are required only for constricting the membrane or already existing tubular structures in the ER.

Just as with *bulldog/sec24d*, *crusher/sec23a* mutants also fail to secrete type-II collagen, whereas a variety of other proteins are sent to the extracellular space. Conceivably, this collagen phenotype could be explained by the large cargo hypothesis. However, this failure to transport likely does not exclusively depend on the size of the trafficked protein. For example, fibronectin is properly secreted from Sec24D-deficient cells, whereas matrilin, which is comparable in size to fibronectin, is not secreted (Koteliansky et al., 1981; Piecha et al., 1999; Sarmah et al., 2010).

Finally, another possibility is that Sec23A and Sec24D have specialized functions in cargo sorting. Although the four Sec24 paralogs are highly divergent from each other, each paralog is conserved among vertebrate species (Figure 1.5). This finding implies that the distinct cargo-binding affinities of Sec24A, Sec24B, Sec24C and Sec24D are also

evolutionarily conserved (Wendeler et al., 2007). Alternatively, Sec24D may recruit an accessory protein that is required for type-II collagen secretion, similar to Tango1 (Saito et al., 2009b), an adaptor required for type VII collagen secretion. This possibility is further strengthened by the fact that fibrillar collagens type I, II and VII are stalled in the ER under various COPII-deficient conditions (Boyadjiev et al., 2006; Lang et al., 2006; Sarmah et al., 2010; Stephens and Pepperkok, 2002; Saito et al., 2009b; Mironov et al., 2003). These data argue for Sec24D being required for sorting cargo as opposed to handling large proteins.

Redundant and specialized functions of cargo adaptors

Another possible explanation for the tissue and stage-specific defects of *bulldog/sec24d* could come from redundancy among Sec24 proteins, especially between Sec24D and its closest paralog, Sec24C. Indeed, in HeLa cells SEC24C and SEC24D recognize similar cargo binding motifs (Wendeler et al., 2007). In zebrafish, Sec24C knockdown by antisense morpholino oligonucleotides does not result in any obvious craniofacial defects, even though *sec24c* morphant embryos are shorter, similar to *bulldog/sec24d* mutants (Sarmah et al., 2010). Nevertheless, although craniofacial primordia migrate in *sec24c* or *sec24d* single morphants, NCC migration is disrupted in *sec2 4c/sec24d* double morphants, chondrocytes fail to form and NCC-derived craniofacial skeletal elements are completely absent. Thus, it appears that either of the two Sec24 paralogs is sufficient for adequate protein transport during neural crest cell migration and the initial stages of chondrogenesis. In contrast, Sec24D is uniquely essential for chondrocyte maturation.

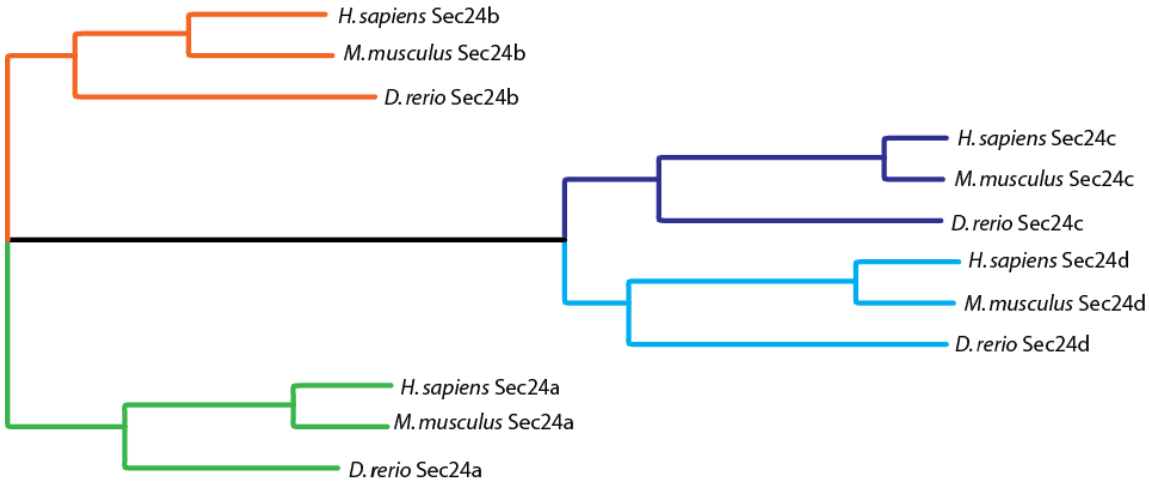

Figure 1.5: Phylogeny of Sec24 paralogs. Phylogram of known zebrafish (*Danio rerio*), human (*Homo sapiens*) and mouse (*Mus musculus*) Sec24 paralogs.

Of note, the eyes of *sec24c* morphant embryos are reduced in size, a defect that is not seen in *bulldog*. Hence, Sec24D cannot compensate for lack of Sec24C during eye development, arguing that there are distinct requirements for the two paralogs in various tissues. Taken together, these results suggest that within the context of a whole organism, Sec24C and Sec24D have both redundant and essential functions.

While the paralog-specific phenotypes seen in Sec24 depletions could be explained by differences in cargo affinity due to primary sequence divergence, the differences in the phenotypes caused by the loss of Sec23A or Sec23B in both humans and zebrafish are less clear. Human mutations in SEC23B result in congenital dyserythropoietic anemia type II (CDAII), an anemia caused by abnormal erythroblast development. In CDAII, erythroblasts have multiple nuclei and membrane abnormalities, possibly caused by impaired glycosylation of membrane proteins. CDAII stands in stark contrast to CLSD, which is caused by a mutation in SEC23A. CLSD has a very similar manifestation to *crusher/bulldog* mutants. CLSD patients are characterized by skeletal defects, including craniofacial abnormalities and late closing fontanels, short stature, neuronal deficits, and sutural cataracts. At the cellular level, CLSD fibroblasts have enlarged ER compartments. In contrast, CDAII patients have no apparent skeletal defects, while CLSD patients do not have a reported anemia; therefore these diseases manifest differently both at the clinical and cellular levels.

SEC23A and SEC23B share >95% similarity other than a string of 18 amino acids. The location of the divergent sequence may provide some clues about the specialized functions of SEC23A and SEC23B and the disease manifestations of the corresponding mutations. The 18 amino acids form a flexible loop near the Sec24D binding site, so it is

possible that they allow the two SEC23 paralogs to partner preferentially with different SEC24 proteins (Figure 1.4). If this is true, then the diverse SEC23A and SEC23B phenotypes might reflect the cargo-sorting affinities of their respective SEC24 partners.

There are also species-specific defects associated with loss of Sec23 proteins. For example, although CDAII patients, who have mutations in SEC23B, do not have skeletal defects, *sec23b* knockdown in zebrafish results in complete loss of the ventral head skeleton, whereas the dorsal skeleton is less affected. This phenotype is more severe than that of *crusher/sec23a*, where both the ventral and dorsal skeleton failings are milder and more similar to the dorsal defects of *sec23b* morphants. The differences in phenotypes may be due to divergent transcriptional regulation and, thus, availability of various COPII components. For example, SEC23B is expressed at 5-fold higher levels than SEC23A in human erythroblasts. Similarly, *sec24c* expression is upregulated in *bulldog* mutants, suggesting that transcriptional regulatory loops may act to offset the loss of individual COPII components. It is possible that such genetic circuits are wired differently among species, resulting in distinct compensatory mechanisms. However, it is also plausible that the differences highlight a null phenotype in the zebrafish and a weak hypomorphic allele of the CDAII patients.

Finally, an interesting aspect of COPII-mediated transport is the phenotype observed during loss-of-function of both Sec23A and Sec23B in *crusher/sec23b* morphants. Although double mutant-morphant embryos are very short and have little head skeleton remaining, they are able to undergo early embryonic patterning. Considering that there are only two known paralogs of Sec23, and Sec23 activity should be required in all cells, it is remarkable that double mutant embryos survive gastrulation,

much less progress beyond 3 days of development with most organs formed and in place. This observation suggests that there are unknown aspects to the secretory machinery, possibly other proteins that can partially compensate for Sec23 (for example Sec24, which has a similar structure to Sec23), or the existence of COPII-independent mechanisms for bulk protein transport.

Conclusions

The recent discoveries outlined above suggest that the various COPII structural components and their paralogs have essential and redundant roles both during embryonic development and in adult tissues. Some of this diversity may be due to preferential cargo affinities and variability in gene expression levels that leads to unique combinations of COPII components. These findings indicate that instead of fulfilling a "housekeeping" role required for basic cellular functions, COPII-mediated anterograde protein transport is a dynamically regulated process, and this regulation plays an important role in development and disease. In this regard, studies in animal models, including the large collection of zebrafish mutants, could shed light on the molecular basis underlying the complexity of protein transport in eukaryotic cells, the secretory "code." This knowledge could eventually help us to treat human diseases caused by defective or excessive secretory activity.

In this dissertation I will first outline my efforts to identify novel genes involved in protein secretion through a forward genetics approach. I will then describe the function the transcription factor Creb3l2 that was found through this approach and has been published in *Disease Models & Mechanisms* (Melville et al., 2011). Finally, I will address

the functional differences between the two Sec23 paralogs, and their relationship to secretion of specific cargos.

In addition to the work outlined here, I have also contributed to other projects through collaborations and written one review article:

Melville, D.B. & Knapik, E.W. (2011) Traffic jams in fish bones: ER-to-Golgi protein transport during zebrafish development. *Cell Adh Migr* **5**, 114-118.

Wang WD. **Melville DB.** Montero-Balaguer M. Barrallo-Gimeno A. Hatzopoulos AK. and EW. Knapik (2011) Tfap2a and Foxd3 regulate early steps in the development of the neural crest progenitor population. *Dev Biol* **360**(1):173-85.

Bradley, K.M., Breyer J.P., **Melville, D.B.,** Broman, K.W., Knapik E.W., & Smith J.R. (2011) A SNP-Based Linkage Map for Zebrafish Reveals Sex Determination Loci. *G3: Genes, Genomes, and Genetics* G3 **1**(1):3-9.

Liu, D., Wang W., **Melville D.B.,** Cha Y.I., Yin Z., Issaeva N., Knapik E.W. & Yarbrough W.G. (2011) Tumor suppressor Lzap regulates cell cycle progression, doming, and zebrafish epiboly. *Dev Dyn* **240**, 1613-1625.

Sarmah, S., Barrallo-Gimeno, A., **Melville, D. B.,** Topczewski, J., Solnica-Krezel, L., and Knapik, E. W. (2010). Sec24D-dependent transport of extracellular matrix proteins is required for zebrafish skeletal morphogenesis. *PLoS ONE* **5**, e10367.

CHAPTER II

FORWARD GENETICS AND POSITIONAL CLONING OF *Danio rerio* CRANIOFACIAL MUTANTS

Introduction

Forward genetic approaches are a powerful method for identifying novel genes involved in developmental pathways. Because forward genetic screens are phenotype driven, the mutations identified are physiologically relevant. 1-ethyl-1-nitrosourea (ENU) mutagenesis has been especially effective in zebrafish and mouse model systems (Knapik, 2000). ENU is an alkylating agent that typically introduces single nucleotide changes that are the most common type of spontaneously occurring mutations.

The Boston mutagenesis and screen (Driever et al., 1996), was a large-scale, phenotype-driven genetic screen (Figure 2.1) that identified 48 mutations in 34 genetic loci affecting craniofacial development (Neuhauss et al., 1996). Two of these mutations, *crusher* (Lang et al., 2006) and *bulldog* (Sarmah et al., 2010), were previously identified by our laboratory as mutations in the COPII machinery components. In an attempt to discover other genes of the trafficking machinery important for craniofacial development, we have utilized positional cloning and genetic linkage analysis strategy to identify the genes responsible for phenotypes similar to *crusher* and *bulldog*.

Physical and Genetic maps

Because of its mechanism, ENU mutagenesis does not leave any sort of “tag” to easily identify mutation sites, however the sites can be identified through a positional

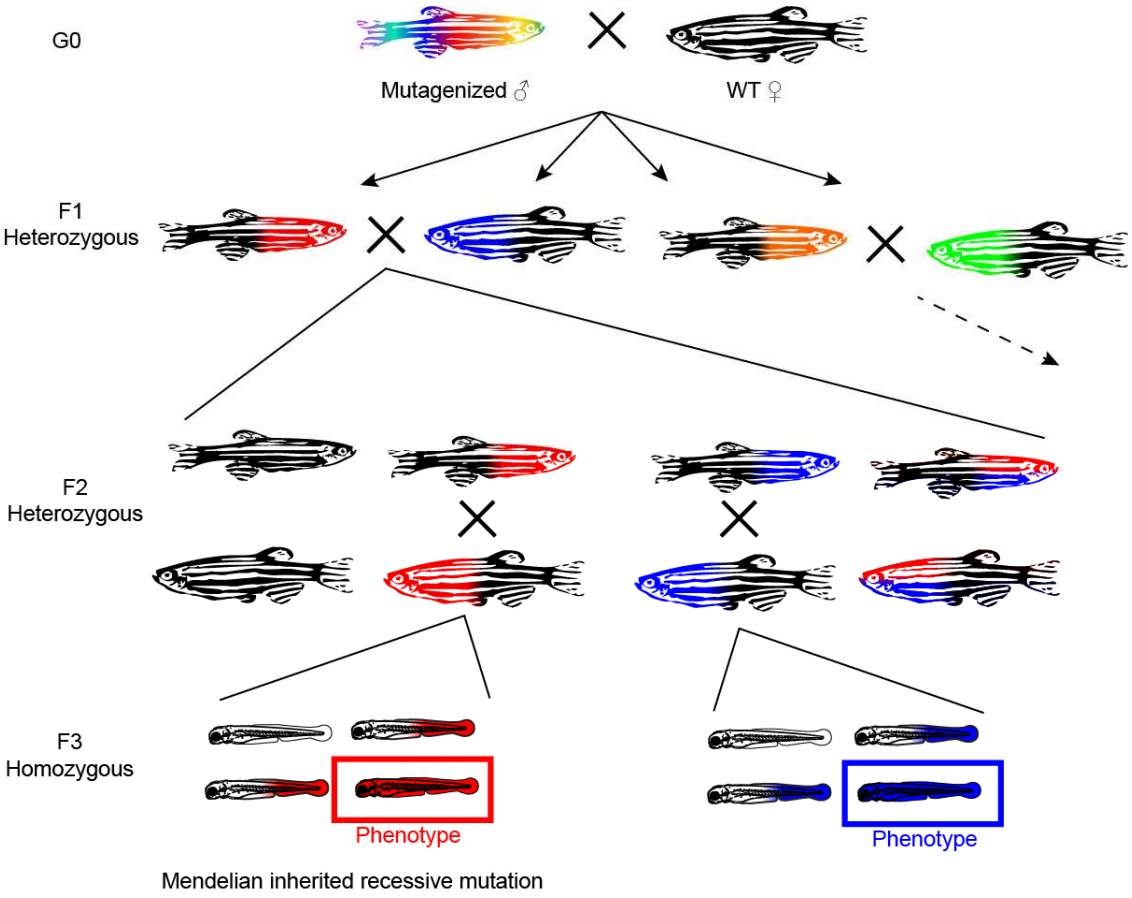

Figure 2.1: Schematic of a phenotype-based F3 Genetic Screen. A mutagenized G_0 male is crossed to a wild-type female to produce heterozygous F_1 fish, each with unique mutations. F_1 fish are intercrossed to produce the heterozygous F_2 generation, which carry the mutations from only two F_1 fish. F_2 siblings are intercrossed, allowing the mutations to reach homozygosity in one fourth of F3 embryos, which are screened for phenotypes.

cloning strategy. For positional cloning, two essential tools are required: a physical map and a genetic map. A physical map is conceptually straightforward; it is based on the actual DNA sequence of a chromosome. Genetic maps take advantage of recombination events during meiosis. They order markers along the length of a chromosome based on the number of recombinations occurring between them during tested meiosis, which translates to a statistical likelihood that two markers are next to each other. Genetic maps measure distances in centimorgans (cM). A centimorgan represents a region on a chromosome where there is a 1% chance of a crossover event/recombination during a single meiosis. In zebrafish, a cM usually represents a physical length of approximately 600-700 kb of DNA (Postlethwait et al., 1994), however certain regions of a chromosome may have altered recombination rates. For example, suppression of recombination at the centromere alters the physical distance in base pairs that a centimorgan represents.

Strategy

We used genetic linkage analysis to initiate positional cloning of craniofacial mutations. In linkage analysis, markers are identified that are polymorphic and can differentiate between the wild-type and mutant grandparental (G_0) zebrafish. These markers are then tested in F_2 mutant fish to measure the number of recombination events per meioses tested that occur between the mutation and the marker (Figure 2.2). Zebrafish can easily generate ~1000 F_2 mutant embryos, which would translate to ~2000 meiosis (two meiosis per embryo, one for each of the parents), these allow for fine mapping of the region where the mutation is located down to an interval as small as 0.1 cM, or ~60kb. Genomic regions of this size generally contain a small number of genes,

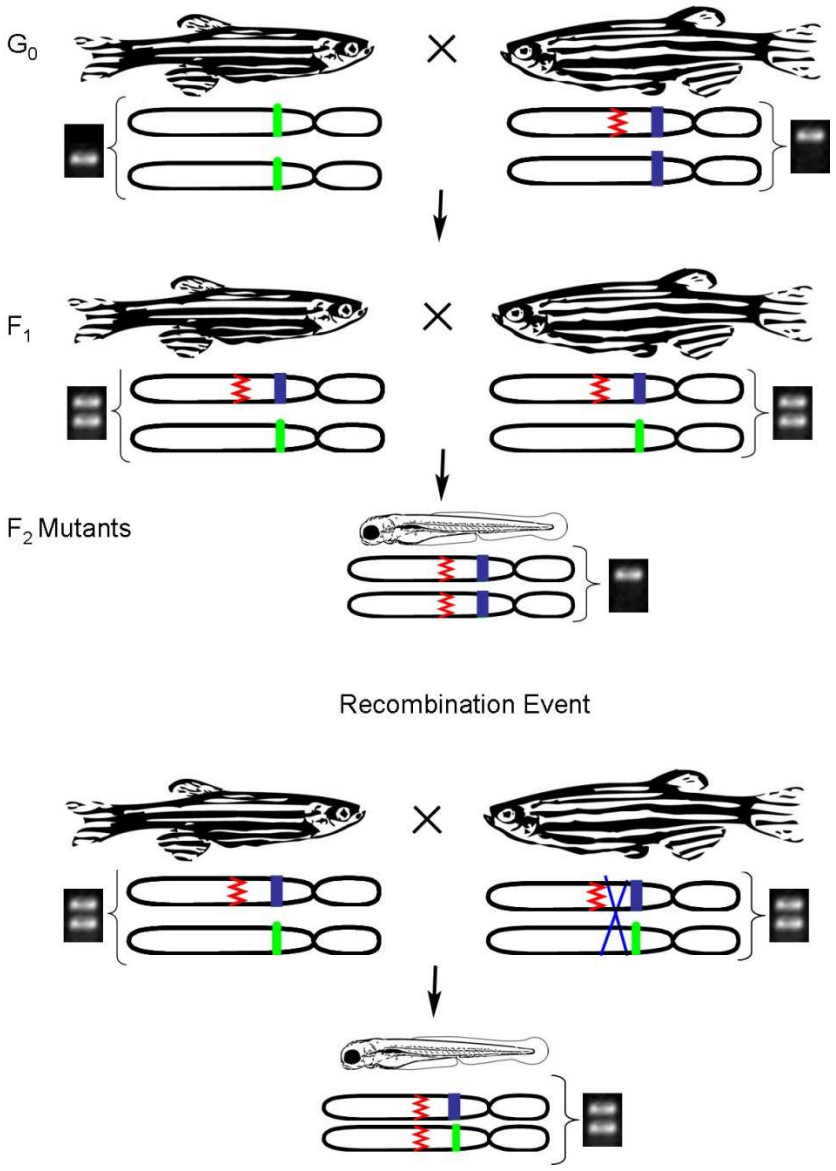

Figure 2.2: Schematic of linkage analysis for positional cloning. Heterozygous and one wild-type G_0 fish of different genetic backgrounds are crossed. The F1 generation is screened to identify mutation-carrying heterozygous fish. Heterozygous F_1 carriers are intercrossed, and DNA is extracted from homozygous mutant embryos. Markers that can differentiate the G_0 genetic backgrounds are analyzed by gel electrophoresis. If they segregate with the mutation then the marker and the mutation are linked. However, in a small percentage of embryos, a recombination event will have occurred between the marker and the mutation, causing the linked marker to have the wild-type allele. The frequency of these recombination events is used to determine the genetic distance between the marker and the mutation site.

which can be sequenced to identify mutations. Once a mutation is identified (generally a SNP) phenocopy and rescue experiments can be used to confirm that it is the causative mutation for the phenotype.

We begin the positional cloning of a mutation by establishing its chromosomal localization through bulk segregant analysis using the zebrafish simple sequence length polymorphism (SSLP) genetic map (Knapik et al., 1998) on a pedigree of pooled map cross DNAs. We then use DNA from individual F_2 mutants and closely linked markers from the genetic map to establish a critical interval containing the mutation. Testing each fish individually allows for the identification and tracking of embryos whose chromosomes had recombination events that occurred close to the mutation site. This "rec" DNA can be used to confirm the location of known markers already positioned on the genetic maps and new markers (developed to increase marker density in a critical region) relative to the mutation. The relative location of the markers of the genetic map is highly reliable, and the location of many of these markers has already been established on the physical map. This allows for a transition to using both the physical and genetic maps to continue fine mapping of the mutation.

When the markers of the genetic map have been exhausted, it is usually necessary to design new markers to further restrict the critical region. This process is expedited by using sequence from the physical map of the zebrafish whole genome sequence. Sequencing of the zebrafish genome started in 2001, making it one of the earliest completed. The current assembly, Zv9, is accessible through Ensembl (www.ensembl.org). Much of the assembly is derived from the sequence of bacterial artificial chromosomes (BAC) clones. BAC clone sequence is at 10-fold coverage and

the physical map is highly accurate when based on sequence from overlapping BACs. Unfortunately, there are significant regions of the genome where coverage by sequenced BAC clones is incomplete, and this leads to "BAC islands," sequence from one or more BACs that is flanked on either side by less reliable Whole Genome Shotgun (WGS) sequence. The inaccuracy of the WGS sequence means that many BAC islands are placed in the wrong order relative to each other, sometimes even on the wrong chromosome. This necessitates that the physical map must be viewed in the context of BAC islands to avoid using inaccurate sequence as a basis for marker design and identification of candidate genes.

Unless both markers flanking a mutation are located on the same BAC island, it is important to determine the relative locations of BAC islands and to build a manually annotated, more accurate physical map of the critical region. The ultimate goal is to restrict the critical region to an interval consisting entirely of overlapping BAC clones, as to be confident that there are no gaps in the sequence that might contain the mutation of interest, and small enough so as to contain only a few genes, which can be readily sequenced. There are several methods that can be used to bypass the gap in sequence between BAC islands (Figure 2.3), and their relative locations can then be confirmed by designing new primers on the BAC islands and performing linkage analysis on the map cross DNA.

Trace Walking

WGS sequence is automatically assembled and sometimes manual assembly can produce superior results. NCBI's trace archive has the individual sequence reads used for

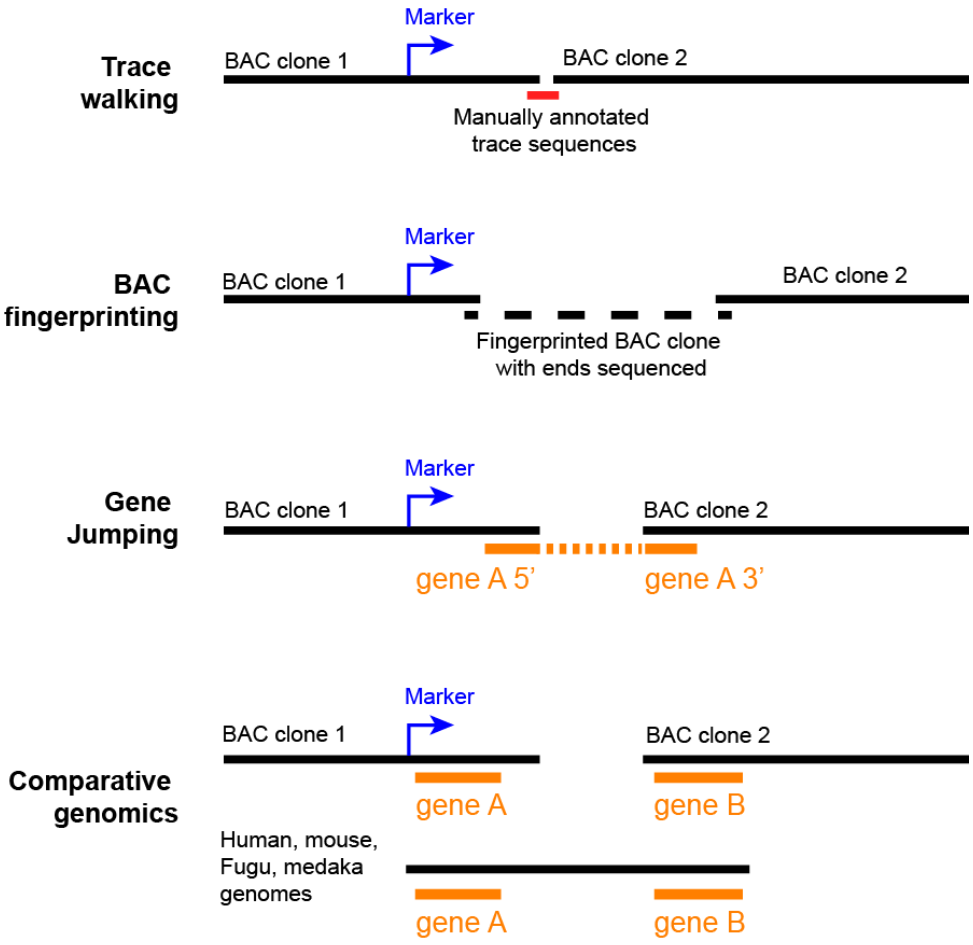

Figure 2.3: Schematics for methods used to connect gaps in the reliable sequence of the zebrafish genome assembly.

the genome assembly, including sequence from BACs as well as WGS sequence. It is possible to search these sequences for the end of the current BAC clone of interest, find individual sequence reads that overlap and extend away from the BAC, and use the non-overlapping portion for a new search. By repeating this process many times, it is possible to create several kilobases of manually annotated contiguous sequence that may bridge a gap between BAC clones.

BAC fingerprinting

The Zebrafish Genome Fingerprinting Project has been undertaken by the Wellcome Trust Sanger Institute, in which sequenced and unsequenced BAC clones are "fingerprinted" by RFLP, which allows for detection of overlapping BAC clones, even if some of those clones have not been fully sequenced. Sometimes these unsequenced BAC clones bridge a gap between two BAC islands. Moreover, the ends of BAC clones have been sequenced even if the whole clone hasn't, and this end sequence can be used as a starting point for trace walking.

Gene Jumping

Sometimes a gene with known cDNA sequence will begin on one BAC clone and end on another. This cDNA sequence can then be used to bridge gaps between BAC clones. GENSCAN (http://genes.mit.edu/GENSCAN.html) software can be used to identify partial genes near the end of a BAC clone or in sequence generated by trace walking. The gene sequence can then be used to search against known cDNAs, and if a matching cDNA can be found, the rest of its sequence can then in turn be used to search

against the whole genome sequence (in hope finding a BAC clone with the other end of the gene) or as a new starting point for trace walking.

Comparative genomics

The order of genes within a chromosomal region is often conserved between species and therefore can be used to infer neighboring genes in zebrafish. The human and mouse genomes are useful because of the reliability of the sequence, while other fish genomes (medaka, fugu, tetraodon, stickleback) are useful for their closer evolutionary relationship to zebrafish. If two genes are adjacent in other genomes but on different BAC islands in zebrafish, then it is likely that the BAC islands are adjacent.

Designing new markers

Once a BAC clone has been identified as potentially being in the region of interest, markers must be designed to confirm its relative location. One method of designing markers (that does not require prior knowledge of variations between the sequences of the two strains used in the map cross) is simple sequence length polymorphisms (SSLPs). SSLPs are repeating sequence of two to four base pairs. The exact number of repeats can change across generations due to slippage during replication (Tautz and Schlötterer, 1994). I wrote a software program to search large DNA sequences for these repeats and to design primers in the flanking sequence. It is then possible to amplify a ~200 base pair fragment containing the repeat and run the fragment on agarose or acrylamide gel to detect differences in the length of the amplimers. Roughly one sixth of the markers I designed were able to differentiate the grandparental strains and were therefore useful for

mapping purposes.

Use of these approaches has allowed for identification of candidate genes for several mutants during my training. Here I outline five of them.

Materials and methods

Genetic mapping and cloning. Mutations were mapped as described in results. Primers used listed in Table 2.1.

Cartilage staining. Embryos (80 hpf or 5 dpf) were fixed in 4% phosphate buffered PFA overnight. After two washes in PBS (1X) for 5 min, embryos were bleached with 10% H_2O_2 and 30 µl of 1M KOH for 1h. Following two washes in PBT for 5 min, embryos were incubated in 0.1% Alcian blue solution overnight at room temperature (RT) on a shaker. After one wash in acidic ethanol (70% ethanol, 5% HCl) followed by an overnight destaining in fresh acidic ethanol, embryos were dehydrated in 85% and 100% ethanol for 15 min each and transferred to 80% glycerol.

Histology. Histological sections were prepared in JB-4 plastic resin medium (Polysciences). Phosphate buffered PFA (4%) fixed 5 dpf embryos were washed with PBS and subsequently dehydrated with 25%, 50%, 70% and 95% ethanol (each step for 5 minutes). Dehydrated embryos were equilibrated with JB-4 infiltration solution for 10 min at RT which was prepared by adding 0.0625g benzyol peroxide plasticized to JB-4 embedding solution. The embryos were then placed in plastic molds. Blocks were

Table 2.1: Sequence of newly developed markers used in fine mapping of the novel mutations: *rnd, brk, mgt, stn, zhi.*

Marker	Mutant	Forward Primer 5' to 3'	Reverse primer 5' to 3'
Bu074420.4	*strangelove*	TGAGACATGAGATACACCTA	CCAACACTAGTTCAAACAAC
gfpt1.1	*zhivago*	GGTTCGTGTGCATGAAGTT	TACAGTAGCGAAGAGCCAA
Fd417C7.1	*zhivago*	CACAATGATGAAGAAGTGGGAG	CTCAATTGGATTCTGACAAGGC
Cu468685.1	*zhivago*	GATCCTCCATGGTATCACAC	GGGCATCCACTGTGTAAAA
Cu468685.3	*zhivago*	GGCACCTTGACCTCAAAAT	CGTCCATTTGACATCCACA
zgc:56525.1	*zhivago*	GCAGCTCAGCTATAAGGTG	GTCTGTTGTCCTGTAAGGT
Bx120008.4	*brak*	CGGCGAGAGATGATTCTGAT	AAGACTGTCGATGCCGAAGC
Ct573285.1	*brak*	CACTTCGAATGTTGACAACT	GGTTTGTTCACTAGACTATC
Cu682355.6	*maggot*	GGAGGTCGTACCGTACGGTT	CAGGCAGCAGATTAGTAGCA
Cu682346.2	*maggot*	ATGGTCTTGACTCCTGAGAC	GGTTGAAGGACAGACAGACA
Cu682777.3	*maggot*	TTCACAAGATGCTGCCAGAG	TCTGCAGCAACTGTGTGATG
Cu633932.2	*maggot*	CCAGCTGTGTGTGAATGTGT	GTTGTGAACGAAGCTCTCAG
Cu633888.2	*maggot*	ACCTGGTGTGGCCAGTCGGT	AGTCTGTGATGCAGCAACAG
Cu929143.1	*maggot*	GTGTAGTTCACGGATGGTGT	AGTGAAGGCAGGTGCCATTG
Cu633916.1	*maggot*	TTCAGCAGTTCAGGGTGAAG	GGATCTCGAAGCAGGAGTAT
Cu633889.4	*maggot*	CTGGTGAGAGACAGACAGGT	GCCTGAACGTGTCAGTTTCA
Bx511310.1	*round*	CAGACCGTAACCACCATGAG	AAACACAGTGAGAGTGCAGG
Cu694481.4	*round*	GGGACTCCCATAGCTGTAAT	CTGAAGACAGGCTAGATGCA

sectioned in 5 μm thickness using a Leica RM2265 microtome. Sections were collected on adhesive coated slides (*Superfrost* plus, Fisher), dried on a heating plate and stained with metachromatic dye Toluidine Blue (Sigma) and mounted using cytoseal-XYL as a mounting medium as previously described (Granero-Moltó et al., 2008).

Immunofluorescence and Wheat Germ Agglutinin staining. Type-II collagen and WGA staining was performed as previously described (Sarmah et al., 2010), whole mount embryos were fixed in 4% PFA at 4°C overnight, and incubated with 1:200 diluted primary antibody against collagen type II (Polysciences) and WGA-Alexa Fluor 488 conjugate (1:200) followed by 1:300 Alexa Fluor 555 fluorescently conjugated secondary antibody (Molecular Probes). The WGA lectin binds to N-acetylglucosamine and N-acetylneuraminic acid residues of membrane and matrix glycoproteins.

Pigment recovery assay. 24 hpf embryos were placed in egg water containing 4 μg/ml 4-hydroxyanisole (Sigma) for 48 hours, after which they were washed with egg water, allowed to recover for 24 hours, and then imaged.

Results

Strangelove

The *stranglove (stn^{m617})* mutant is characterized by severely reduced cartilage elements as revealed by alcian blue staining (Figure 2.4A). Similar to the *crusher/sec23a* mutant, all elements of the ventral skeleton are present; however they are significantly

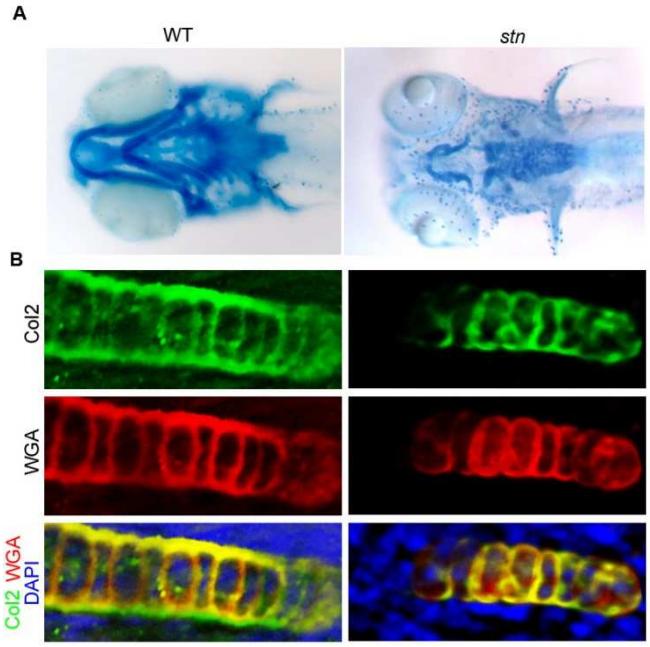

Figure 2.4: The *strangelove* mutation leads to abnormal craniofacial skeleton development. (A) Alcian blue staining of cartilage element in wild-type (WT) and *strangelove (stn)* head skeleton preparations ventral views. (B) Immunostaining of type-II collagen (Col2) and wheat germ agglutinin (WGA) in the 4th pharyngeal arch of 4 dpf embryos.

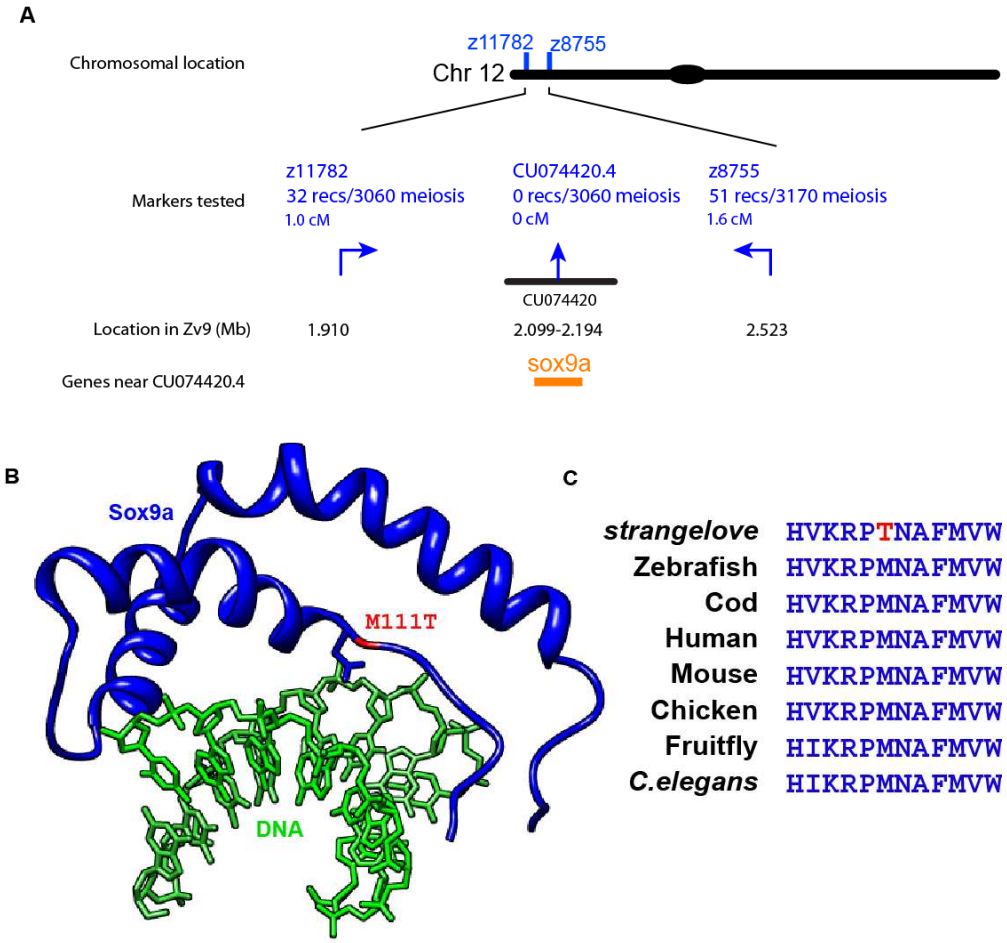

Figure 2.5: The *strangelove* mutation carries a missense mutation in *sox9a*. (A) The *strangelove* mutation was mapped to chromosome 12 between SSLP markers z11782 and z8755. A novel marker was developed and found to have 0 recombinations out of 3,060 meioses. (B) Predicted structure of zebrafish Sox9a DNA binding domain region based on the human SOX9 solved structure (McDowell et al.; 1999) showing the *strangelove* mutation in red. (C) Comparison of the DNA-binding domain predicted protein sequence of Sox9 across phylogeny. The amino acid changed in *strangelove* mutants is in red.

more reduced than in *crusher*. Immunofluorescence staining of type-II collagen and WGA, a lectin which binds N-glycosylated proteins, reveals that unlike *crusher*, trafficking of collagen to the extracellular space is not disrupted in *strangelove* mutants (Figure 2.4B).

strangelove was mapped to a 2.6 cM region on the proximal arm of chromosome 21 using the zebrafish genetic linkage map (Knapik et al., 1998) (Figure 2.5A). Unfortunately, none of the closely flanking markers have been located on BAC clones; however a combination of BAC fingerprinting, trace walking, and gene jumping identified the BAC clone CU074420, which contains a strong candidate gene, *sox9a*, as possibly located in the critical region. We developed SSLP markers for this BAC clone and found 0 recombinants out of 3,060 meioses, establishing that CU074420 is in the critical region and possibly contains the mutation site.

Sox9a is a transcription factor that regulates collagen expression and is essential for craniofacial development (Yan et al., 2002; Bell et al., 1997). We sequenced the *sox9a* transcript and found a T>C transversion at base pair 332 that results in a M111T missense mutation in the highly conserved DNA binding domain of Sox9a (Figure 2.5B,C) (McDowall et al., 1999). This is likely a hypomorphic allele as the phenotype is less severe than that of previously characterized *sox9a* mutants (Yan et al., 2002).

Zhivago

zhivago (*zhi*^{m315}) mutants have a skeletal phenotype very similar to *crusher* (Figure 2.6A), however, like *strangelove*, collagen trafficking is not disrupted (Figure 2.6B). Initial mapping of *zhivago* was performed using a newly developed SNP-based

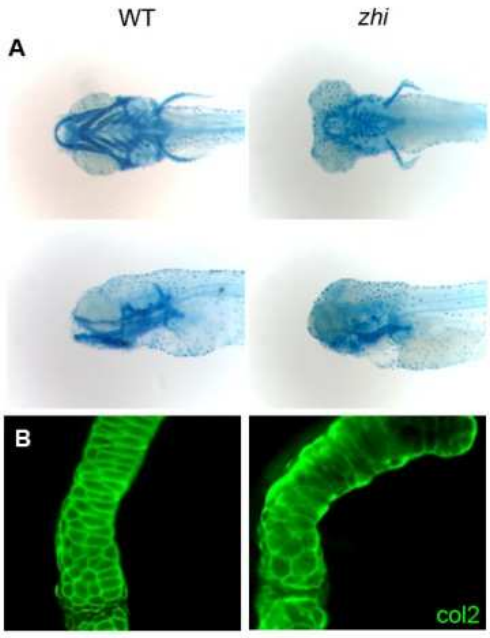

Figure 2.6: The *zhivago* mutation leads to deformities of the craniofacial skeleton. (A) Alcian blue staining of cartilage elements in wild-type and *zhivago (zhi)* head skeletons, ventral view top, lateral view bottom. Immunostaining of Col2 in the Meckel's cartilage at 4 dpf.

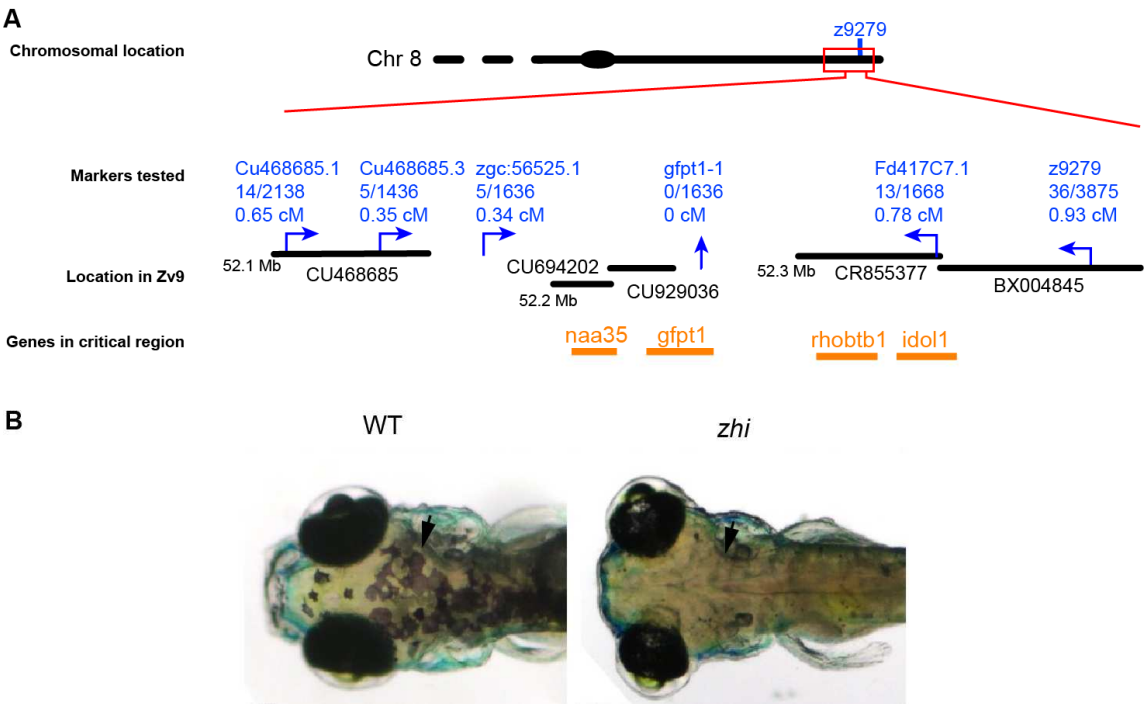

Figure 2.7: The *zhivago* mutation likely disrupts *gfpt1*. (A) The *zhivago* mutation was mapped to chromosome 8 near SSLP marker z9279. Novel SSLP markers with the indicated number of recombinants reduced the critical interval to a ~1 cM region that contains four genes. (B) Dorsal view of *zhivago* mutants after pigment regeneration assay. Arrows indicate pigment that failed to regenerate in *zhivago*.

genetic map in collaboration with the Jeffrey Smith laboratory (Bradley et al., 2007) using illumina GoldenGate genotyping technology. The mutation site was localized on the distal arm of Chromosome 8, near the SSLP marker z9279 (Figure 2.7A).

We then built a physical map using a combination of BAC fingerprinting, trace walking, gene jumping and comparative genomics. We confirmed the accuracy of our physical map by developing simple sequence length polymorphism (SSLP) and single strand conformation polymorphism (SSCP) markers from BAC or contig sequences and counting recombination events in a 1,636 meioses F2 map cross. Finally, we restricted the critical interval to a 1.12 cM region containing the gene *gfpt1*. A SSCP marker within the *gfpt1* gene had zero recombinants out of 1,636 meioses. A *gfpt1* mutant was previously identified in a screen for defects in pigment regeneration(Yang et al., 2007), but was also found to have craniofacial defects similar to *zhivago.* We performed a pigment regeneration assay, and confirmed that *zhivago* has an identical phenotype to *eartha/gfpt1* (Figure 2.7B). Combined with the mapping data, it is highly likely that a mutation in *gfpt1* is responsible for the *zhivago* phenotype.

Brak

brak (*brk*^{m452}) mutants have a pigmentation phenotype (Figure 2.8A) in addition to the previously identified skeletal phenotype (Neuhauss et al., 1996). *brak* was mapped to a 2 cM interval on the distal arm of chromosome 14, near the centromere (Figure 2.8B). Because recombination is suppressed near the centromere, the genetic distance underestimates the physical distance in the genome for z6847, previously established as a

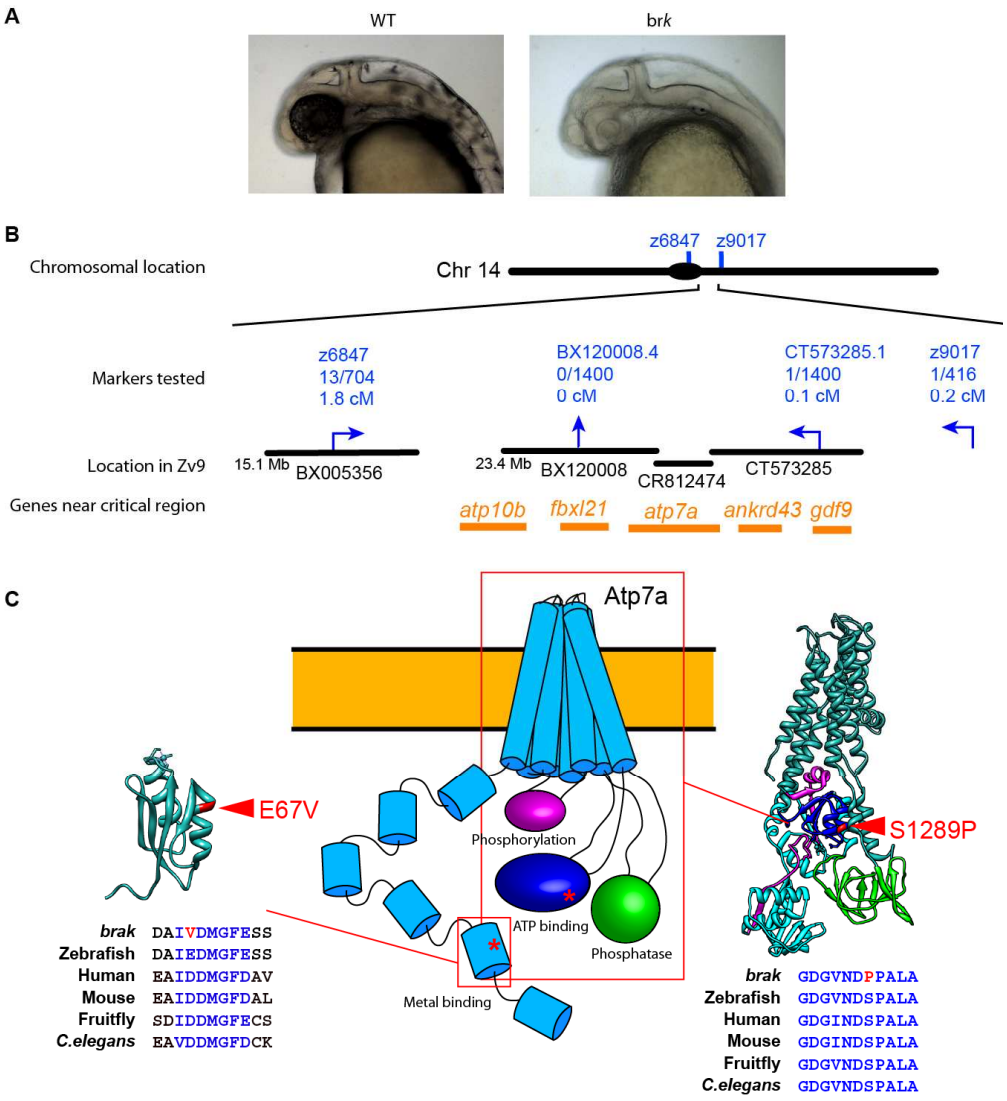

Figure 2.8: The *brak* mutation. (A) Lateral view of 30 hpf WT and *brak* live embryos. (B) The *brak* mutation was mapped to chromosome 14 between SSLP markers z6847 and z9017. Novel SSLP markers with the indicated number of recombinants highlighted a genomic region that contains five genes. (B) Predicted structure of Atp7a based on PDB structures 3RFU (Gourdon et al., 2011) and 1KVJ (DeSilva et al., 2005), including comparison of *atp7a* across several species. The amino acids changed in *brak* are highlighted in red, conserved residues are in blue.

centromere marker (Shimoda et al., 1999). The other flanking marker is not mapped to the genome as of Zv9, however, a combination of BAC fingerprinting, trace walking, and gene jumping identified several BAC clones in the critical region. I developed SSLP markers for these BAC clones and found two polymorphic markers with 0 and 1 recombinants out of 1,400 meioses. There are five genes in this region, one of which, the copper transporter *atp7a*, a copper transporter, has a previously identified zebrafish mutant, *calamity*, which was identified in a genetic screen for mutants phenocopied by copper deficiency (Mendelsohn et al., 2006). Because *calamity* and *brak* have similar phenotypes, although *brak* is less severe, we performed a complementation test and found that *calamity* and *brak* fail to complement each other, indicating that they result from mutations in the same gene. We sequenced *atp7a* in *brak* mutants and found two missense mutations in conserved regions of the gene (Figure 2.8C). Because *brak* is less severe than *calamity*, and results only in missense mutations, it is probably a hypomorphic allele.

Maggot

maggot (*mgt*^{m350,m503,m635}) mutants have craniofacial defects that are more severe than *crusher/sec23a* (Figure 2.9A); however the phenotype is distinguishable by notochord defects before the craniofacial defects are obvious. Immunofluorescence staining reveals that collagen deposition in the notochord appears to be disrupted in *maggot*, while trafficking of WGA-labeled glycoproteins appears normal (Figure 2.9B).

maggot was mapped to the distal arm of chromosome 23 using the zebrafish genetic linkage map (Knapik et al., 1998) (Figure 2.9C). We constructed a physical map

from BAC clone sequence using the Zv9 assembly, and restricted the critical interval to a

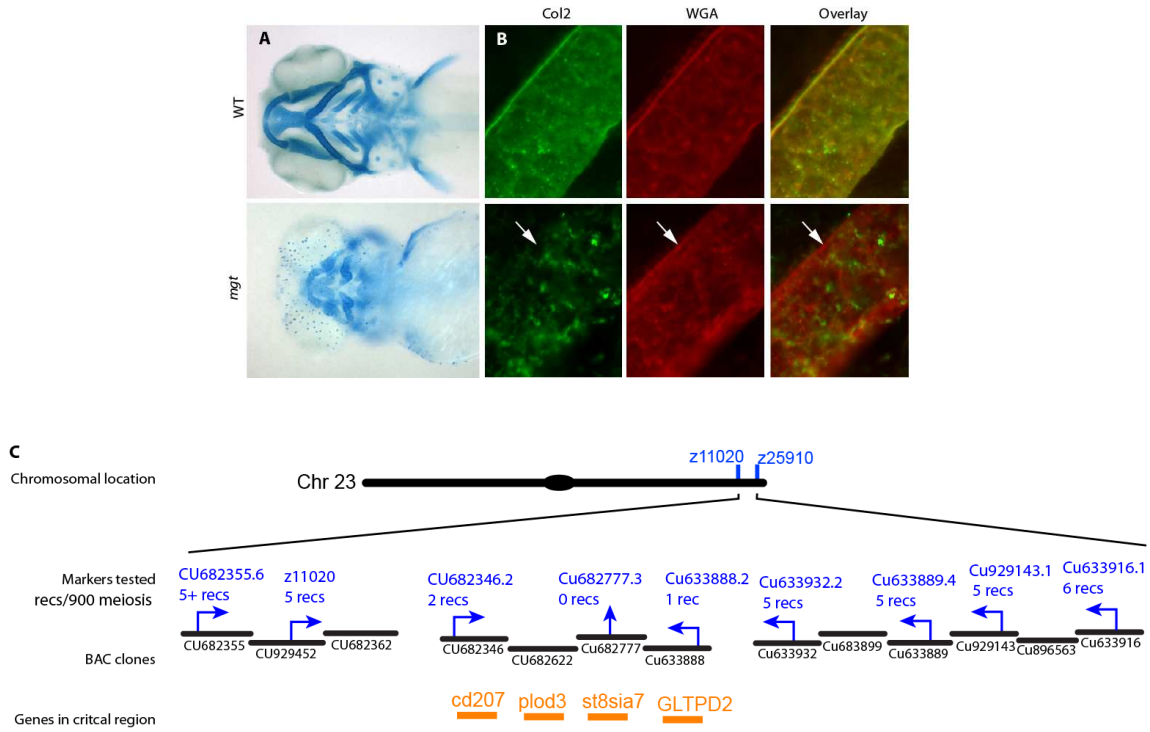

Figure 2.9: The *maggot* mutation. (A) Alcian blue staining of cartilage element in wild-type (WT) and *maggot (mgt)* head skeleton preparations ventral views. (B) Immunostaining of type-II collagen (Col2) and wheat germ agglutinin (WGA) in the notochord of 28 hpf embryos. (C) The *maggot* mutation was mapped to the distal arm of chromosome 23 between SSLP markers z11020 and z25910. Novel SSLP markers with the indicated number of recombinants reduced the critical interval to a ~160 kb region that contains four genes.

0.33 cM region containing four genes. One of those genes, *plod3*, has a previously characterized mutant, *diwanka*, which was found in a screen for motility defects (Zeller and Granato, 1999). *diwanka* mutants also have defects in collagen secretion. In order to test whether *maggot* mutants have defects in motility similar to *diwanka* we observed the response of 48 hpf embryos to prodding with forceps, and found that while wild-type siblings immediately swim away, *maggot* mutants do not. It is therefore possible the *maggot* mutation is caused by a defect in *plod3*, but this needs to be confirmed by sequencing or a complementation test with *diwanka* mutants.

Round

round (*rnd*^{m211,m641,m713,m715}) mutants have craniofacial defects and kinked fins similar to *crusher/sec23a* mutants (Figure 2.10A). Toluidine blue histological staining revealed that the ECM staining is lighter and more diffuse than in wild-type siblings (Figure 2.10B), this result is similar to that seen in *crusher/sec23a* mutants, and is consistent with a defect in trafficking of ECM components. Immunofluorescence staining shows diffuse, likely intracellular, distribution of type-II collagen (Figure 2.10C). While this staining is consistent with a trafficking defect, it is distinct from what is seen in *crusher/sec23a* mutants. In *crusher*, the collagen is backlogged within the ER and appears as bright conglomerations within the cell (Figure 1.3), not diffuse and widespread like in *round* mutants. WGA labeled proteins have a similarly diffuse staining, suggesting that the defect seen in *round* may represent a post-Golgi defect, because the sialic acid moieties that WGA primarily recognizes are not added to glycoproteins until they reach the Golgi.

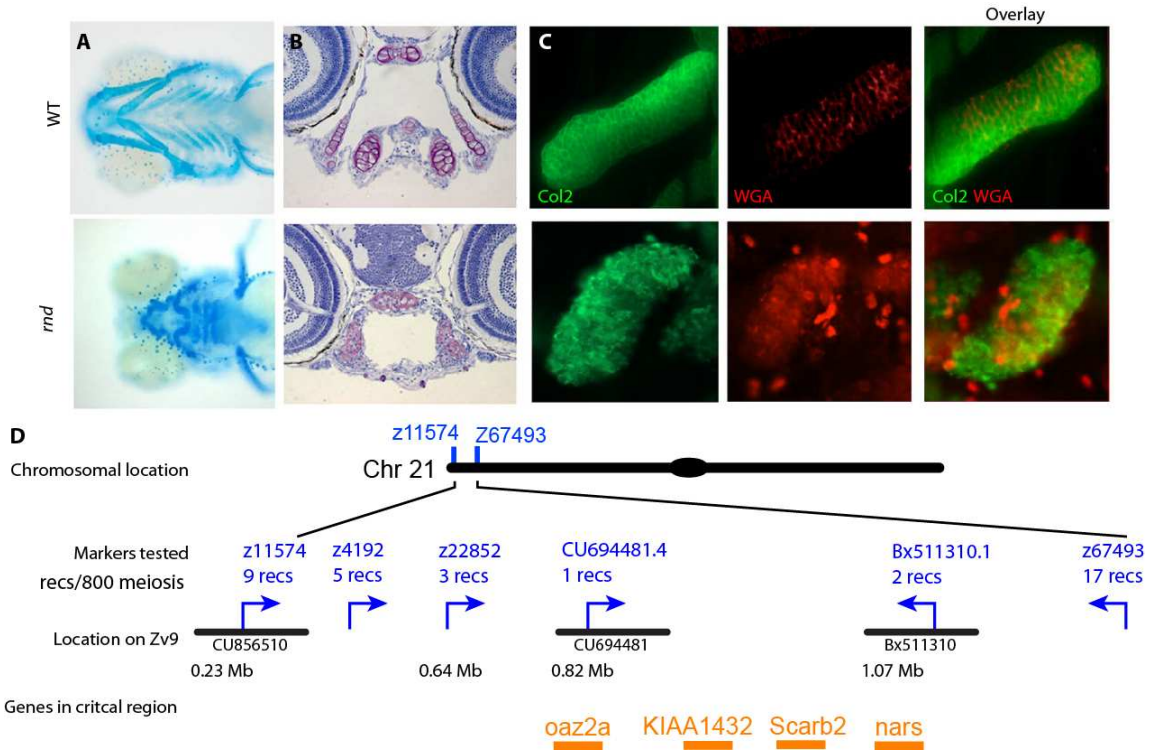

Figure 2.10: The *round* mutation leads to abnormal craniofacial skeleton development and disrupted protein trafficking. Alcian blue staining of cartilage element in wild-type (WT) and *round (rnd)* head skeleton preparations ventral views. (B) Toluidine blue staining of transverse sections of the jaw at the level of the optic nerve. Nuclei stain blue, whereas ECM stains purple. (C) Immunostaining of type-II collagen (Col2) and wheat germ agglutinin (WGA) in the 4th pharyngeal arch at 4 dpf embryos. (D) The *round* mutation was mapped to chromosome 21 between SSLP markers z11574 and z67493. Novel SSLP markers with the indicated number of recombinants reduced the critical interval to a 0.4 cM region that contains four genes.

round was mapped to the proximal arm of chromosome 21 using the zebrafish genetic linkage map (Knapik et al., 1998) (Figure 2.10D). Unfortunately, BAC coverage of that region of the genome is low, and the order of the genes is not conserved in mammalian genomes, making comparative genomics difficult. Through a combination of BAC fingerprinting, trace walking, and gene jumping we identified two non-overlapping BACs within the critical region and by developing markers for each of those BACs we restricted the critical interval to 0.38 cM, which should correspond to ~230 kb. This distance is consistent with the distance between those two markers in the Ensembl database, increasing confidence that the critical region, although not composed entirely of BAC clone sequence, may be correctly assembled. The Ensembl assembly of the critical interval contains four genes, and comparative genomics indicates that two of them, *oaz2a* and *kiaa1432* are neighboring genes in other species, giving further confidence that the ensembl assembly may be correct. Due to their distance from the flanking markers, the two most likely candidate genes for *round* are *scarb2* and *kiaa1432*. *scarb2* is an especially good candidate as it has been implicated in membrane trafficking of the endosome (Kuronita et al., 2002). We are currently sequencing these genes.

Discussion

Through positional cloning I have helped to identify either exact mutation sites or likely candidate genes for seven different mutants. These include the five discussed above, the *feelgood* mutant discussed in the next chapter, as well as the *kimble* mutant, which was found in collaboration with another graduate student and has become the basis for his dissertation research.

Several of these mutations were in genes that had been identified in other forward genetic screens, which highlights one disadvantage of forward genetic approaches, it is possible to expend resources searching for mutations in genes that have already been studied. However, the fact that they have been discovered in multiple screens highlights their physiological importance. Moreover, having multiple mutations in the same gene, an allelic series, is a powerful tool for dissection of the protein domains important for function.

At least three of the mutations identified so far appear to be hypomorphic alleles. This highlights the physiological relevance of ENU mutagenesis, and again emphasizes the importance of these genes, given that even without complete loss of function they result in a specific phenotype. The location and nature of the mutation may also provide insights into gene function. Deep sequencing has been proposed as a method of identifying mutation sites (Sun et al., 2012), but when the causative mutation does not result in a stop codon or frameshift, deep sequencing may lead to difficulties in determining which mutations in a mutagenized genome is the causative mutation for the phenotype.

CHAPTER III

PARALOG SPECIFIC REGULATION OF THE COPII MACHINERY BY Creb3L2 IS REQUIRED FOR COLLAGEN SECRETION AND CHONDROCYTE MATURATION

Introduction

Extracellular matrix (ECM) serves as a structural scaffold and a reservoir for biologically active molecules (Hynes, 2009). Cartilage formation and skeletal morphogenesis depend on timely and abundant deposition of ECM proteins (DeLise et al., 2000). Failure to produce adequate mature ECM or form proper collagen fibers can lead to many developmental defects and diseases, such as osteogenesis imperfecta, typically characterized by fragile bones (Rauch and Glorieux, 2004), scoliosis, short stature, hearing loss and teeth defects (Rauch and Glorieux, 2004). In adults, failure to maintain the ECM of the bone can lead to degenerative diseases such as osteoporosis, a debilitating condition characterized by a loss in bone density. Similarly, interstitial fibrosis leading to organ failure after injury, or pathological conditions in aging patients such as arthritis, have been associated with dysregulated protein secretion (Trojanowska et al., 1998; Heinegård and Saxne, 2011; Goldring and Goldring, 2007; Löppönen et al., 2004).

The initial step of protein trafficking occurs when proteins leave the site of synthesis in the endoplasmic reticulum (ER) and are transported to the Golgi. This step is primarily conducted by Coat Protein II complex (COPII) vesicular carriers (Barlowe et al., 1994; Dancourt and Barlowe, 2010; Miller and Barlowe, 2010). The COPII complex is recruited to the ER membrane by the Sar1 GTPase and consists of an inner coat of Sec23–Sec24 heterodimers and an outer coat of Sec13–Sec31 proteins. Vertebrate

genomes carry two highly similar paralogs of Sec23; Sec23A and Sec23B, and four paralogs of Sec24; Sec24A, Sec24B, Sec24C and Sec24D. Sec23 paralogs act as GTPase-activating proteins for Sar1, whereas Sec24 proteins play a role in cargo sorting (Wendeler et al., 2007).

Mutations in genes encoding COPII components have been implicated in a variety of human disorders with defects in close paralogs causing widely different phenotypes (Boyadjiev et al., 2006; Schwarz et al., 2009; Aridor and Hannan, 2002; Routledge et al., 2010). For example, mutations in SEC23B lead to Congenital Dyserythropoietic Anemia type II (CDAII), a disease characterized by ineffective erythropoiesis, bi- and multinucleated erythroblasts, and hypoglycosylation of red blood cell membrane proteins (Bianchi et al., 2009; Schwarz et al., 2009). In contrast, a point mutation in SEC23A leads to Cranio-lenticulo-sutural dysplasia (CLSD), the distinctive marks of which include craniofacial skeleton malformations and short stature (Boyadjiev et al., 2006). Zebrafish *crusher/sec23a* mutant and *sec23b* morphant embryos present phenotypes similar to the corresponding human diseases, establishing zebrafish as a model system to study the molecular and cellular bases of COPII-deficiencies (Schwarz et al., 2009; Lang et al., 2006).

Further establishing the paralog-specific defects seen with loss of COPII components, another zebrafish mutant, *bulldog/sec24d*, was recently described (Sarmah et al., 2010). Loss of Sec24D activity in zebrafish also results in craniofacial defects, whereas Sec24C morphants undergo normal development of head skeletal structures. Loss of *bulldog/sec24d* does not prevent neural crest migration, formation of pharyngeal condensations, or proliferation of chondrocytes, but hinders normal maturation of highly

secretory chondrocytes. Strikingly, the combined loss of Sec24C and Sec24D results in neural crest migration and condensation deficits, indicating that Sec24D activity is essential for chondrocyte maturation, but Sec24C or Sec24D compensate for each other in early stages of cartilage development (Melville and Knapik, 2011).

Considering the high levels of similarity between COPII paralogs and the basic cellular function that they perform, these findings suggest that COPII-dependent anterograde protein transport is a highly regulated process both during development and under physiological conditions in adulthood, and therefore is likely to be a factor in many more diseases than those already characterized. However, the mechanisms of this regulation are still in the early stages of being understood.

Forward genetic screens in model organisms, such as the one that isolated the *crusher* and *bulldog* mutants (Neuhauss et al., 1996), provide an unbiased approach to discover physiologically relevant mutations that affect skeletal development. Here, we have characterized the *feelgood* (*fel*^{m662}) mutant that belongs to the same phenotypic series as *crusher* and *bulldog.* We found that the *feelgood* mutation disrupts head skeleton and notochord development through loss of secretory capacity. The *feelgood* defect decouples the transport of collagens from that of other extracellular matrix proteins such as laminins by manifesting disrupted trafficking specifically in collagens. We show that the *feelgood* phenotype is caused by a missense mutation in the DNA binding domain of the transcription factor *creb3l2*. We provide the first evidence of paralog-specific regulation of COPII components by showing that loss of Creb3l2 activity decreases the expression of *sec23a, sec23b* and *sec24d*, but not *sec24c*. Our results suggest that Creb3l2 acts primarily as a transcriptional regulator of specific COPII

components, establishing a mechanism that enables cell-type, cargo, and tissue-specific functions of COPII vesicles during development and providing a possible mechanism for the diverse disease manifestations caused by loss of COPII. Our results also suggest that skeletal development is highly sensitive to the level of Creb3l2 activity in vivo and advance Creb3l2 as a candidate for skeletal diseases of unknown genetic origin.

Material and methods

Fish maintenance and breeding. Fish were reared under standard laboratory conditions at 28.5°C as previously described (Barrallo-Gimeno et al., 2004; Montero-Balaguer et al., 2006). *feelgood* (allele designated *m662*, isolated in the MGH genetic screen (Driever et al., 1996; Neuhauss et al., 1996)) was kept in AB genetic background for phenotypic analysis. Embryos were staged and fixed at specific hours (hpf) or days (dpf) post-fertilization as described by Kimmel et al, 1995. For some experiments embryos were incubated in 0.2 mM 1-phenyl-2-thiourea (Sigma) to block pigmentation.

Genetic mapping and cloning. The *feelgood* locus was mapped in a F2 intercross using bulked segregate analysis. DNA samples were PCR-genotyped with SSLP markers evenly spaced across the zebrafish genome. The mapped *feelgood* mutation was confirmed by sequencing genomic DNA flanking the mutation site from three homozygous wild-type F2 animals, five heterozygous F2 animals, six homozygous mutant F2 animals, and six animals each from three different genetic backgrounds of wild-type fish (AB, IN, and TL).

Cartilage staining. See detailed method in Chapter II.

Histology. See detailed method in Chapter II.

Immunofluorescence and Wheat Germ Agglutinin staining. Detailed method in Chapter II. For staining on sections, embryos were fixed in 4% or 2% PFA, embedded in 1.5% agarose in 5% sucrose, and stored in 30% sucrose solution at 4°C overnight. Agarose blocks were mounted with O.C.T. (Sakura Finetechnical Co.). Fifteen micrometer sections were cut using a Leica CM 3050 cryostat at −20°C and transferred onto *Superfrost* slides (Fisher). Sections were washed in PBS, blocked in 2 mg/ml BSA, 2% goat serum, 2% DMSO in PBS and incubated with collagen type II antibody (1:250 dilution), collagen type IV antibody (1:200 dilution, Lab Vision), Laminin Ab-1 (1:100; LabVision) or WGA (1:250) at 4°C overnight. Alexa Fluor 555 conjugate was applied as secondary antibody (1:500). TO PRO-3 (Molecular Probes) was used for nuclear counterstaining. Confocal images were taken with a Zeiss LSM510 inverted confocal microscope (Vanderbilt Cell Imaging Shared Resource).

Electron microscopy. After being anesthetized with *tricaine* (Sigma) zebrafish embryos were placed into fresh 2% gluteraldehyde and incubated overnight at 4°C. Fish were washed in PBS, transferred to 1% osmium textroxide, and washed in diH_2O. Fish were stained *en bloc* in 1% aqueous uranyl acetate for 1 h, and washed in diH_2O. The samples were taken through a series of dehydration steps starting with 30% and followed

by 50%, 70%, 95%, and absolute ethanol. Propylene oxide was used as a transitional solvent to replace the dehydration solution. Samples were transferred to a 1:1 araldite: propylene oxide mixture then placed in pure araldite in a vacuum oven. Pure resin specimens were then transferred into embedding molds containing fresh resin and finally placed into a 16° C oven overnight. Ultra-thin serial sections (50-60 nm) from polymerized blocks were obtained using a Leica UCT Ultracut microtome (Leica Microsystems), transferred to Formvar-coated slot grids, and examined using a Phillips CM10 TEM (FEI Company, Hillsboro, OR) equipped with an Advantage Plus 2 mega pixel Digital CCD System for CM10 TEM (Advanced Microscopy Techniques, Danvers, MA).

Western Blotting. Proteins were isolated by homogenizing 4 dpf embryos in RIPA buffer containing protease inhibitor (Sigma). Glycoproteins in lysate were cleaved by Endo H (NEB) or PNGase F (NEB) according to manufacturer specifications. Proteins were separated by sodium dodecyl sulfate-polyacrylamide gel electrophoresis (SDS-PAGE) on 10% Mini-Protean TGX gels (Bio-Rad). For immunoblotting, proteins were transferred to polyvinylidene fluoride (PVDF) membrane using an electrophoretic transfer apparatus (Bio-Rad). The membrane was blocked with 1% Non-fat milk (Bio-Rad) and incubated with 1:1,000 diluted primary antibody against type-II collagen (Polysciences), or N-Cadherin (Sigma) followed by 1:10,000 HRP conjugated anti-rabbit secondary antibodies (Promega). Signal detection was performed using Pico West Chemiluminescent Substrate (Thermo Scientific).

Generation of Tol2kit based transgenic fish. The *bactin2:creb3l2:mcherry*

construct was created using the "Tol2 kit" approach (Kwan et al., 2007). In brief, PCR was used to add attB1 and attB2 sites to the coding region of *creb3l2,* and the product was recombined into pDONR221 to create a middle entry clone. A construct containing the N301K mutation was created using the QuikChange Site-Directed Mutagenesis Kit (Stratagene).

The final constructs were created by recombining the middle entry clone with p5E-bactin2, p3E-mCherrypA and pDestTol2pA2 as described in the Invitrogen Multisite Gateway manual. PCR products were purified using the Qiaquick gel extraction kit (Qiagen).

5′ capped sense synthetic mRNAs were synthesized using a construct encoding the transposase and the mMessage mMachine kit (Ambion). 30 pg of the *bactin2:creb3l2-mCherry* construct and 20 pg of the transposase sRNA were simultaneously injected into embryos at the one-cell stage.

Phylogenetic analysis. Protein sequences were aligned using ClustalW2 (http://www.ebi.ac.uk/Tools/clustalw2/index.html). Phylogenetic tree was constructed using the neighbor joining method (Saitou and Nei, 1987).

RNA Isolation and RT-PCR Analysis. RNA was extracted and reverse transcription performed as described (Müller et al., 2006). cDNA was used as template for PCR analysis of *creb3l2* expression between one-cell stage and 5 dpf. The exon-spanning primers amplified a 235 bp fragment and were as follows:

β-actin 5′gactcaggatgcggaaactg3', 5′aagtcctgcaagatcttcac3′

Creb3l2 5′cacagaaccaccaccatgag3’, 5′acaggagagtcgcaggaaaa3′.

Morpholino knockdown. Antisense morpholino oligonucleotides (MOs) (Gene Tools) were designed to target the *creb3l2* 5′UTR (MO-1: CAGACCTGGACAACAGCATGACACT), or the *creb3l2* intron3-exon4 boundary (MO-2: TTCTGGGGTCGTTGAAGCGACGCTG). MO concentrations were determined spectrophotometrically and 1 nl was injected into 1–2 cell stage embryos at increasing doses (0.25 ng–8 ng) to determine optimal concentrations. MO-1 was injected at 7 ng, and MO-2 was injected at 0.5 ng and 3 ng (Figure 3.8 B-F, live images and Alcian blue stains are of embryos injected at 0.5 ng). Both morpholinos produced similar phenotypes, and MO-2 was used for all experiments pictured. MO-2 effectiveness was evaluated at 3 ng using primers indicated in Figure 3.8A, with sequences: e3f 5′CTTGAACCTCTCGCCTAAAG3′, i3f 5′GCCATGATTGAGCGTTCAGT3′, e5r 5′ATCCTTCAGCAATGAGGGTC3′, e6f 5′ACAGGAGAGTCGCAGGAAAA3′, e6r 5′CACAGAACCACCACCATGAG3′.

***In situ* hybridization.** The *creb3l2* probe was made by cloning 427 nucleotides from the 3’UTR of *creb3l2* cDNA into pGEM-T Easy vector (Promega) with primers 5′ATCTACTGCGCTGGGGCGAT3′, 5′AATATTTTCCTTAATAAAAGCA3′. Whole-mount *in situ* hybridization was performed as previously described (Sachdev et al., 2001).

Pigment aggregation assay. 3 dpf embryos were placed in egg water containing 0.5 μg/ml 4-hydroxyanisole (Sigma) for 3 days and imaged. 6 dpf embryos were placed

in egg water containing 1 nM melanin concentrating hormone (Sigma) for 10 minutes (Logan et al., 2006).

Luciferase Assay. Effector protein expression plasmids were generated by sub-cloning full length and cytosolic domain (1-374) Creb3l2 and N301KCreb3l2 into pCS2+ vector. The *firefly* luciferase reporter plasmid was generated by subcloning 895 bp of promoter sequence upstream of zebrafish *sec23a* into the pGL3 luciferase reporter vector (Promega). Human Foreskin Fibroblasts (System Biosciences) were grown to 95% confluency and transfected using Lipofectamine 2000 (Invitrogen) according to the manufacturer's specifications with reporter plasmid (0.4 µg), a reference plasmid pRL-SV40 (0.04 µg) carrying the *Renilla luciferase* gene under the control of the SV40 enhancer and promoter (Promega) and the corresponding effector plasmids (0.4 µg). After 30 h, luciferase activities were measured using the Dual-Luciferase Reporter Assay System (Promega) according to the manufacturer's protocol. *Firefly* luciferase activity was normalized to that of *Renilla* luciferase.

Quantitative PCR analysis. Q-PCR was performed as described previously (Sarmah et al., 2010). Total RNA was extracted from approximately 30 embryos at different embryonic time points using the TRIzol reagent (Sigma). Two micrograms of total RNA were reverse transcribed to cDNA using M-MLV reverse transcriptase (Promega) and poly-T primer. Each PCR reaction was performed with 1 µl of cDNA using iQ^{TM} SYBR Green Supermix (Bio-Rad) and 5 µM of each primer. Primer sets used were:

β-actin: 5′gactcaggatgcggaaactg3′, 5′aagtcctgcaagatcttcac3′,

Creb3l2: 5′ACAGGAGAGTCGCAGGAAAA3′, 5′CACAGAACCACCACCATGAG3′,

Sec23a: 5′AGGTGGACGTGGAGCAATAC3′, 5′CGAGAACGTCTCGGAGAAAC3′,

Sec23b: 5′ATGCTGGGACTGATGAAACC3′, 5′TCCTGTGTTTGGGAAAGTCC3′,

Sec24D: 5′TTTGCTGACACCAACGAGAG3′, 5′TGATTGGGGAACAGGAAGAG3′,

Sec24c: 5′CAGGGAAGAGAGTGGACTGC3′, 5′GTCTTCAGCTCCTGGCAAAC3′,

S1P: 5′GGATGTGGCGGTGTCTTACT3′, 5′CCTCTTACTGCGTGGAGGAG3′,

Bip: 5′CAGGAAAGAGTAAAACAGCAACCG3′,

5′CCGAAATTTTGCTCTCACTGCATC3′, and

Sil1: 5′CAGGAAAGAGTAAAACAGCAACCG3′,

5′CCGAAATTTTGCTCTCACTGCATC3′.

Three independent experiments in triplicates were performed using β-actin as internal control. Thermal cycling was carried out in an iQ5 (Bio-Rad) and relative expressions were calculated following previously described methods (Livak and Schmittgen, 2001).

Statistical Analysis. Data in bars represent average ± s.d. Statistical analyses were performed using unpaired two-tailed Student's *t*-test and *p* values <0.05 were considered as significant.

Results

The zebrafish *feelgood* mutation causes craniofacial defects

The primary features of the *feelgood* phenotype include a reduced lower jaw, shortened body length, and compact head, trunk and tail as measured from the posterior edge of the ear capsule to the tip of the tail (Figure 3.1A-D). Alcian blue staining (Figure 3.1 E-F′) reveals that all cartilage elements of the head skeleton are present in *feelgood* mutants, but they are shortened and malformed, including abnormal curvature of the Meckel's and ceratohyal cartilages, and failure of the Meckel's to taper towards the anterior end (Figure 3.1F′).

Histological analysis by toluidine blue staining (Figure 3.1G,H) shows reduced extracellular matrix (ECM) surrounding the chondrocytes and tightly packed nuclei in *feelgood* mutants (Figure 3.1H, arrow). Furthermore, the overall pattern of chondroblast intercalations and stacking is disrupted. These features are shared with the head skeleton defects observed in the *crusher/sec23a* and *bulldog/sec24d* mutants (Melville and Knapik, 2011; Lang et al., 2006; Sarmah et al., 2010).

Type-II collagen trafficking is disrupted in *feelgood* mutant chondrocytes

To investigate whether abnormal cartilage shape is associated with trafficking deficits of extracellular matrix proteins as with *crusher/sec23a* and *bulldog/sec24d*, we examined the cellular distribution of Collagen2α1 (Col2α1) in chondrocytes at 80 hpf, the

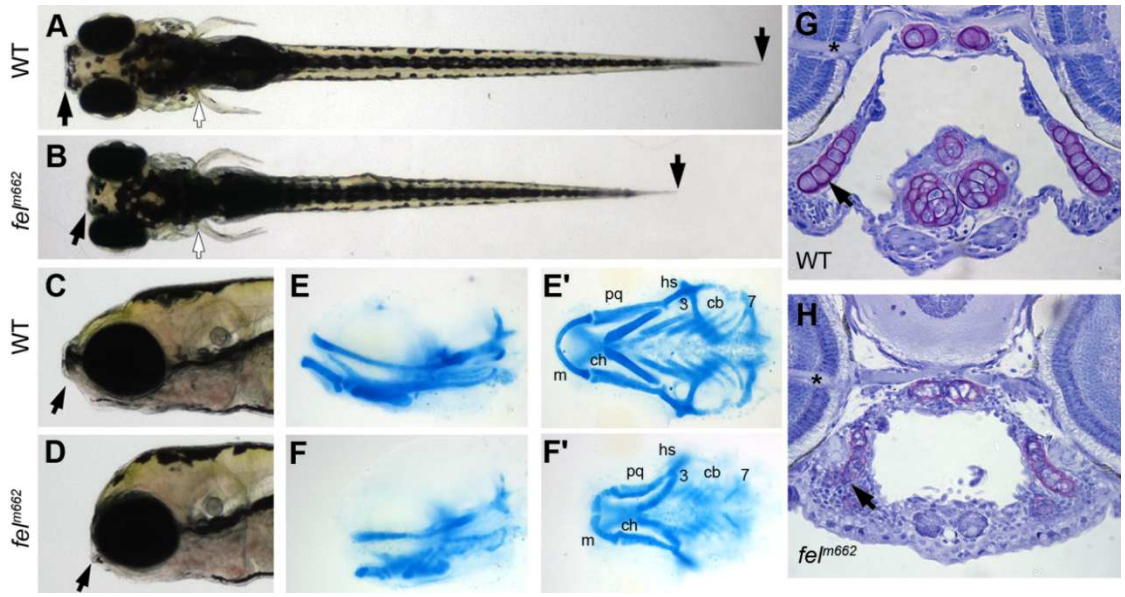

Figure 3.1: The *feelgood* (*fel*^{m662}) mutation affects craniofacial skeletal development. (A-D) Live images of wild-type (WT) and *feelgood* embryos at 5 dpf. Arrows indicate reduced length of head and trunk in dorsal (A,B) and lateral (C,D) views. (E-F) Alcian blue staining of cartilage elements in head skeleton in lateral (E,F) and ventral (E′,F′) views. (G,H) Toluidine blue staining of transverse sections of the jaw at the level of the optic nerve. Nuclei stain blue, while ECM stains purple. Abbreviations: cb, ceratobranchials 3-7; ch, ceratohyal; hs, hyosymplectic; m, Meckel's cartilage; pq, palatoquadrate.

earliest stage at which *feelgood* mutants can be clearly identified, and at 5 dpf embryos. In addition, we compared collagen trafficking to bulk transport of secreted glycoproteins by staining N-acetylglucosamine or sialic acid residues with wheat germ agglutinin (WGA).

In 80 hpf wild-type embryos, both Col2α1 and WGA-labeling is primarily localized to the extracellular space (Figure 3.2A-A″), with small clusters of intracellular staining likely representing the Golgi apparatus (Allen et al., 1989). In *feelgood* mutants, WGA staining also appears in the extracellular space and the Golgi apparatus (Figure 3.2B), suggesting that *feelgood* mutants traffic the bulk of WGA-binding glycoproteins at close to normal levels. In contrast, immunofluorescence staining in *feelgood* reveals deposition of Col2α1 to the extracellular space but also accumulation in small cytosolic vesicle-like structures, which are larger and denser than the corresponding intracellular compartments in wild types (Figure 3.2A′,B′). By 5 dpf, *feelgood* and wild-type WGA staining patterns are similar (Figure 3.2C,D), whereas the intracellular type-II collagen accumulation in *feelgood* chondrocytes has increased (Figure 3.2C′,D′).

To identify the intracellular localization of protein accumulation, we used transmission electron microscopy (TEM). TEM images show that chondrocytes are regularly stacked in wild-type embryos with abundant ECM (Figure 3.2E,I), whereas in *feelgood,* chondrocytes have a round morphology and are irregularly spaced, suggesting stacking defects (Figure 3.2G,K). At this stage, rough ER, identified as ribosome dotted membranes, is severely, but not uniformly, distended in *feelgood* mutants (Figure 3.2F,H). By 5 dpf, chondrocytes in wild-type embryos have become hypertrophic, lacking dense rough ER (Figure 3.2I,J). Conversely, chondrocytes in *feelgood* appear arrested at earlier

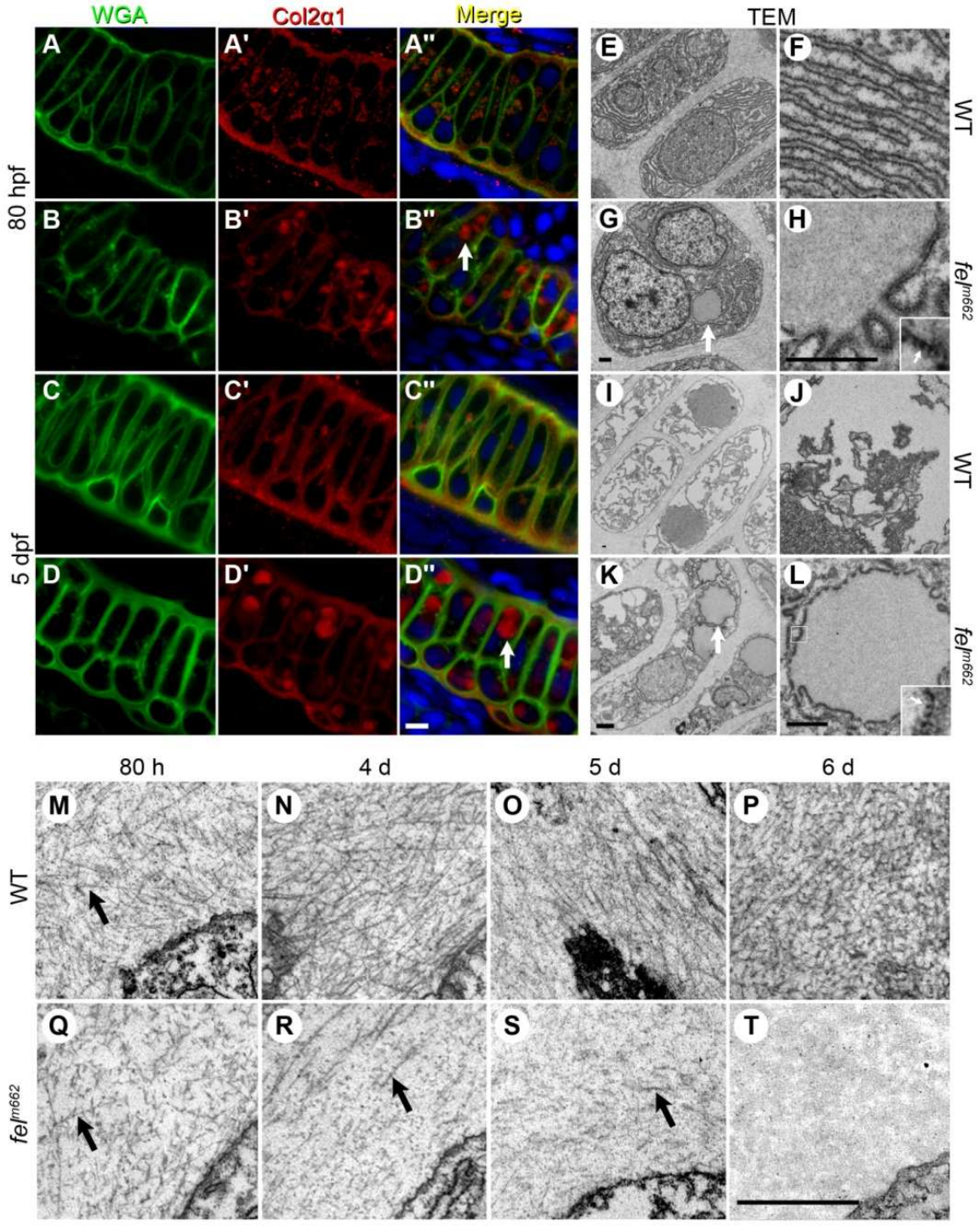
WGA
Col2α1
Merge
TEM
80 hpf
5 dpf
WT
fel^m662
WT
fel^m662
A
A'
A''
B
B'
B''
C
C'
C''
D
D'
D''
E
F
G
H
I
J
K
L
80 h
4 d
5 d
6 d
WT
fel^m662
M
N
O
P
Q
R
S
T

Figure 3.2: Protein trafficking is disrupted in *feelgood* mutants. (A-D) Immunostaining of WGA (A-D) and Col2α1 (A′-D′) of the Meckel's cartilage at 80 hpf (A-B′′) and 5 dpf (C-D′′) in wild-type (WT) and *feelgood* embryos. Arrows in merged images indicate aberrant intracellular collagen localization in *feelgood*. (E-L) TEM images of 80 hpf (E-H) and 5 dpf (I-L) WT and *feelgood* chondrocytes. Arrows indicate distended ER membranes in *feelgood* cells. Scale bars are 1 micron. (M-T) TEM images of collagen fibrils in the extracellular space of *feelgood* mutants and wild-type (WT) siblings at 80 hpf and 4, 5 and 6 dpf. Arrows point to representative individual collagen fibrils. Scale bar is 1 micron.

stages of maturation, containing large vacuoles of distended ER membranes filled with electron dense material (Figure 3.2K,L).

These data indicate that the jaw deformity in *feelgood* mutants is likely a consequence of abnormal collagen secretion and continuous intracellular protein buildup, leading to a progressively more severe phenotype. They also suggest that the maturation of *feelgood* chondrocytes toward a hypertrophic state is delayed or stalled, subsequent to insufficient matrix deposition, which is known to cause deficits in matrix-mediated intracellular signaling (Hickok et al., 1998).

Cartilage matrix is progressively lost in *feelgood* mutants

Cartilage matrix is continuously turned over during development and tissue homeostasis. Maintenance of cartilage matrix requires synchronization of a number of cellular functions, including coordinated protein secretion, cell-matrix signaling and protein degradation. To query how the intracellular defect in collagen transport affects ECM formation, we compared the ultrastructure of cartilage matrix in TEM images of wild-type and *feelgood* embryos (Figure 3.2M,Q). In this analysis, we examined tissue sections from the earliest stage we can morphologically distinguish the *feelgood* phenotype at 80 hpf, followed by analyses on days 4, 5 and 6 of development. We found that *feelgood* mutant matrix at 80 hpf contains collagen fibrils (Figure 3.2Q) suggesting that collagen is successfully synthesized and secreted by chondrocytes at the initial stages of chondrogenesis. However, as collagen fibrils grow progressively denser in wild-type cartilage (Figure 3.2M-P), ECM matrix in *feelgood* becomes gradually more sparse and devoid of collagen bundles with an almost complete absence of organized fibrils by 6 dpf

(Figure 3.2Q-T).

Thus, cartilage collagen is being initially secreted by *feelgood* chondrocytes, albeit at lower levels than in wild types. However, the typical increase in matrix secretion during cartilage differentiation at the 4 dpf stage is absent, suggesting that *feelgood* is required for sustained, high-volume traffic of ECM proteins.

Notochord sheath formation, but not secretion of glycosaminoglycans (GAGs), is disrupted in *feelgood* mutants

feelgood mutant embryos are shorter than wild types, pointing to disrupted notochord development. In zebrafish embryos, the notochord functions as a hydrostatic skeleton; the mechanical properties of which depend on an external fibrous sheath, that consists primarily of collagen and laminin matrix, and numerous internal vacuoles in notochord sheath cells, that enclose secreted glycosaminoglycans (GAGs) with high affinity for water (Scott and Stemple, 2005; Adams et al., 1990). Both of these biomechanical components exert the appropriate notochord stiffness that is essential for embryo lengthening and maintenance of straight posture.

To determine the secretory status of GAG proteins in the notochord sheath, we used WGA staining. The results show that at 28 hpf, WGA-stained proteins are trafficked through the notochord sheath cells of *feelgood* embryos to extracellular space (Figure 3.3A,B,E,F). The major components of the notochord sheath are type II and type IV collagen fibrils that are interlinked with laminins, nidogen and fibulins; the typical components of basement membranes (Timpl and Brown, 1996). We analyzed the

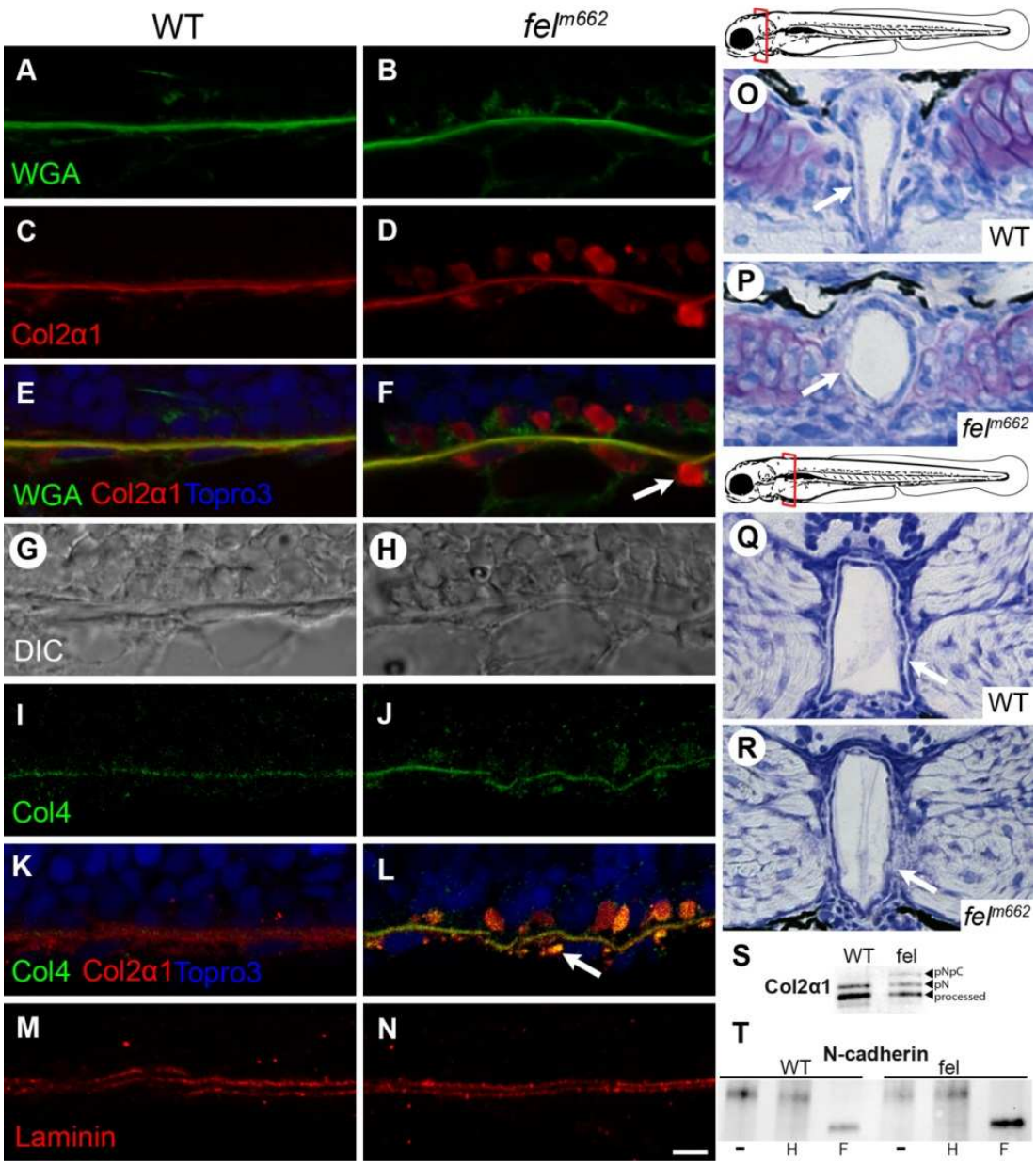
WT
felm662
A
WGA
B
C
Col2α1
D
E
WGA Col2α1Topro3
F
G
DIC
H
I
Col4
J
K
Col4 Col2α1Topro3
L
M
Laminin
N
O
WT
P
felm662
Q
WT
R
felm662
S
WT fel
Col2α1
pNpC
pN
processed
T
N-cadherin
WT
fel
-
H
F
-
H
F

Figure 3.3: Collagen trafficking is preferentially disrupted leading to notochord defects of *feelgood* mutants. (A-F) Immunofluorescence of WGA, Col2α1 and merged images of 15 μm sagittal sections of the notochord of 28 hpf embryos. Arrows indicate vesicle-like collagen staining outside the notochord sheath; (G-H) DIC images of the corresponding sections in A-F. (I-N) Immunofluorescence of type-IV and Type-II collagen (I-L) and laminin (M,N) in 15 μm sagittal sections of the notochord at 28 hpf. (O-R) Toluidine blue staining of transverse sections through the notochord at the level of the posterior of the parachordal plate (O,P) and posterior medulla oblongata (Q,R) in 80 hpf embryos. Schematic diagrams depict the area of the corresponding sections. Arrows indicate the less robust notochord sheath in *feelgood* compared to wild types. (S) Immunoblot analysis of type-II collagen processing. Molecular forms are indicated as: processed, the fully processed form; pN, pN-collagen II; pNpC, unprocessed procollagen II. (T) EndoH sensitivity assay for N-cadherin. Embryo lysates were either untreated (-) or treated with either EndoH (H) or PNGase F (F) before immunoblotting for N-cadherin.

secretory status of the type II and type IV collagens by immunofluorescence and found that both are abnormally localized within large vesicle-like structures similar to those seen in the craniofacial cartilage (Figure 3.3 C-F, I-L).

To determine whether secretory defects extend to other ECM proteins, we analyzed the localization of laminin in the notochord and somitic boundaries, and we detected no deficits in deposition in *feelgood* embryos compared to wild types (Figure 3.3M,N, and data not shown). Histological analysis of transverse sections stained with Toluidine blue at 80 hpf embryos further corroborated the findings at earlier stages and revealed less robust notochord sheath in *feelgood* compared to wild types (Figure 3.3O-R). These data suggest that the transport of GAGs to internal vacuoles, as well as the secretion of WGA-binding glycoproteins and laminin is not disrupted in *feelgood* mutants. In contrast, *feelgood* specifically affects the secretion of type II and type IV collagens resulting in overall weaker and smaller fibrous sheath surrounding the notochord, consistent with the shorter body length of *feelgood* embryos.

To further assess the secretory capability of the *feelgood* embryos, we analyzed total protein extracts from 4 dpf embryos on Western blots probed with antibodies against type-II collagen. We found an increase in unprocessed procollagen, consistent with a trafficking defect (Figure 3.3S).

Furthermore, we analyzed an immunoblot using N-cadherin antibody and protein extract and found that N-cadherin in *feelgood* mutant embryos was resistant to endoglycosidase H (Endo H) (which cleaves mannose rich structures) but sensitive to PNGase F (which cleaves high-mannose as well as complex-type N-glycans). This indicates that N-cadherin is normally processed and progresses along the intracellular

secretory pathway consistent with its plasma membrane localization in *feelgood* chondroblasts (Fig. 3T, and data not shown).

The *feelgood* mutation affects melanosome maturation

To test whether the *feelgood* phenotype affects other cell types characterized by high levels of protein trafficking, including those that do not secrete collagen, we analyzed pigment cell maturation. This process involves intensive protein transport during the biogenesis of melanosomes, a set of morphologically and functionally unique organelles that accumulate melanin and translocate within melanocytes in response to pigment modulating stimuli (Marks and Seabra, 2001). Our results show that while pigment appears normal, the ability of *feelgood* melanocytes to respond to stimuli is disrupted (Figure 3.4A-D). Specifically, when stress was induced by a low concentration of the melanotoxic 4-hydroxyanisole (Riley et al., 1975), melanosomes in wild-type pigment cells responded by aggregating into small dense structures as previously described (Logan et al., 2006). However, in *feelgood* embryos, melanosomes failed to aggregate when stimulated with 4-hydroxyanisole and melanosome concentrating hormone (Figure 3.4C,D, and data not shown).

To gain insight on pigment aggregation phenotype, we compared the ultrastructural characteristics of melanosomes between wild-type and *feelgood* fish (Figure 3.4E-G). TEM images revealed that in wild types, melanosomes mature to flattened, oval shape structures, whereas in *feelgood* mutants, they appear uniform in size and circular in shape (Figure 3.4F,G). This phenotype is similar to the melanosome maturation defects observed in the murine and zebrafish *silver* mutants (Theos et al.,

2006; Schonthaler et al., 2005). The *silver* phenotype is caused by failure to transport

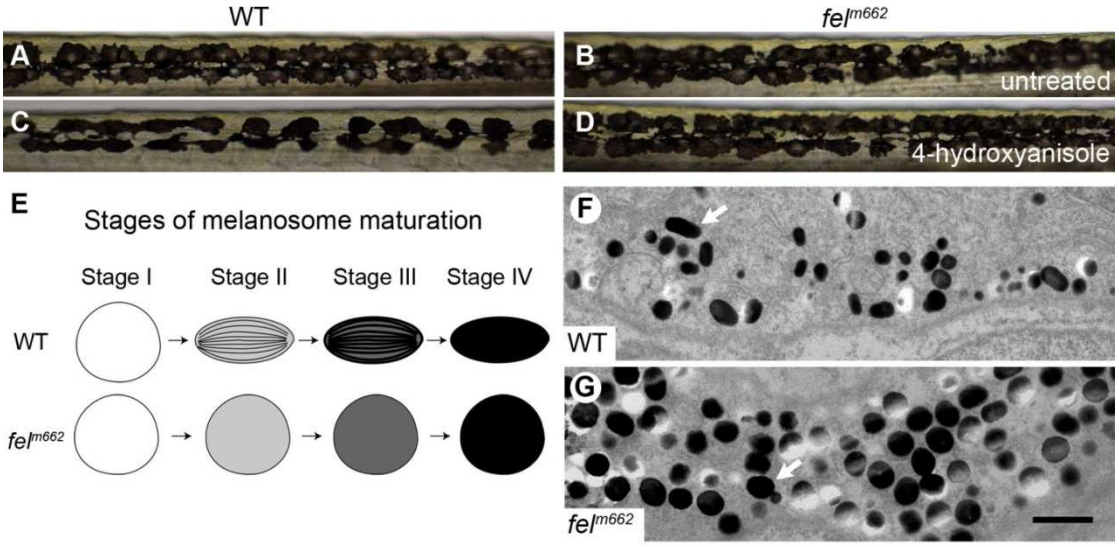

Figure 3.4: Melanophore development is disrupted in *feelgood* mutants. (A-D) Live image of melanophores in the trunk of 6 dpf wild-type and *feelgood* mutants in untreated (A,B) and 0.5 μg/ml 4-hydroxyanisole treated (C,D) embryos. (E) Summary drawing of the stages of melanosome maturation comparing normal and *feelgood* melanocytes. (F,G) TEM images of 5 dpf melanosomes. Arrows point to a mature melanosome in wild type (F), and a round, dark, stage IV melanosome in *feelgood* (G). Scale bar is 1 micron.

Pmel17, a structural protein that is required to maintain the oval shape of melanosomes, across the ER membrane (Theos et al., 2006).

Taken together, these results show that *feelgood* disrupts normal melanosome maturation in melanocytes. Thus, *feelgood* has critical functions in distinct cell types and not only in collagen-producing cells.

The *feelgood* mutation disrupts the *creb3l2* locus

The similarities between the *feelgood* phenotype and the phenotypes of the *crusher/sec23a* and *bulldog/sec24d* mutants, which abolish the function of two key COPII components, suggested that the *feelgood* locus encodes a protein participating in COPII-mediated transport. To identify the chromosomal location of the *feelgood* mutation, we utilized a positional cloning strategy. We genotyped fish from an F2 intercross and used the zebrafish genetic linkage map (Knapik et al., 1998; Bradley et al., 2007) to establish that the *feelgood* mutation is located in a 5.2 cM region on the proximal arm of chromosome 4 (Figure 3.5A). We then built a physical map of the critical region between these markers using the Zv7 genomic assembly to obtain contigs, and bridged the gaps between contigs using BAC information from the Zebrafish Genome Fingerprinting Project and sequences from the Ensembl trace repository. We confirmed the accuracy of our physical map by developing SSLP markers from BAC or contig sequences and counting recombination events in a 2,510 meioses F2 map cross. Finally, we restricted the critical interval to a 58 kb region flanked proximally by a marker within an intron of the *cAMP responsive element binding protein 3-like 2* (*creb3l2*) gene, and distally by a marker in intron 20 of the *diacylglycerol kinase, iota* (*dgki*) gene.

No other known genes are present in the critical region (Figure 3.5A).

Sequencing of the coding region of the two candidate genes revealed a single C>G transversion at base pair 1128 of the *creb3l2* gene that results in a N301K missense mutation (Figure 3.5B,C). The Creb3l2 protein contains a basic leucine zipper domain consisting of a basic motif that mediates sequence specific DNA binding, a leucine zipper motif that facilitates protein dimerization (Vinson et al., 1989; Hope and Struhl, 1987), and a single pass transmembrane domain preceding a Site-1 protease (S1p) recognition site (Figure 3.5B). The *feelgood* mutation is located within the DNA binding basic motif of Creb3l2, in a segment that is conserved from *C. elegans* to man (Figure 3.5D). *Creb3l2* belongs to a family of 5 paralogs that are highly conserved among vertebrate species including zebrafish. Phylogenetic analysis showed that zebrafish *creb3l2* is the most similar zebrafish paralog to human *CREB3L2* (Figure 3.6).

To determine whether loss of Creb3l2 function is responsible for the *feelgood* phenotype, we designed a Tol2-based rescue construct (Kwan et al., 2007) containing wild-type *bactin2:creb3l2-mCherry* that was injected into *feelgood* mutants to create chimeric transgenic fish overexpressing wild type and mutant proteins (Figure 3.5E). Approximately 1/4 of the injected *feelgood* mutant embryos showed a partial rescue of the *feelgood* phenotype as indicated by the longer jaw, which protrudes past the eyes, and the presence of cartilage elements whose shape closely resembles that of wild types (Figure 3.5F,H). A similar construct that contained the putative *feelgood* (N301K) mutation in *creb3l2* failed to rescue, indicating that the N301K substitution disturbs *creb3l2* function and accounts for the *feelgood* mutant phenotype (Figure 3.5G,I,J).

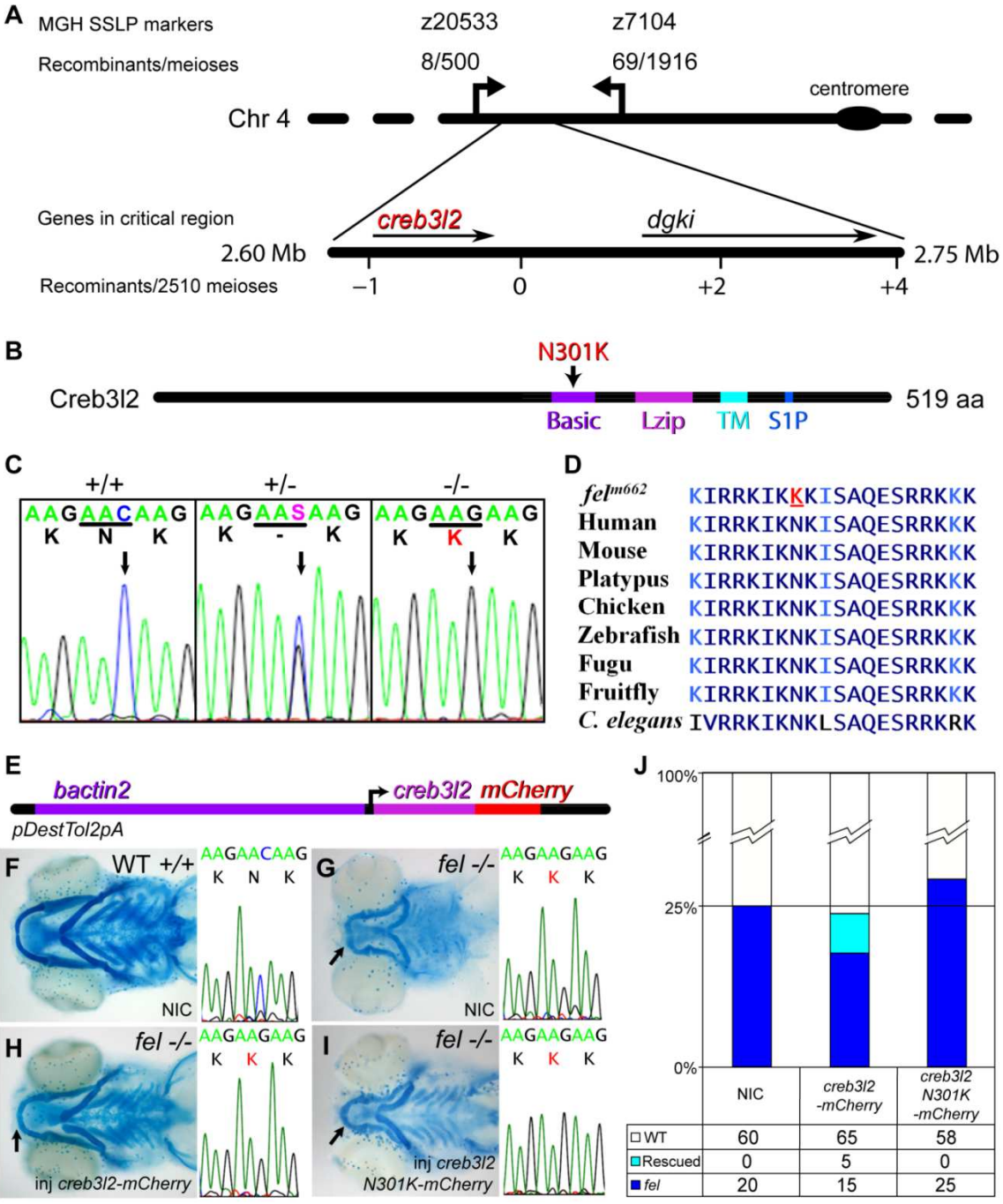
A
MGH SSLP markers
z20533
z7104
Recombinants/meioses
8/500
69/1916
centromere
Chr 4
Genes in critical region
creb3l2
dgki
2.60 Mb
2.75 Mb
Recominants/2510 meioses
−1
0
+2
+4
B
N301K
Creb3l2
519 aa
Basic
Lzip
TM
S1P
C
+/+
+/-
-/-
AAGAACAAG
K N K
AAGAASAAG
K - K
AAGAAGAAG
K K K
D
fel m662 KIRRKIKKKISAQESRRKKK
Human KIRRKIKNKISAQESRRKKK
Mouse KIRRKIKNKISAQESRRKKK
Platypus KIRRKIKNKISAQESRRKKK
Chicken KIRRKIKNKISAQESRRKKK
Zebrafish KIRRKIKNKISAQESRRKKK
Fugu KIRRKIKNKISAQESRRKKK
Fruitfly KIRRKIKNKISAQESRRKKK
C. elegans IVRRKIKNKLSAQESRRKRK
E
bactin2
creb3l2 mCherry
pDestTol2pA
F
WT +/+
NIC
G
fel -/-
NIC
H
fel -/-
inj creb3l2-mCherry
I
fel -/-
inj creb3l2 N301K-mCherry
J
100%
25%
0%
NIC
creb3l2 -mCherry
creb3l2 N301K -mCherry
WT 60 65 58
Rescued 0 5 0
fel 20 15 25

Figure 3.5: The *feelgood* line carries a missense mutation in *creb3l2*. (A) The *feelgood* mutation was mapped to Chromosome 4 between SSLP markers z20533 and z7104. Novel SSLP markers with the indicated number of recombinants reduced the critical region to a ~50 kb region that contained two genes. The physical map of the critical region was based on the Zv7 assembly. (B) Schematic diagram of the Creb3l2 primary structure illustrating a missense N301K mutation in the DNA binding Basic motif. Abbreviations: Basic: Basic motif, Lzip: Leucine zipper motif, TM: transmembrane domain, S1p: Site-1 protease recognition sequence. (C) Electropherograms of wild-type (+/+), heterozygous (+/–) and *feelgood* (–/–) genomic DNA. The arrow points to the C→G transversion that results in lysine for asparagine substitution at position 301 (N301K). (D) Comparison of the DNA binding basic motif of *creb3l2* across several species. The amino acid changed in *feelgood* mutants is underlined in red. (E) Schematic diagram of the Tol2 kit-based construct containing *mCherry*-tagged *creb3l2* under the ubiquitous *beta-actin* (*bactin2*) promoter. (F-I) Alcian blue staining of cartilage elements at 5 dpf of non-injected (NIC) wild-type embryo (F); non-injected *feelgood* embryo (G); *creb3l2-mCherry* rescued *feelgood* mutant embryo (H); and mutant embryo injected with *feelgood* (N301K*) creb3l2–Cherry* that failed to rescue the phenotype (I). The chromatograms of sequences surrounding the *feelgood* lesion for the embryos shown in F-I have been included in the corresponding adjacent images. Arrows indicate an increased length of lower jaw in rescued mutant (H) compared to NIC *feelgood* control (G). (J) Quantification of the number of mutant, wild-type, and rescued phenotypes in the *bactin2 creb3l2-mCherry* injection experiments. The *feelgood* genotype of these fish was confirmed by sequencing.

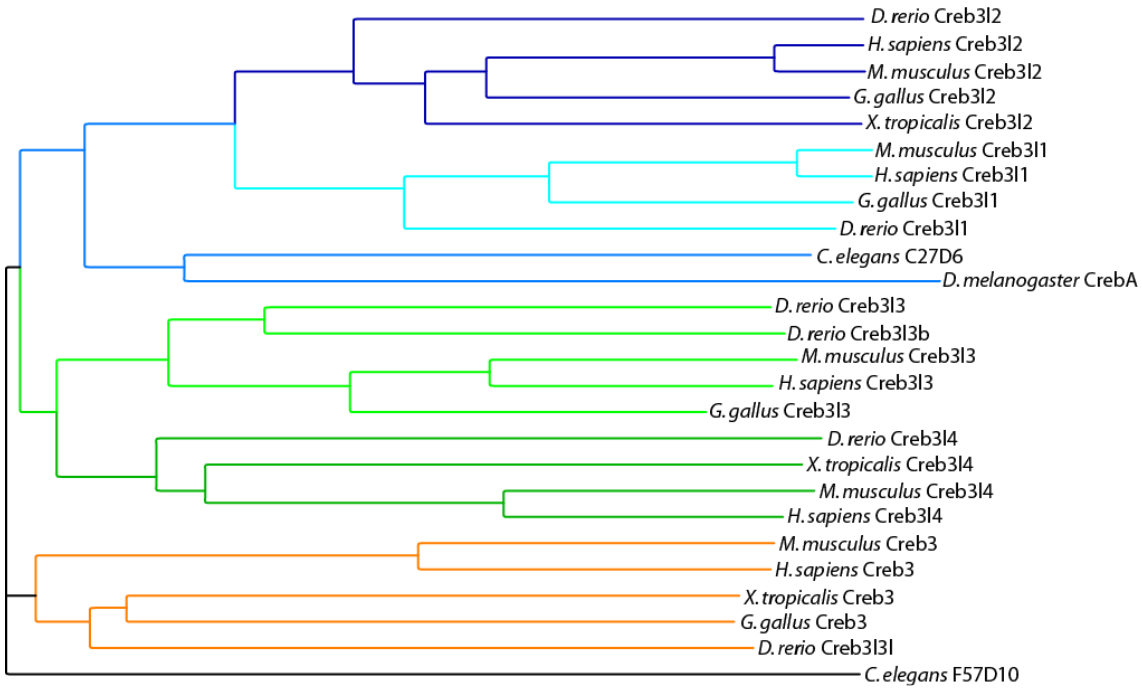

Figure 3.6: Phylogeny of Creb3 like paralogs. Phylogram of known zebrafish (*Danio rerio*), human (*Homo sapiens*), mouse (*Mus musculus*), chicken (*Gallus gallus*), frog (*Xenopus tropicalis*), fruitfly (*Drosophila melanogaster*), and nematode (*Caenorhabditis elegans*) Creb3 like paralogs.

creb3l2 is expressed in the developing pharyngeal arches

To determine whether the spatio-temporal expression pattern of *creb3l2* during development matches the structures mostly affected in *feelgood* mutants, we analyzed RNA samples by RT-PCR and embryos by whole mount *in situ* hybridization at sequential developmental time points. RNA analysis revealed that *creb3l2* mRNA is maternally deposited and that the amount of transcript decreases after the onset of zygotic transcription at the mid-blastula transition. As development proceeds, *creb3l2* is steadily expressed throughout morphogenesis with the highest level at 4 dpf (Figure 3.7A). Probing embryos by *in situ* hybridization with digoxigenin-labeled *creb3l2* riboprobes showed that *creb3l2* is ubiquitously expressed during early development (Figure 3.7B). By 36 hpf, *creb3l2* RNA becomes primarily localized to the developing jaw, pectoral fins, and the otic capsule (Figure 3.7C) and expression is maintained throughout jaw development (Figure 3.7D-E′). These results show that Creb3l2 is highly expressed in tissues that show developmental deficits in *feelgood* embryos, consistent with a direct role for Creb3l2 in craniofacial morphogenesis.

creb3l2 knockdown phenocopies the *feelgood* defects

The *feelgood* mutation most likely disrupts the DNA binding ability of Creb3l2, resulting in partial or complete loss of function. To determine whether *feelgood* is a null or a hypomorphic allele, we knocked-down Creb3l2 protein using two morpholinos (MO-1 and MO-2; Figure 3.8A). Although both produced similar results, MO-2, which

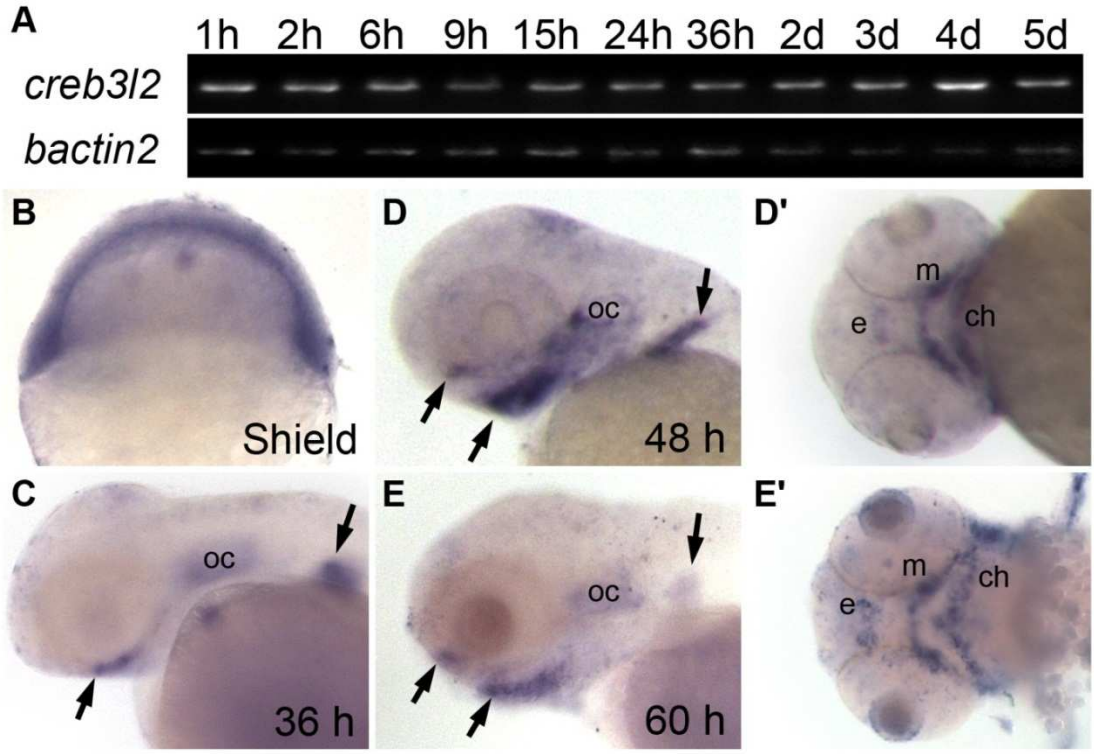

Figure 3.7: Expression of *creb3l2* during zebrafish development. (A) RT-PCR analysis of *creb3l2* expression with *beta-actin* as a loading control. (B-E') Whole mount in situ hybridization of *creb3l2* expression. Arrows indicate increased expression at the developing pharyngeal skeleton and fin between 36 and 60 hpf. C-E, lateral views, D′,E′ ventral views of D,E. Abbreviations: e, ethmoid plate; m, Meckel's cartilage; ch, ceratohyal; oc, otic capsule.

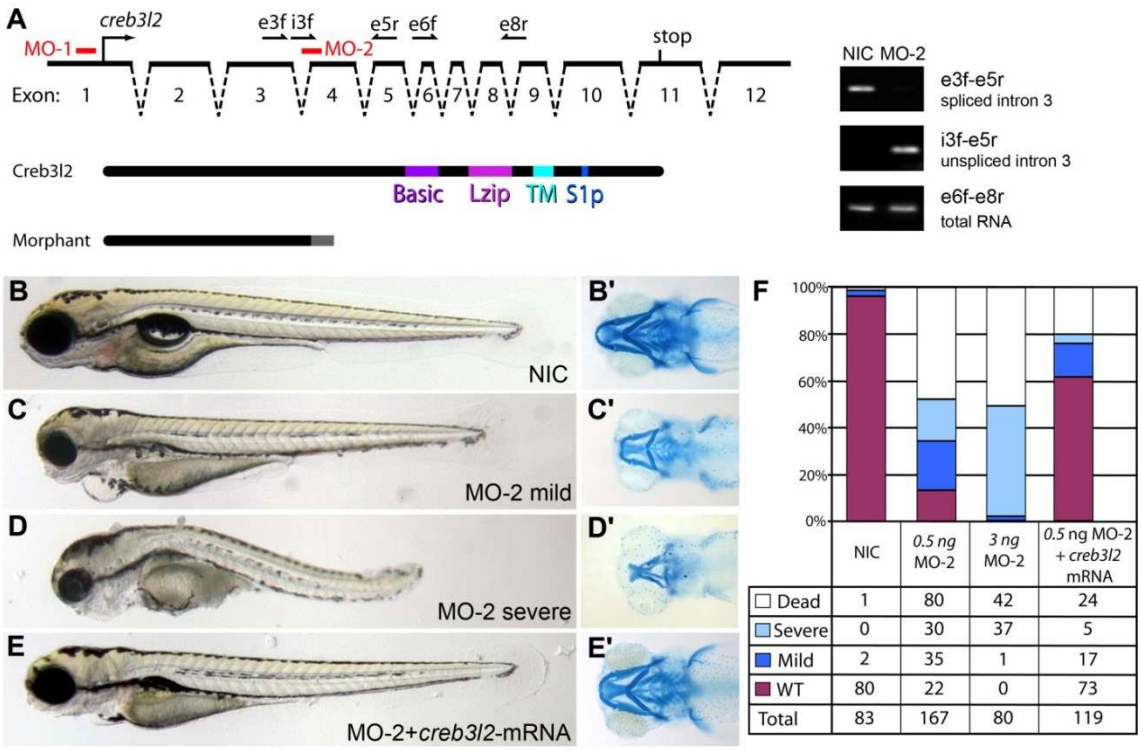

	NIC	0.5 ng MO-2	3 ng MO-2	0.5 ng MO-2 + creb3l2 mRNA
Dead	1	80	42	24
Severe	0	30	37	5
Mild	2	35	1	17
WT	80	22	0	73
Total	83	167	80	119

Figure 3.8: Decreased Creb3l2 function is responsible for the *feelgood* phenotype. (A) Schematic representation of the *creb3l2* gene structure and positions of the two morpholinos MO-1 and MO-2 used in knockdown experiments. The names, position and orientation of specific primers used to evaluate the effectiveness of MO-2 are shown on top of the genomic locus diagram. Exonic primers are indicated by an 'e', intronic primers are indicated by an 'i'. The predicted truncated form of the protein caused by MO-2 compared to the full-length wild-type protein is shown below. PCR amplification products representing spliced and un-spliced *creb3l2* mRNA as compared to total *creb3l2* mRNA in embryos injected with 3 ng MO-2 is shown on the left gel electrophoresis images. The primers used for amplification are shown on the right. (B-E′) Live (lateral, B-E) and Alcian blue stained (ventral, B′-E′) images of 80 hpf embryos injected with 0.5 ng MO-2 (C,D), or MO-2 plus *creb3l2*-mRNA (E). NIC, (non-injected control) is shown in B. (F) Quantification of knockdown and mRNA rescue experiments indicates the percentage of embryos in the four phenotypic classes observed.

straddles the exon 4 splice acceptor site of the *creb3l2* gene locus in order to disrupt transcript processing, was more effective. MO-2 is predicted to cause a frame shift generating a stop codon at amino acid 209 and leading to a truncated peptide lacking all functional domains (Figure 6A). Injection of MO-2 resulted in depletion of the spliced *creb3l2* transcript as evaluated by RT-PCR (Figure 3.8A). The observed MO-2 phenotype is similar to *feelgood*, although the morphant defects are more severe than those found in *feelgood* mutants (Figure 3.8B-D). Decreasing the amount of morpholino results in a milder phenotype more similar to *feelgood* (Figure 3.8C,C′, quantified in Figure 3.8F). To determine the specificity of the MO-2 phenotype, we co-injected morphants with mRNA of correctly spliced *creb3l2* and observed a suppression of the MO-2 phenotype in live larvae and Alcian blue skeletal preparations (Figure 3.8E). Because the depletion of zygotic *creb3l2* transcript results in more severe defects than the ones in *feelgood*, it is likely that the *feelgood* mutation represents a hypomorphic allele with partial loss of Creb3l2 function.

The *feelgood* mutation reduces the transcriptional activity of Creb3l2

The *feelgood* variant results in a change of a single amino acid residue (N301K) within the DNA binding domain of Creb3l2. To assess whether this change affects transcriptional activity, we cloned zebrafish cDNAs encoding wild-type Creb3l2, a processed Creb3l2 lacking its transmembrane domain, and the corresponding *feelgood* variants into expression vectors (Figure 3.9A). We also cloned the 895 bp fragment of the zebrafish *sec23a* promoter that is located immediately upstream from the translation start site in front of the *Luciferase* reporter gene. We chose this fragment because it

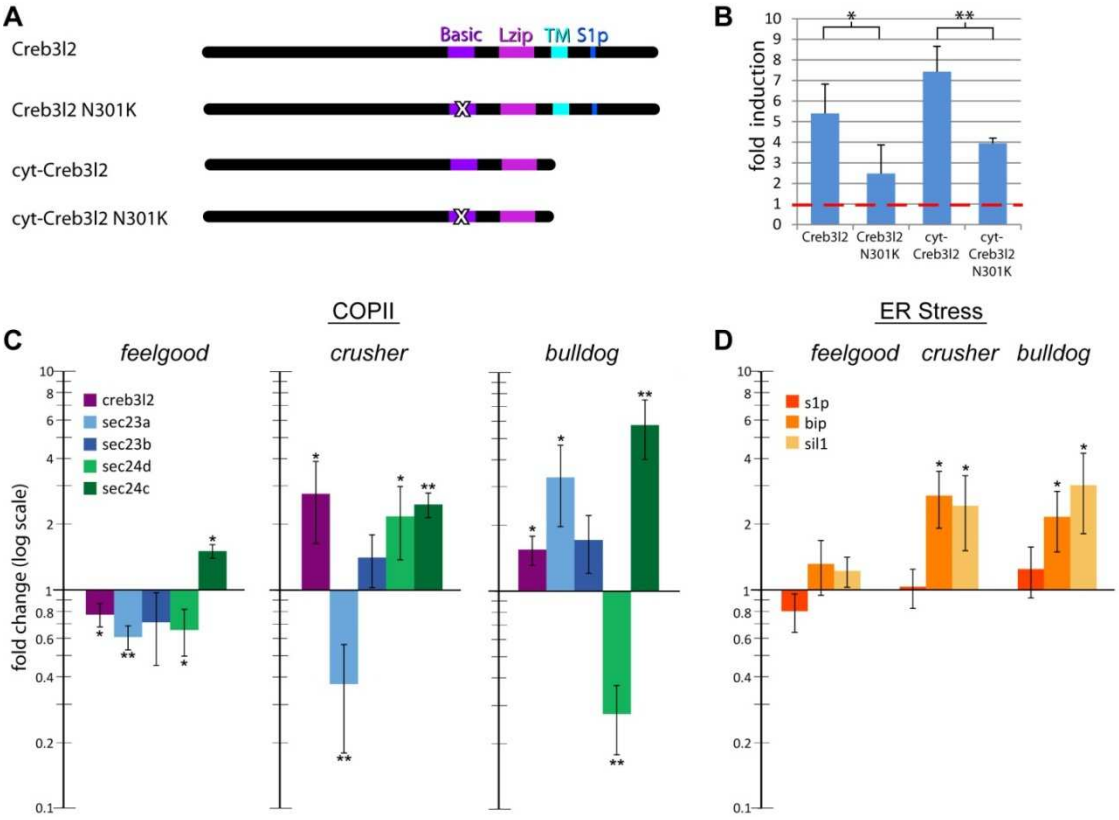

Figure 3.9: Expression of gene transcripts encoding COPII components is reduced in *feelgood*. (A) Schematic of zebrafish Creb3l2 expression constructs. "X" in Basic domain marks the *feelgood* N301K mutation. (B) Luciferase reporter assays. Human fibroblasts were transfected with the indicated expression constructs and the firefly luciferase reporter containing 0.8 kb of the zebrafish *sec23a* promoter. *Renilla* luciferase control plasmid was also used as transfection efficiency control. Luciferase activities were compared to cells transfected with empty vector to determine fold induction. Red line indicates baseline activity adjusted to *Renilla* luciferase values. (C-D) qPCR analysis of the fold expression change of COPII-related transcripts *creb3l2, sec23a*, *sec24d*, and *sec24c* in *feelgood*, *cru/sec23a* and *bul/sec24d* (C), and ER-stress-related transcripts *s1p, bip*, and *sil1* (D) in *feelgood, crusher/sec23a* and *bulldog/sec24d* mutants compared to wild types. RNA was extracted form whole embryos at 80 hpf. All results are normalized to beta-actin and then to wild-type. * indicates $p<0.05$, ** indicates $p<0.005$.

contains three putative CREB-binding elements: –5'-TGACGTGG-3' at position -3 to -10; 5'TCACGTTT-3' at -347 to -354 and 5'-AGACGTCT-3' at -888 to -895 bp from the transcriptional start site.

Transient transfection experiments in human fibroblasts showed that the wild-type Creb3l2 and the processed, cytosolic Creb3l2 activate the reporter gene by 5.5- and 7.5-fold, respectively (Figure 3.9B). In contrast, both the full length and cytosolic *feelgood* Creb3l2 variants were considerably less active, inducing the promoter by 2.5- and 4.0-fold, respectively. The transcriptional activity assays suggest that the N301K *feelgood* variant diminishes the transcriptional activity of Creb3l2 by approximately 50%. Thus, the molecular data are consistent with the genetic and MO-mediated mutational analyses described above (Figures 3.5 and 3.8), which show that *feelgood* is a hypomorphic allele. The fact that both the full length and the processed Creb3l2 mutants display a similar loss of activity compared to the corresponding wild-type proteins strongly suggests that the primary molecular defect in *feelgood* leads to loss of transcriptional activity, or nuclear transport rates, rather than incorrect processing by S1P or inefficient transport of Creb3l2 from ER to Golgi.

The *feelgood* mutation leads to decreased expression levels of select cargo adaptor proteins

Collectively, our results indicate that *feelgood/creb3l2* mutants have a similar, although milder, craniofacial phenotype to *crusher/sec23a* and *bulldog/sec24d* mutants (Lang et al., 2006; Sarmah et al., 2010). This raises the possibility that the *feelgood* deficit leads to lower expression levels of *sec23a* and *sec24d.* Sec23A was previously

shown to be a direct target of Creb3l2 (Saito et al., 2009b). We also found that Creb3l2 itself has a conserved *cre* site in its promoter, and therefore might be self-regulated.

In order to determine whether the putative Creb3l2 targets *creb3l2, sec23a* and *sec24d* are misregulated in *feelgood* mutants, we analyzed total RNA samples from 80 hpf embryos. We also included *sec24c* for comparison. Quantitative real-time PCR results show that the expression levels of *creb3l2, sec23a,* and *sec24d* are decreased in *feelgood* mutants relative to wild types (Figure 3.9C). In contrast, *sec24c* levels are upregulated in *feelgood* mutants as compared to wild-type embryos. This outcome could be either due to *sec24c* upregulation through Creb3l2-independent, compensatory mechanisms, or a Creb3l2-mediated, indirect suppression of *sec24c*.

To determine whether expression levels of Creb3l2 targets are altered by disruption of ER-to-Golgi protein trafficking independently of Creb3l2, we analyzed RNA samples from *crusher/sec23a* and *bulldog/sec24d* mutants. The results show that the expression levels of *creb3l2, sec23a,* and *sec24d* are increased in these mutants relative to wild-type embryos, except *sec23a* and *sec24d* in their respective mutants, possibly due to nonsense-mediated decay (Figure 3.9C), whereas *sec24c* is upregulated in all three mutants.

Together, these results demonstrate that Creb3l2 plays an important role in regulating multiple components of COPII carriers, as well as regulating its own expression. Interestingly, there is no evidence that the expression of *sec24c* is regulated by Creb3l2, consistent with the lack of craniofacial dysmorphology phenotype in *sec24c* morphants (Sarmah et al., 2010).

The *feelgood* mutation does not cause ER stress response

To test whether the unfolded protein response (UPR) is disrupted in *feelgood* mutants, we analyzed the expression of *bip* and *sil1* (Figure 3.9D), both of which are induced in *crusher/sec23a* and *bulldog/sec24d*. Neither was upregulated in a statistically significant manner in 80 hpf *feelgood* mutants compared to wild-type embryos, suggesting a lack of ER stress response. Finally, expression differences in the Creb3l2 processing enzyme S1P were negligible in the three mutants. The lack of UPR likely reflects the less severe nature of the *feelgood* phenotype, consistent with the hypothesis that the primary *feelgood* defect is in collagen trafficking.

Discussion

Here we show that the zebrafish *feelgood* mutation manifests skeletal phenotypes resembling those observed in *crusher/sec23a* and *bulldog/sec24d, i.e.,* accumulation of type II and type IV collagens within enlarged rough endoplasmic reticulum in chondrocytes and notochord sheath cells. At the molecular level, the *feelgood* mutation causes an amino acid substitution within the DNA binding domain of the transcription factor Creb3l2.

Developmental stage specificity

feelgood mutants present deficits in the late developmental stages of the craniofacial skeleton formation. The early stages of head skeleton development, including neural crest migration, mesenchymal condensation, and specification into type-II collagen secreting chondrocytes, proceed normally, indicating that these steps do not

depend on fully functional Creb3l2. However, in the later developmental steps, characterized by robust collagen secretion by chondrocytes, ECM fails to densify and mature, leading to skeletal elements that are specified, but structurally malformed. This phenotype of normal skeletal patterning and misshapen individual elements is similar to human birth defects including CLSD (Boyadjiev et al., 2006; Fromme et al., 2007), and as such, *feelgood* may provide a powerful tool for understanding the etiology of this class of congenital dysmorphologies. Moreover, the initial presence of collagen fibrils in the extracellular space, but lack of ECM maintenance seen in *feelgood* mutants is reminiscent of adult-onset diseases characterized by microarchitectural skeletal deterioration such as observed in osteoporosis or arthritis (Goldring and Goldring, 2007; Heinegård and Saxne, 2011).

Tissue specificity

Our results uncovered that Creb3l2 function is not confined to skeletal tissues, but is also required in other cell types. Specifically, *feelgood* mutant embryos display defects in the maturation of melanosome organelles that are similar to those previously described in the zebrafish and mouse mutation *silver* (Theos et al., 2006; Schonthaler et al., 2005). The *silver* locus encodes Pmel17, a type I membrane-inserted glycoprotein that is an integral part of the melanosomal matrix. Pmel17 is trafficked from the ER to endosomes and finally to melanosomes (Theos et al., 2005; Harper et al., 2008). In *feelgood*, as revealed by TEM, the trafficking of melanosome matrix proteins that are responsible for change in melanosome shape is de-coupled from pigment synthesis and secretion, indicating that Creb3l2-mediated regulation of cargo secretion extends to different cell

types.

The role of Creb3l2 in protein trafficking

Creb3l2 is a protein of 519 amino acids, coded by 12 exons spanning a genomic region of over 120 kbp. The overall genomic structure as well as the amino acid sequence of the DNA binding domain have been highly conserved from zebrafish to human (Storlazzi et al., 2003). Creb3l2 is part of a class I membrane bound basic leucine zipper proteins that must be cleaved by Site-1 protease (S1P) and Site-2 protease (S2P) in order to be activated (Figure 3.10) (Seidah et al., 1999; Kondo et al., 2007). Because Creb3l2 is synthesized in the ER, whereas the proteases that cleave it are localized in the Golgi, Creb3l2 proteolysis may be regulated by the availability of the COPII machinery as with the similarly cleaved Sterol Regulatory Element Binding Proteins (Espenshade et al., 2002). Thus, by virtue of being an ER resident protein, Creb3l2 is in an optimal location to optimize both the availability and composition of the ER-to-Golgi trafficking machinery by selective regulation of secretory pathway components.

Previously Creb3l2 was shown to directly bind the promoter of *Sec23a* in mouse (Saito et al, 2009). Our analysis using the zebrafish *sec23a* promoter and constructs encoding wild-type and mutant Creb3l2 show that the *feelgood* Creb3l2 has lost approximately 50% of its transcriptional activity. This result further corroborated the mild skeletal defects observed in *feelgood* mutants. Thus, we conclude that the *feelgood* mutation represents a hypomorphic allele that is much less severe than the zebrafish *creb3l2* morphants and knockout mouse, both resulting in very severe skeletal deficits.

The analysis of Creb3l2 KO mice has suggested that Creb3l2-mediated Sec23a

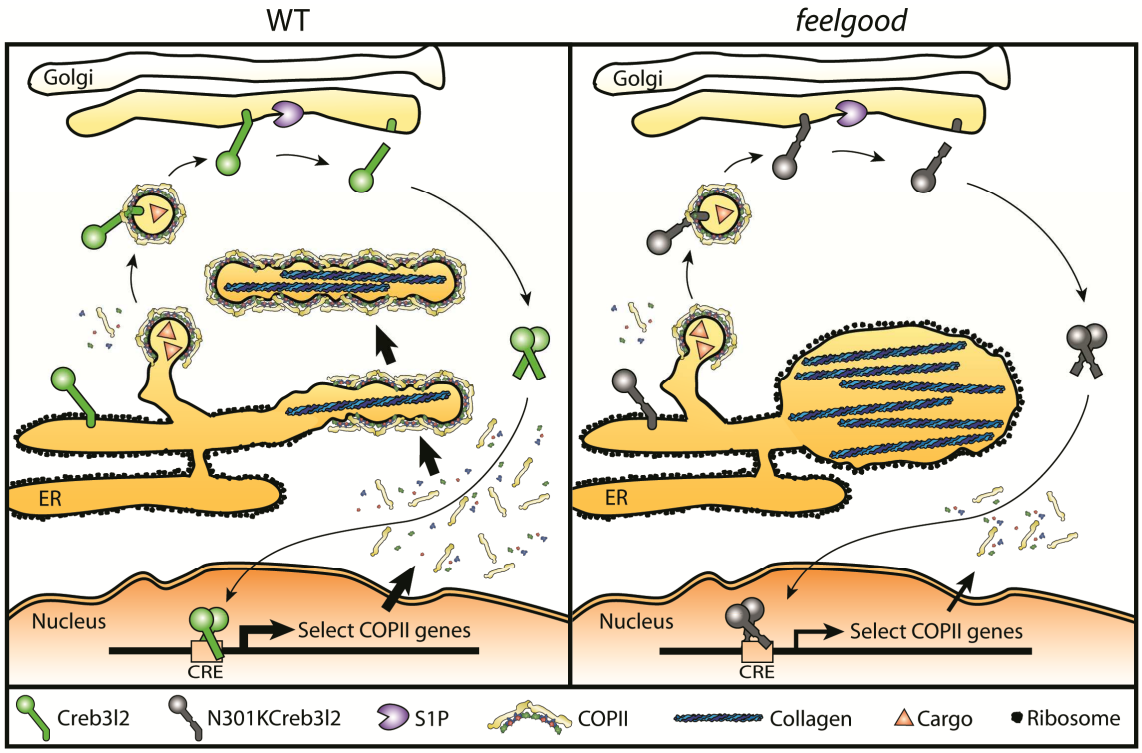

Figure 3.10: Model of Creb3l2 function and the phenotype of the *feelgood* mutation. When the secretory load of a cell increases beyond the capacity of the basal level of COPII protein expression, Creb3l2, which is normally localized in the ER, is cleaved by cis-Golgi resident Site-1 protease. After cleavage Creb3l2 dimerizes and enter the nucleus to bind cre sites in the promoters of select COPII genes, upregulating their expression and increasing the secretory capacity of cell (left panel). In *feelgood* mutants, the missense mutation in the DNA binding domain of Creb3l2 likely leaves the regulatory steps of cleavage and dimerization unaffected, but leads to inefficient binding of Creb3l2 to cre sites and diminished upregulation of expression of COPII components. The lack of adequate secretory machinery leads to distended ER filled with collagen, while trafficking of small cargos such as glycosaminoglycans and some large cargos such as laminin is unaffected (right panel). This may be due to insufficient levels of COPII components to build the more complex structures required for large cargos, or large cargos may be displaced by smaller ones when the secretory capacity is limited, or, because Creb3l2 differentially regulates COPII paralogs Sec24C and Sec24D, leading to deficient Sec24-dependent cargo sorting caused by an improper balance of Sec24 paralogs.

pathway regulates the ER stress response machinery during chondrogenesis (Saito et al., 2009b). We detected similar increases in the ER stress response in *crusher/sec23a* and *bulldog/sec24d* mutants, but not in *feelgood*. It has been difficult to discern which aspects of the phenotype are due to over-activation of the ER stress response and which are due to the inability of cells to secrete proteins to build normal ECM. However, the hypomorphic nature of the *feelgood* allele allowed us to parse the ER stress response phenotype from the requirement of Creb3l2 for COPII-dependent ER-to-Golgi transport. We postulate that the primary function of Creb3l2 is not direct regulation of the ER stress response. This conclusion is consistent with our preliminary results using additional ER stress response markers as CHOP and Xbp1 (Tabas and Ron, 2011, data not shown). These experiments did not reveal significant upregulation of ER stress response in *feelgood* or in much more severe *creb3l2*-morphants.

Paralog Specificity of Creb3l2

We have shown that Creb3l2 does not only regulate *sec23a* expression, but also other COPII components, namely *sec23b* and *sec24d.* While we observed diminished expression of *sec24d* in *feelgood,* we did not find any evidence that Creb3l2 regulates the expression of its closest paralog *sec24c*. Therefore, it is likely that the *feelgood* mutation mostly affects the Creb3l2/Sec24D secretory axis without influencing Sec24C-dependent cargos. The loss-of-function phenotypes of *creb3l2*, *sec24d* and *sec24c* mutants/morphants support this model (Melville and Knapik, 2011; Sarmah et al., 2010). For example, the four *bulldog/sec24d* zebrafish alleles, which abolish Sec24D function, share many features with *feelgood*, i.e., they display intracellular backlogs of collagen

molecules and sparse extracellular matrix, but relatively normal trafficking of other ECM molecules such as fibronectin (Sarmah et al., 2010). In contrast, chondrocyte maturation and skeletal development proceed normally in *sec24c* morphants.

The differential transcriptional regulation of COPII components could also explain the tissue specific deficits observed in some human syndromes. For example, mutation in SEC23B result in the human disease CDAII, which manifests in anemia but not skeletal defects, while mutations in SEC23A result in the human disease CLSD, which is characterized by skeletal defects but not anemia (Boyadjiev et al., 2006; Bianchi et al., 2009). The differences in phenotypes might be due to divergent transcriptional regulation, resulting in differential availability of various COPII components in different cell types. This hypothesis is supported by the finding that SEC23B is expressed at 5 fold higher levels than SEC23A in human erythroblasts (Schwarz et al., 2009). Because both Sec23 paralogs are *Creb3l2* targets, it is likely that additional unknown regulators modulate availability of Sec23A, Sec23B, Sec24C and other COPII associated proteins. Future discovery research in this area is likely to help crack the secretory code.

Cargo specificity of Creb3l2

The high ECM secretory load has been postulated as cause of the craniofacial dysmorphology in the COPII mutants (Fromme et al., 2007; Lang et al., 2006). Our results suggest that Creb3l2 is also required for the secretion of certain protein classes independently of secretory volume. For example, Collagen II and IV secretion to the extracellular space is affected in both chondrocytes and notochord sheath cells, yet the latter produce far fewer collagen fibrils than the former. Moreover, although fibrillar

collagens accumulate in intracellular compartments, other abundantly deposited extracellular matrix proteins such as laminins, as well as vacuolar GAG proteins are well trafficked to the extracellular space.

There are several explanations of how this phenotype might occur. It is plausible that large fibrillar molecules such as collagen compete less efficiently with other protein classes that are synthesized in the ER and destined for transport to Golgi and subsequent destinations. This may occur because, while cargo-free self-assembled COPII vesicles are 40-80 nm in diameter (Barlowe et al., 1994; Miller and Barlowe, 2010; Dancourt and Barlowe, 2010), fibrillar procollagen bundles form rigid 300 nm rods (Fraser et al., 1979; Canty and Kadler, 2005; Stephens and Pepperkok, 2002). Hence, collagen transport requires specialized, oversized COPII structures and ample supply of coat proteins (Stagg et al., 2008; O'Donnell et al., 2011). As a result, in cells with high levels of protein trafficking, the availability of COPII carriers may become a limiting factor, and other proteins may displace collagen molecules. Or, there may be insufficient levels of COPII components to build the more complex tubular structures required for large cargos, leading to intracellular backlogs of collagen within distended ER compartments (Figure 3.10, right).

Craniofacial and skeletal dysmorphologies account for the majority of birth defects and most of them are of unknown origin. The fact that random mutagenesis screens in zebrafish have yielded multiple mutants that disrupt the transport machinery suggests that at least some of the birth defects of unknown nature are due to abnormal protein transport (Neuhauss et al., 1996). Besides developmental defects, a host of adult-onset human diseases, including arthritis or interstitial fibrosis after organ injury, have

been linked to dysregulated collagen production (Goldring and Marcu, 2009; Goldring and Goldring, 2007; Heinegård and Saxne, 2011; Trojanowska et al., 1998). The decoupling of collagen transport from that of other cargos as well as the hypomorphic nature of the *feelgood* allele has important implications in the understanding of human diseases linked to collagen defects. Because the genetic basis for these diseases is often highly complex, tools such as *feelgood* are important for identifying potential candidate genes and regulatory networks. Better understanding the roles of the regulatory and structural components of the intracellular transport machinery could lead to better diagnostic tools and novel treatments of human diseases.

CHAPTER IV

PARALOG SPECIFIC FUNCTIONS OF Sec23a AND Sec23b

Introduction

Trafficking of secretory proteins from the endoplasmic reticulum (ER) to the Golgi is primarily conducted by Coat Protein II complex (COPII) vesicular carriers, which were originally discovered in yeast (Barlowe et al., 1994). The yeast COPII complex is anchored to the ER membrane by the Sar1 GTPase and consists of an inner coat of Sec23p–Sec24p heterodimers and an outer coat of Sec13p–Sec31p proteins. Vertebrate genomes carry two Sec23p paralogs, Sec23A and Sec23B, and four Sec24p paralogs: Sec24A, Sec24B, Sec24C and Sec24D. Sec23A and Sec23B act as GTPase-activating proteins for Sar1, whereas Sec24 paralogs play a role in protein cargo selection (Wendeler et al., 2007; Mancias and Goldberg, 2008).

Recently, the genetics of COPII components have attracted increasing attention because mutations in their corresponding genes have been implicated in a wide variety of human disorders (Boyadjiev et al., 2006; Schwarz et al., 2009; Aridor and Hannan, 2002) and animal models show diverse, paralog specific defects (Lang et al., 2006; Sarmah et al., 2010; Merte et al., 2010; Ohisa et al., 2010). For example, loss of Sec24D activity results in craniofacial defects, while Sec24C morphants undergo normal development of head skeletal structures (Sarmah et al., 2010). Loss of *bulldog/sec24d* does not prevent neural crest migration, formation of pharyngeal condensations, and proliferation of chondrocytes, but hinders normal maturation of highly secretory chondrocytes.

Strikingly, the combined loss of Sec24C and Sec24D results in neural crest migration and condensation deficits, indicating that Sec24D activity is essential for chondrocyte maturation, but Sec24C or Sec24D compensate for each other in early stages of cartilage development.

A possible explanation for these stage specific requirements for Sec24 paralogs in the development of neural crest derived chondrocytes is that each step requires unique cargos. Immunostaining in *bulldog* mutants show that Sec24D is required for type-II collagen secretion, which is essential for chondrocyte maturation, but does not appear to be required for fibronectin or integrin trafficking, which are the cargos required for neural crest migration and condensation. It is therefore likely that either Sec24C or Sec24D is sufficient for secretion of these cargos. The earliest steps of neural crest induction and specification, which rely on small secreted morphogens (Wang et al., 2011), do not appear disrupted even with loss of both Sec24C and Sec24D.

The Sec24 paralogs are known for cargo sorting functions, and these could explain cargo-specific loss-of-function phenotypes, however, the two Sec23 paralogs have not been recognized for cargo sorting abilities. Sec23 paralogs are highly similar at the sequence level, sharing 82% identity; however, Sec23A and Sec23B loss-of-function result in disparate phenotypes.

Mutations in SEC23B lead to Congenital Dyserythropoietic Anemia type II (CDAII), a disease characterized by ineffective erythropoiesis, bi- and multinucleated erythroblasts, and hypoglycosylation of red blood cell membrane proteins (Bianchi et al., 2009; Schwarz et al., 2009). In contrast, a point mutation in SEC23A leads to Cranio-lenticulo-sutural dysplasia (CLSD), the distinctive marks of which include craniofacial

skeleton malformations and short stature (Boyadjiev et al., 2006). Zebrafish *crusher/sec23a* mutant and *sec23b* morphant embryos present phenotypes similar to the corresponding human diseases, establishing zebrafish as a model system to study the molecular and cellular bases of COPII-deficiencies (Lang et al., 2006; Schwarz et al., 2009).

One potential explanation for distinct phenotypes between *sec23a* and *sec23b* is differential expression, and indeed the transcription factor Creb3l2 regulates *sec23a* more strongly than *sec23b* (Melville et al., 2011). While both paralogs are ubiquitously expressed, *sec23a* is enriched in the developing head skeleton (Lang et al., 2006) while SEC23B expression is higher in erythroblasts (Bianchi et al., 2009). Alternately, the structural differences between the two Sec23 paralogs could explain the functional differences. Specifically, the highly divergent 18 amino acid flexible loop that resides near the Sec24 binding site is a plausible candidate (Figure 4.1).

Here we test the structure-function hypothesis and demonstrate that the 18 amino acid divergent loop contributes significantly to Sec23a and Sec23b specific functions. We show that *sec23b* is likely the ancestral gene and is essential for fibronectin secretion, while *sec23a*, the evolutionarily more recent paralog, is required for normal collagen secretion. Replacement of the divergent loop from Sec23b with the loop from Sec23a results in an enhanced ability of the overexpression construct to carry on collagen secretion, while replacement of the Sec23a loop with that of Sec23b leads to a decrease in collagen secretion. These results suggest that Sec23 may indirectly regulate cargo sorting via differential interaction with distinct Sec24 paralogs. This may provide a potential

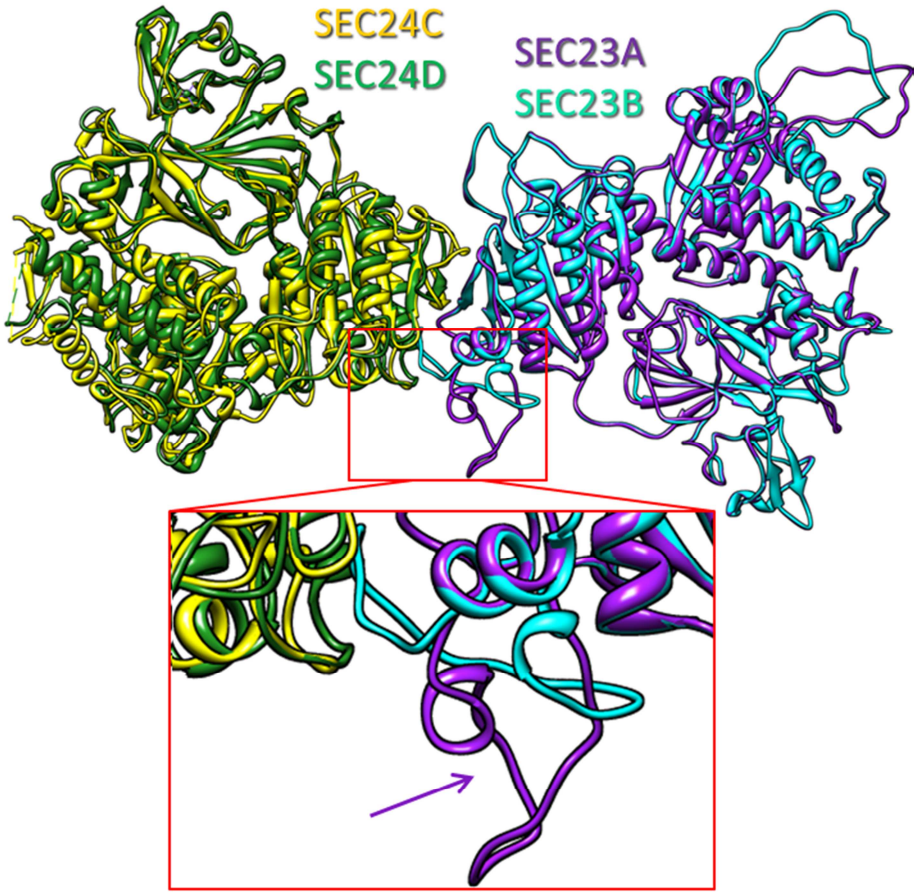

Figure 4,1: SEC23A and SEC23B have a divergent loop near the SEC24 binding site. Structure of human SEC24C, SEC24D, SEC23A, and SEC23B in heterodimer complex. Divergent 18 amino acid loop highlighted with inset and arrow.

explanation for the structure-function differences seen in Sec23 paralogs loss-of-function phenotypes and create a starting point for understanding the mechanisms underlying the secretory code of vertebrates intracellular protein traffic.

Materials and methods

Immunofluorescence and Wheat Germ Agglutinin staining. Method as in Chapter III with the addition of fibronectin antibody (1:200 dilution, Sigma).

Generation of Tol2kit based transgenic fish. The *bactin2:sec23a:polyA* and *bactin2:sec23b:polyA* with *cmlc2:egfp* transgenesis marker constructs was created using the "Tol2 kit" approach, as in Chapter III. Constructs containing swapped 18 amino acid divergent loops were created by PCR amplification with mutagenizing primers sec23btoaF 5'GCCGCTCAAGCGGGACGCGGACCACAGCAGCCTCAGGTTCCTCC CTCCAACAGATTTCTCCAGCCTGTGC3' and sec23atobF 5'ACATCCGGCCAACAA GGAAAACCACTGGCGCCTCATGATGCTGCAGCATCCTGCAGGTTTCTCCAGC CGGTGC3' followed by dpnI digestion of parental plasmid and ligation.

Phylogenetic analysis. Method as in Chapter III.

Morpholino knockdown. Antisense morpholino oligonucleotides (MOs) (Gene Tools) targeting *sec23a* and *sec23b* from (Lang et al., 2006), method as in Chapter III. Antisense morpholino (MO) oligonucleotides (Gene Tools) were targeted to the sec23a 5'

untranslated region (sec23a-MO5'UTR 5'CTGAATCCTTGATTTTGTGTCTCCT3', 1.1 ng injected); the sec23a 5' translation start site (sec23a-MOAUG 5'AACTCCTGGAAGGTCGCCATCGCAC3', 1.8 ng injected) and the sec23b translation start site (sec23b-MO 5'CCATGACAGCGCGAACAACTTTTTA3', 3.5 ng injected).

Statistical Analysis. Data in bars represent average ± s.d. Statistical analyses on continuous data were performed using unpaired two-tailed Student's t-test, analysis on categorical data were performed using two-tailed Fisher's exact test.

Results

Vertebrate Sec23b is more related to the ancestral Sec23 gene than Sec23a

In order to determine the evolutionary relationship between Sec23a and Sec23b and discover which paralog is closest to the ancestral gene, we compared their sequence by phylogenetic analysis. We assumed that the single yeast Sec23 paralog likely represents the ancestral gene. ClustalW analysis of vertebrate sequences comparing Sec23a and Sec23b indicates that Sec23b is most closely related to the yeast gene and therefore likely to the ancestral paralog (Figure 4.2A).

To test whether sequence conservation translates to conserved function, we performed gene replacement experiments in yeast. While both zebrafish Sec23a and Sec23b partially complement the growth defect of a yeast *ts sec23-1* temperature sensitive mutant (TGY526-7C), Sec23b is more effective (Figure 4.2B). These findings were also true for the SEC23 human paralogs used in the *ts sec23-1* rescue experiments.

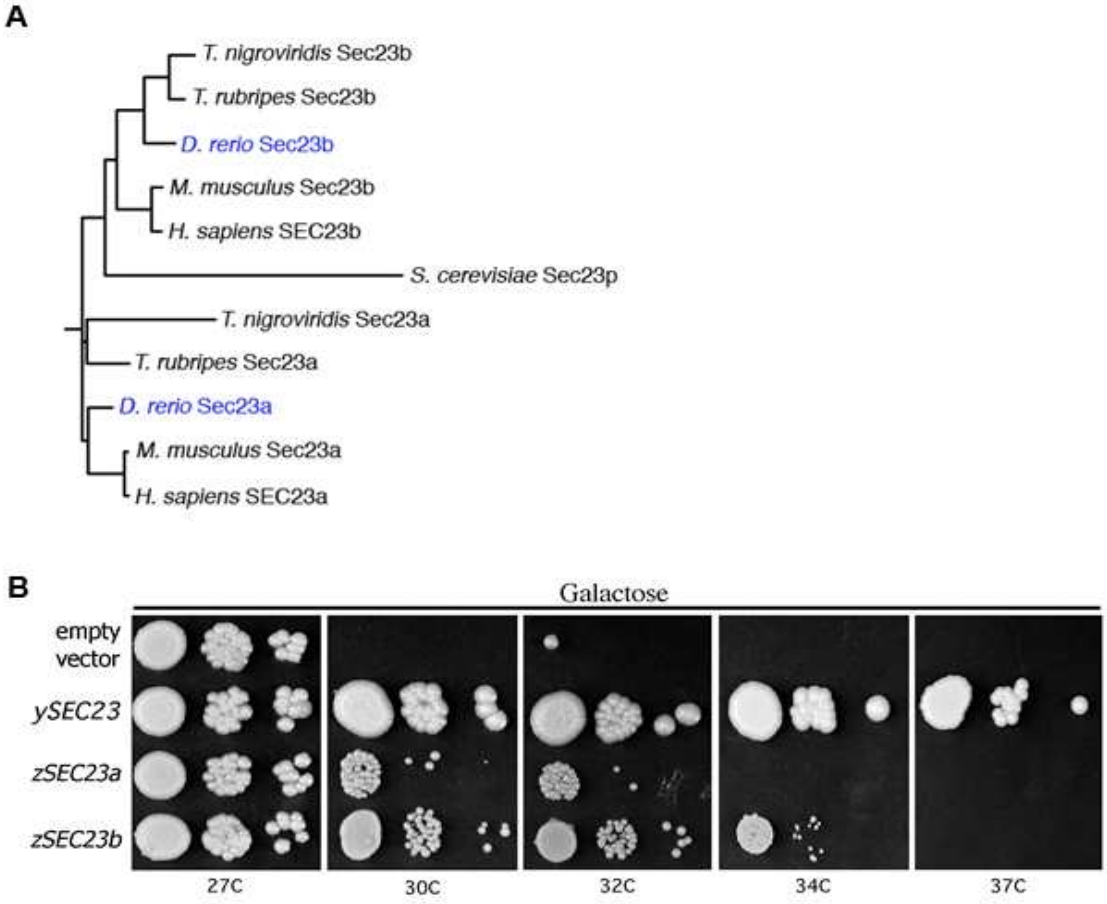

Figure 4.2: Evolutionary relationship of Sec23 paralogs. (A) Phylogram of known zebrafish (*Danio rerio*), human (*Homo sapiens*), mouse (*Mus musculus*), Tetraodon (*Tetraodon nigroviridis*), and Fugu (*Takifugu rubripes*) Sec23 paralogs. (B) Gene replacement experiments in yeast *ts sec23-1* (TGY526-7C).

Collectively, these data show that Sec23 paralogs are highly conserved in sequence and function throughout phylogeny, with Sec23b being more closely related to the ancestral Sec23 gene. The zebrafish loss-of-function phenotypes and yeast replacement experiments reveal potential functional differences between the two Sec23 paralogs. To further explore the mechanisms underlying the Sec23 paralog-specific functions during development, we used zebrafish embryology approaches.

Sec23b, but not Sec23a is essential for neural crest migration

To test the requirement of the two Sec23paralogs in neural crest cell migration, we injected *sec23a and/or sec23b* antisense morpholinos into transgenic zebrafish line *Tg(sox10(7.2):mrfp)* and inspected facial primordia formation in live embryos at 30 hpf and 48 hpf. While the migratory neural crest of *sec23a* morphants developed normally and were indistinguishable from uninjected controls, *sec23b* morphants showed delayed migration and abnormal patterning of mesenchymal condensations (Figure 4.3). These results indicate that Sec23b is required for normal migration and condensation of neural crest cells while Sec23a is dispensable. These data are consistent with our previously published Sec23b craniofacial dysmorphology phenotype that showed absent cartilage elements of the ventral pharyngeal skeleton.

ECM components of the notochord sheath have differential requirement for Sec23a and Sec23b

We hypothesized that the developmental stage-specific differences in the requirement for Sec23 paralogs may be due to paralog-specific requirements for transport of different cargos. Both *crusher/sec23a* and *bulldog/sec24d* mutants have defects in

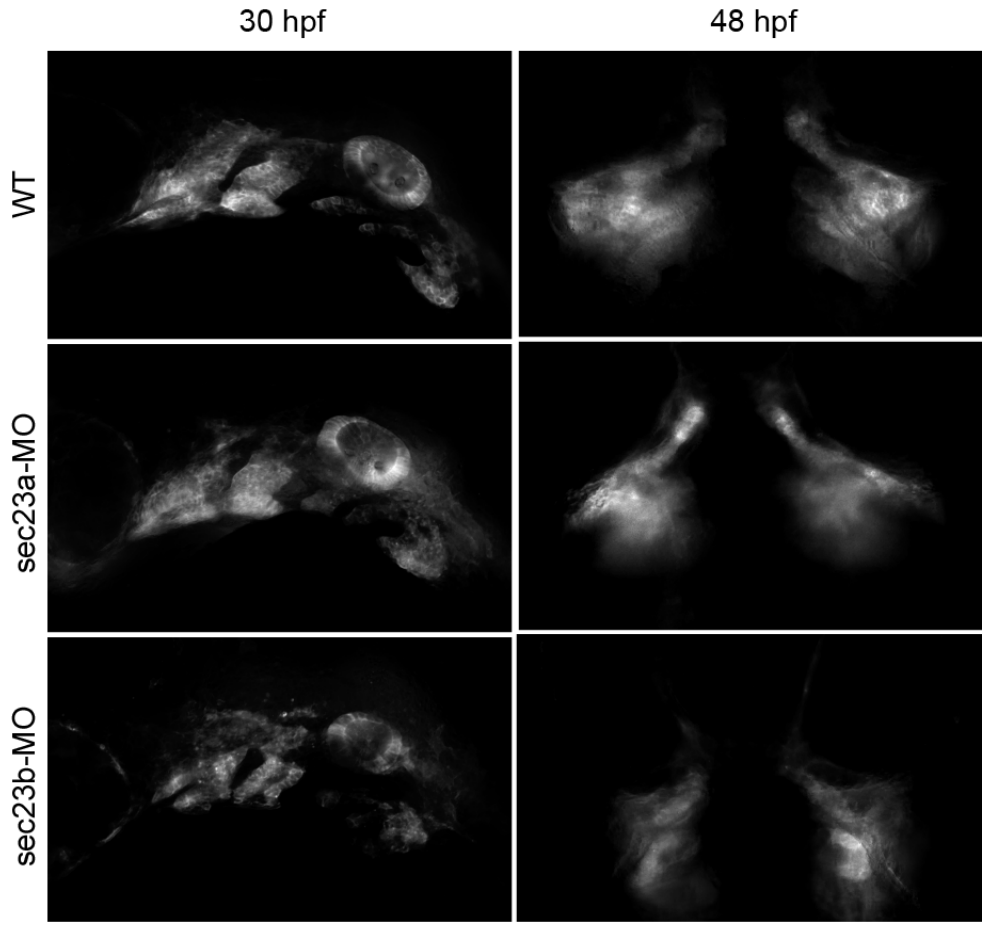

Figure 4.3: Migration of craniofacial primordia in *sec23a* and *sec23b* morphants. Images of transgenic *sox10:mRFP* embryos at 30 hpf (lateral view, anterior to the left) and 48 hpf (ventral view , anterior to the top) after injection with specified morpholino.

collagen secretion. Collagen poses a special problem for the secretory machinery because while cargo-free self-assembled COPII vesicles are 40-80 nm in diameter (Barlowe et al., 1994; Miller and Barlowe, 2010; Dancourt and Barlowe, 2010), fibrillar procollagen bundles form rigid 300 nm rods (Fraser et al., 1979; Canty and Kadler, 2005; Stephens and Pepperkok, 2002). As such, collagen may require auxiliary COPII machinery components to facilitate ER export.

In order to understand whether loss of Sec23b causes collagen trafficking defects similar to loss of Sec23a, we performed immunostaining for type-II collagen of the notochord of *crusher* mutants and *sec23b* morphants. The notochord functions as a hydrostatic skeleton, the mechanical properties of which depend on an external fibrous sheath, which consists primarily of a collagen and laminin matrix (Scott and Stemple, 2005; Adams et al., 1990). We found that in contrast to *crusher/sec23a* mutants, which have large accumulations of collagen II in the notochord sheath, *sec23b* morphant notochords do not accumulate collagen (Figure 4.4A). WGA-labeled proteins such as glycosaminoglycans do not appear disrupted with the loss of either paralog. These data indicate that different Sec23 paralogs have evolved to differentially traffic large cargos, including collagen II.

Because neural crest condensations do not form in *sec23b* morphants and the movement of neural crest cells is dependent on fibronectin and laminin components in the extracellular matrix (Alfandari et al., 2003; Strachan and Condic, 2008; Testaz et al., 1999; Desban and Duband, 1997), we hypothesized that either fibronectin or laminin trafficking may be disrupted in *sec23b*-depleted embryos. To test this hypothesis, we performed immunostaining of the notochords of *crusher* mutants and *sec23b* morphants.

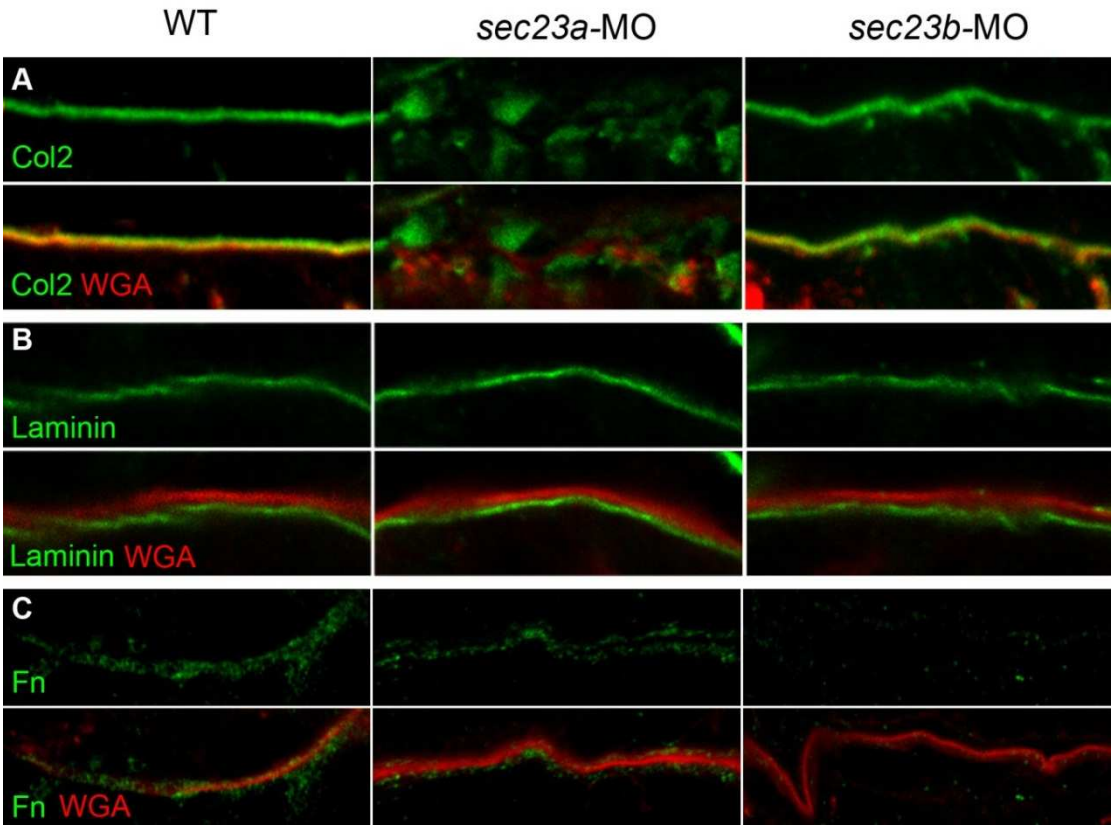

Figure 4.4: Trafficking of collagen, laminin, and fibronectin in the notochord of *sec23a* and *sec23b* morphants. Immunofluorescence of type-II collagen (Col2) (A), laminin (B), and fibronectin (Fn) (C) and wheat germ agglutinin (WGA).

We found that while laminin localization in the notochord sheath is indistinguishable from wild-type embryos (Figure 4.4B), fibronectin secretion is disrupted in *sec23b* morphants but not in *crusher* mutants. Combined, these data indicate that both Sec23a and Sec23b are required to transport distinct cargos, Sec23a for collagen and Sec23b for fibronectin.

A divergent loop of 18 amino acids is important for the distinct functions of Sec23a and Sec23b in the developing fin

We hypothesized that the divergent loop of 18 amino acids near the *sec24* binding site could be responsible for the functional differences between *sec23* paralogs. To test this hypothesis, we utilized a gene replacement strategy. We designed a Tol2-based rescue construct (Kwan et al., 2007) containing either wild-type *sec23a*, wild-type *sec23b*, *sec23a* with the divergent loop from *sec23b* (hereafter referred to as *sec23a>b*) or *sec23b* with the divergent loop from *sec23a* (hereafter referred to as *sec23b>a*). These constructs were cloned into a vector that contained an ubiquitous *beta-actin* promoter and a *cmlc2:egfp* transgenesis marker and injected into *crusher* mutants at the one-cell stage to create chimeric transgenic zebrafish overexpressing individual constructs.

crusher mutants have three easily scorable phenotypes: the head is shortened along the anterior posterior axis, the body length is shortened, and the pectoral fins are kinked. To evaluate the effectiveness of the four *sec23* constructs at rescuing the *crusher* phenotype, we examined fin morphology, which has an easily quantifiable binary readout- kinked/mutant or curved/wild type (Figure 4.5A).

While *crusher* mutants have a negligible number of normally curved fins (<2%), *crusher* mutants injected with wild-type *sec23a* had >40% curved fins (Figure 4.5A). In

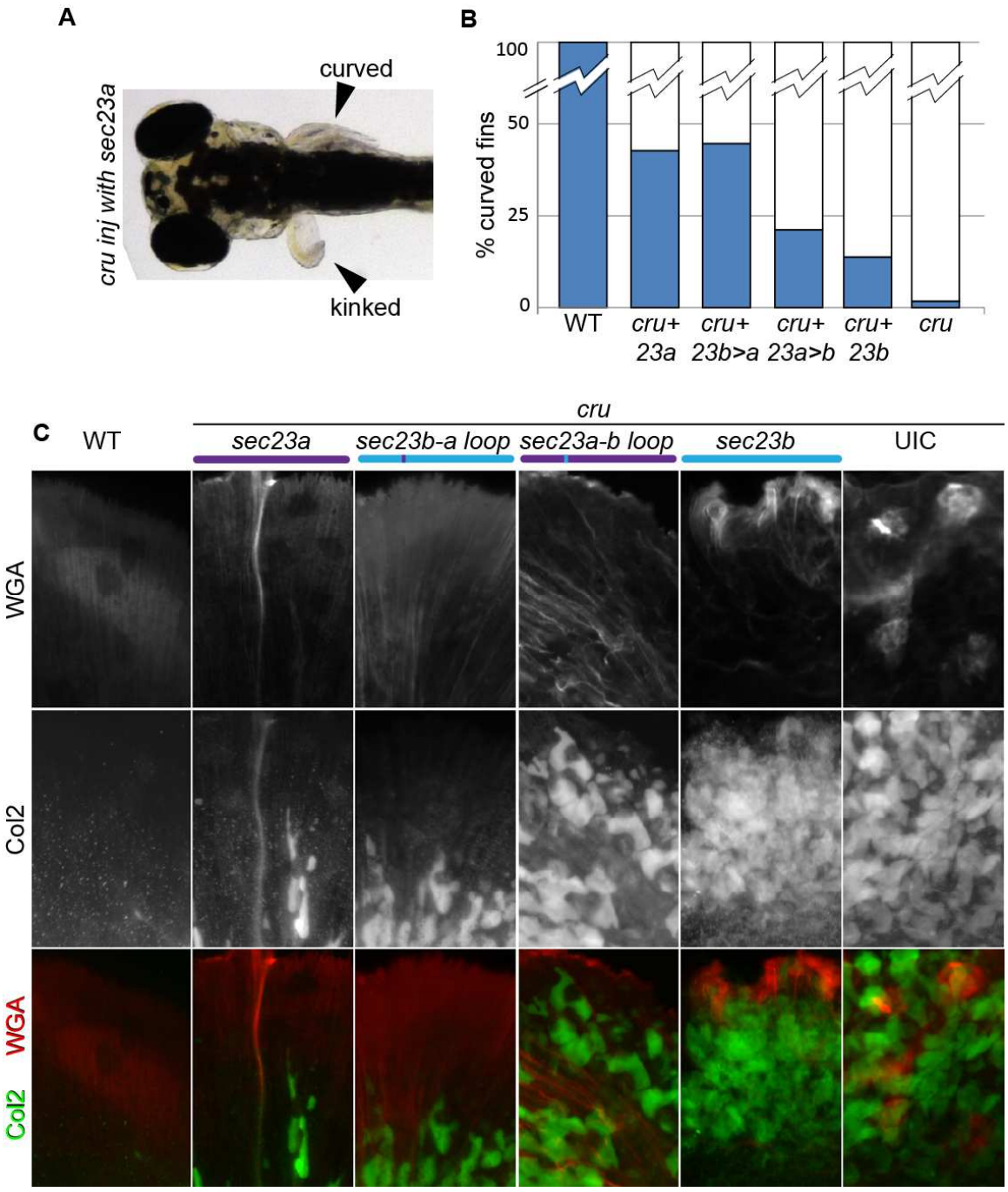
A
curved
cru inj with sec23a
kinked
B
100
50
25
0
% curved fins
WT
cru+ 23a
cru+ 23b>a
cru+ 23a>b
cru+ 23b
cru
C
WT
cru
sec23a
sec23b-a loop
sec23a-b loop
sec23b
UIC
WGA
Col2
WGA
Col2

Figure 4.5: The 18-amino acid divergent loop of Sec23a has a significant role in the ability of Sec23a to rescue fin morphology and collagen trafficking (A) Live image (dorsal view) of 6 dpf *crusher* mutant injected with *sec23a* demonstrating chimeric rescue of fin morphology, one normally curved fin and one kinked fin (B) Quantification of normally curved fins in 6 dpf embryos injected with indicated constructs. (C) Immunostaining of WGA and Col2 in the actinotrichia of the pectoral fin of 6 dpf embryos injected with the indicated constructs.

contrast, wild-type *sec23b* was much less effective at rescuing fin morphology (less than <15% normally curved fins). This is consistent with our previous data in yeast that show incomplete overlap in functions between the two paralogs. Strikingly, *crusher* mutants injected with *sec23b>a* had >40% normally curved fins, indicating that the substitution of the 18 amino acid loop was sufficient to increase the ability of *sec23b* to rescue comparably to that of *sec23a*. However, injection with *sec23a>b* led to just over 20% of fins with normal morphology, significantly lower than wild-type *sec23a*.

The kink of *crusher* fins occurs at the actinotrichia, which are collagen-based, non-calcified spicules found in brush-fashioned groups at the distal end of the fin (Durán et al., 2011; Wood and Thorogood, 1984). To understand molecular basis of the fin phenotype, we performed immunostaining for type-II collagen and WGA-binding proteins. We found that *crusher* mutants have large conglomerations of collagen at the distal end of the fin, and that the deposition of WGA-labeled proteins to the actinotrichia is disrupted (Figure 4.5B). Injection with wild-type *sec23a* or *sec23b>a* partially rescued collagen spicule formation and restores the deposition of WGA-labeled proteins comparable to wild-type fins. In contrast to this, *sec23b* or *sec23a>b* injection rescues collagen spicule formation much less effectively. These data suggest that the Sec23 divergent loop is critical for collagen transport in the developing fin.

The extracellular matrix composition of the actinotrichia is predominantly collagen. To determine whether the functional differences between *sec23a* and *sec23b* were consistent in more complex matrixes, we evaluated the ability of the four *sec23* constructs to rescue short body length of *crusher* mutants.

Zebrafish body length is largely dependent on notochord stiffness, which depends

on both an external fibrous sheath and internal vacuoles within notochord sheath cells (Scott and Stemple, 2005). These biomechanical components rely on matrix composed of diverse proteins including collagens, fibronectin, laminin, and secreted glycosaminoglycans. We measured the trunk and tail from the posterior edge of the ear capsule to the distal tip of the caudal fin in wild-type, *crusher*, and *crusher* injected with each of the four *sec23* constructs embryos (Figure 4.6). We found that injection with all four constructs, *sec23a, sec23b, sec23a>b,* or *sec23b>a,* were sufficient for partial rescue of trunk length, and we found no statistically significant difference in the magnitude of the rescue between *sec23a* and *sec23b*. Combined with the immunofluorescence experiments, these data suggest that both paralogs are required for trafficking of the essential components of the notochord basement membrane.

Discussion

Here we show that the COPII components *sec23a* and *sec23b,* despite being highly conserved paralogs, functional differently. We show that *sec23b* is most closely related to the ancestral gene in yeast; *sec23a* is required for collagen secretion in the notochord and fin, while *sec23b* is required for fibronectin deposition in the notochord and a divergent loop of 18 amino acids plays a critical role in specifying the paralog-specific functions of *sec23a* and *sec23b.* This provides a basis for understanding the divergent human diseases caused by loss of function of SEC23 paralogs as well as providing clues to deciphering the secretory code and the dynamic relationship between COPII and the cargos it transports.

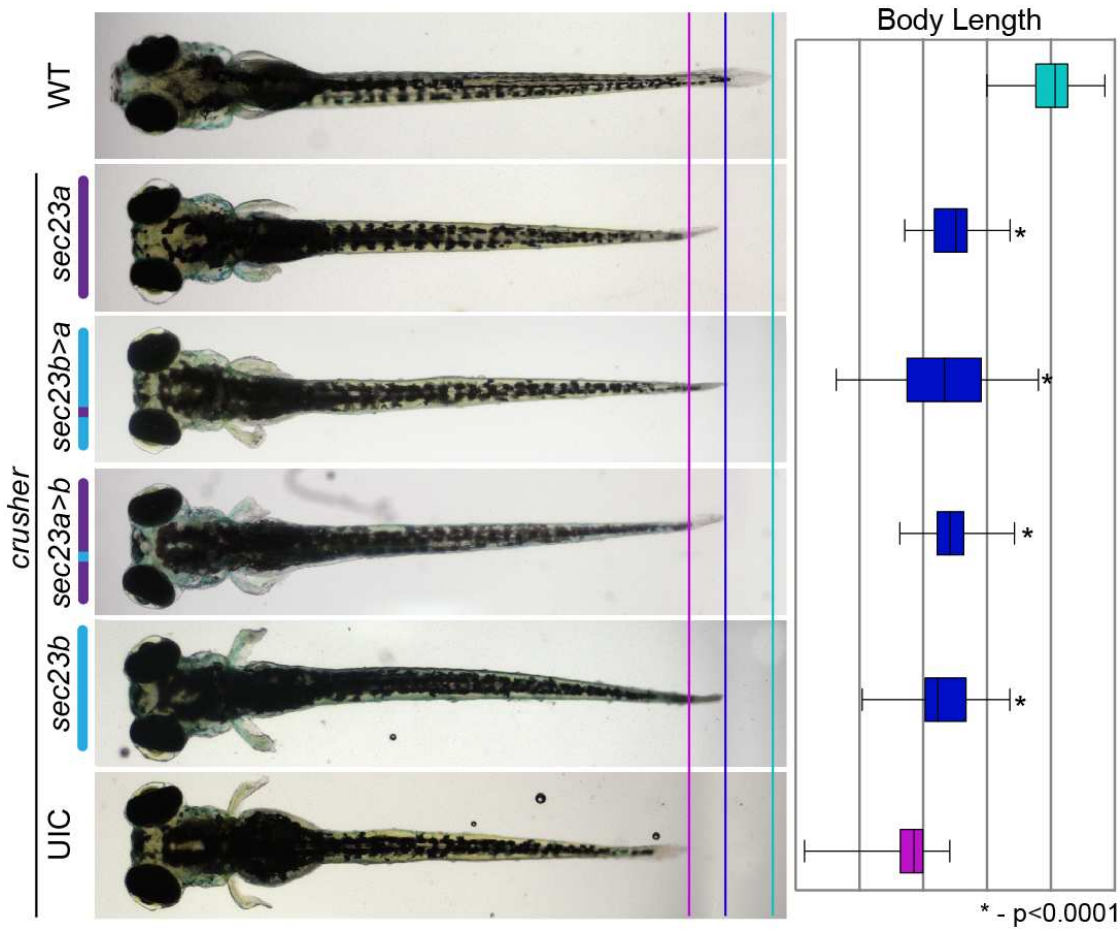

Figure 4.6: Either Sec23a or Sec23b is sufficient to rescue body length defects in crusher mutants. (Left) Live images (dorsal view) of WT and *crusher* embryos injected with indicated constructs. Pink vertical line indicates *crusher* body length, purple line indicates body length of injected embryos, light blue line indicates WT body length. (Right) Quantification of body length of injected embryos relative to *crusher* and WT. (n>20 for each condition).

Evolutionary History

Phylogenetic analysis and gene replacement experiments in yeast indicate that *sec23b* is most closely related to the ancestral gene. In theory, if *sec23b* performs the traditional functions of the ancestral gene, then *sec23a* can evolve new specialized functions. One such potential specialized function is collagen secretion, which does not occur in unicellular organisms such as yeast. It has recently been shown that the ubiquitylation of outer coat component SEC31A is essential for collagen secretion (Jin et al., 2012) and accessory proteins such as TANGO1 may be required for loading of collagen into vesicles (Saito et al., 2009b; Wilson et al., 2011; Saito et al., 2011). Thus, there appear to have been other evolutionary adaptations to facilitate collagen secretion. Considering that *sec23a* is required for collagen secretion and that the overall phenotype of *crusher/sec23a* mutants is mostly restricted to collagen secreting tissues, *sec23a* may have evolved specialized functions in relation to collagen secretion, possibly due to interactions with novel adapter proteins or other COPII components.

Developmental stage and tissue specific functions

Our analysis of migratory neural crest cells in *Tg(sox10(7.2):mrfp* fish indicates that *sec23a* and *sec23b* have developmental stage specific functions. Moreover, *sec23b* overexpression is able to rescue the body length of *crusher* mutants but not fin morphology. What is the mechanism of these stage- and tissue-specific functions? One possible explanation is cargo centric. The defects in *sec23b* morphants could be explained as defects in fibronectin deposition, which is required for earlier steps in chondrogenesis than collagen. Moreover, in the complex basement membrane of the

notochord, *sec23b* overexpression may facilitate efficient secretion of fibronectin or other matrix proteins to partially restore body length.

Sec23 and Sec24

Sec23 paralogs are not known for cargo sorting capacity, and the mechanisms by which this could be accomplished has not been addressed. One potential possibility is through interaction with specific Sec24 paralogs. Sec23 and Sec24 form a heterodimer of the inner COPII complex, and the loop of 18 divergent amino acids that we have shown contributes to functional differences between Sec23a and Sec23b is located adjacent to the Sec24 binding site (Figure 4.1). Potentially, Sec23a may have a higher binding affinity for Sec24D under physiological conditions, and it is the cargo sorting function of Sec24D that conveys cargo specificity of the heterodimer. Alternatively, Sec23 may have its own, currently uncharacterized, cargo sorting function, or the groove created by the Sec23/Sec24 heterodimer may allow for binding of yet unknown auxiliary cargo adapters.

Understanding how the COPII machinery handles specific cargo types and loads in a tissue specific manner will lead to better understanding of this fundamental cellular function as well as human diseases related to protein trafficking, which include both those caused by a failure of secretion, such as osteoporosis (Goldring and Goldring, 2007), and those caused by excessive secretion, such as fibrosis (Trojanowska et al., 1998). Parsing the paralog specific functions of Sec23a and Sec23b represents an important step in cracking the “secretory code” that allows the secretory machinery respond to the each tissues demands during development and adult homeostasis.

CHAPTER V

DISCUSSION AND FUTURE DIRECTIONS

Discussion

The goal of this dissertation was twofold: to identify novel genes involved in protein trafficking that are important for craniofacial morphogenesis, and to dissect the mechanisms by which the COPII machinery responds to unique demands of each tissue. The work presented here outlines the identification of candidate genes for six zebrafish mutants through a positional cloning strategy: *strangelove/sox9a, zhivago/gfpt1, brak/atp7a, maggot/(plod3), round/(scarb2),* and *feelgood/creb3l2*.

I found that *feelgood/creb3l2* is an ER-localized transcription factor that is required for collagen secretion, but not for other cargos. This is because Creb3l2 regulates COPII in a paralog-specific manner, the first transcription factor known to do so. Creb3l2 provides a transcriptional mechanism whereby the COPII machinery can respond to the cargo demands of a cell.

I also identified functional differences between the two highly related paralogs *sec23a* and *sec23b*, components of the COPII inner coat, which are differentially regulated by Creb3l2. I found differential secretion of collagen by Sec23a and fibronectin by Sec23b. This is the first cargo-specific function identified for COPII components other than the cargo-sorting Sec24 paralogs, and suggests that different combinations of COPII components preferentially transport certain protein classes, generating a “secretory code” that customizes the transport machinery in order to meet

the secretory demands of cells. Combined with the paralog-specific transcriptional regulation by Creb3l2, this allows for a COPII coat that is highly dynamic and able to respond to stimuli from cargo.

Strikingly, *feelgood/creb3l2* regulates the expression of *sec23a* and *sec24d*, the two COPII components implicated in collagen trafficking and chondrocyte maturation (Lang et al., 2006; Sarmah et al., 2010), suggesting that there is a regulatory network for collagen that links the special trafficking requirements of the cargo to the secretory machinery. This, combined with the cargo, tissue, and developmental stage-specific defects we have found in *feelgood* and COPII component loss-of-function phenotypes lead to the hypothesis that coat proteins represent a central regulatory target to couple the concentration and composition of COPII carriers to tissues secretory demand thus constantly adapting to the needs of developing and mature organs. The specialized axis of Creb3l2/Sec23a/Sec24D proteins is one such network optimized for collagen transport.

Future directions

Identification and characterization of the genetic network regulated by Creb3l2 during cartilage development

The work outlined here postulates a novel Creb3l2 regulatory network for collagen transport. Beyond Sec23a and Sec24d, however, the specific Creb3l2 targets in chondrocytes are unknown. We hypothesize that Creb3l2 regulates the expression of a broad range of genes involved in protein transport and cartilage maturation. A comprehensive assessment of Creb3l2 targets will uncover novel pathways operating in

tandem to optimize ECM secretion and cartilage formation.

To discover Creb3l2 targets, we will use whole transcriptome shotgun sequencing to compare the RNA expression profiles of wild-type and *feelgood* embryos to identify genes with altered expression levels. This is especially advantageous to do in *feelgood,* because our analysis will be done in intact tissue versus cultured cells, which might alter important cellular characteristics, especially in a cell type as dependent on ECM interactions as chondrocytes. Also, the hypomorphic *feelgood* mutation does not trigger an ER stress response, which will eliminate many false positives by uncoupling of the primary Creb3l2 function from the secondary effects of ER stress. Due to the unbiased nature of this approach, it has high potential for discovering new mechanisms relevant to cartilage development and human disease.

One potential problem with this approach is noise introduced by using the whole embryo. A potential solution to this problem is to use Fluorescence Activated Cell Sorting (FACS) to enrich for chondrocytes and other skeletal cell types. Other labs at Vanderbilt have gotten FACS to work well with zebrafish (Liu et al., 2011), so it is likely to be a viable approach. One tool that we have to facilitate FACS is a Tol2 construct with GFP-CAAX under the type-II collagen promoter. This construct will allow us to generate transgenic animals that express GFP in the chondrocytes and notochord, our ideal tissues for analysis.

To validate putative Creb3l2 targets found by expression profiles, we will compare our datasets of up- and down-regulated transcripts with public databases of skeletal-specific genes in zebrafish (http://zfin.org). Also, we will select genes that contain putative Cre regulatory sites in their regulatory regions. Our bioinformatics

analysis shows that 829 skeletal genes from the zebrafish database have at least one Cre binding site in their promoter, and thus could be potentially regulated by Creb3l2.

To determine whether Creb3l2 directly regulates these identified targets, we will perform chromatin immunoprecipitation sequencing (ChIP-seq) to test whether Creb3l2 binds directly to their promoter. For ChIP-seq we will use human fibroblasts. This provides several benefits. There is an antibody against human Creb3l2 that works for ChIP (Saito et al., 2009a) so we can perform ChIP with endogenous protein. Fibroblasts are more amenable to maintaining a consistent cellular state than chondrocytes, which must be carefully maintained to prevent hypertrophy (Bruckner et al., 1989), and their physiological relevance to trafficking diseases have been shown, as fibroblasts in CLSD patients present a collagen-filled distended ER similar to zebrafish *crusher* mutants. Moreover, doing ChIP in human cells while doing RNA-seq in zebrafish confirms that any identified Creb3l2 targets are relevant across species.

These experiments will assemble a collection of genes regulated directly and indirectly by Creb3l2 (Figure 5.1). We expect that we will find genes that are already known to be targets of Creb3l2 such as *sec23a* and *sec24d* and discover which of the remaining COPII components are also regulated by Creb3l2. In addition, we expect to assemble a novel collection of Creb3l2 targets involved in pathways independent of but cooperative with the COPII structural components, which will provide a conceptual framework explaining the way secretion is regulated in chondrocytes.

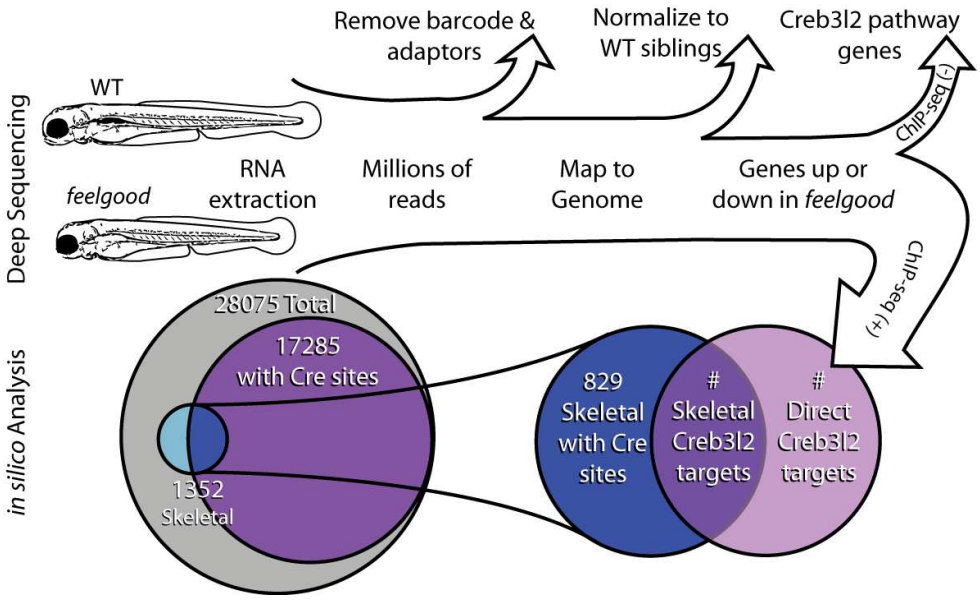

Figure 5.1: Identification of novel Creb3l2 targets. Experimental design of RNA profiling combined with bioinformatics approaches. The expected number of genes to be targeted by Creb3l2 is based on bioinformatics analysis of existing public databases.

In silico identification of novel regulatory components and networks involved in protein trafficking

The approaches outlined above will allow us to identify novel factors downstream of Creb3l2, however there may also be important upstream factors. Moreover, there are likely other regulatory networks governing the secretory demands of different tissues. One method of identifying candidate genes for these processes is through an *in silico* approach.

To identify novel upstream regulators of the secretory pathway, I can utilize the Over-represented Transcription Factor Binding Site Prediction Tool (OTFBS) (Zheng et al., 2003) to analyze the promoters of COPII components. OTFBS compares a group of sequences that are thought to be similarly regulated and determines if any known transcription factor binding sites are present at levels above baseline. After identification of over-represented transcription factors, I can evaluate the effect of overexpression or loss-of-function of that transcription factor on the expression levels of COPII components and the secretory capacity of cells.

To identify novel regulatory networks involving COPII components I can utilize the correlative expression data of the Multi-experiment matrix (Adler et al., 2009). This tool will identify genes whose expression is similar to a gene of interest across a variety of experimental conditions. I can then build a database containing each COPII paralog and all the genes identified to have similar expression patterns to it. I then can compare the results for each COPII paralog to each other and determine if there are clusters of genes from a common pathway or tissue of origin that are identified with only a single COPII paralog or a subset of COPII paralogs. If so, this would suggest that those COPII

paralogs may be part of the same regulatory network as the gene cluster, and merit further analysis.

Identification of the mechanism for cargo-specific functions of Sec23a and Sec23b

We found that Sec23a is essential for collagen secretion while Sec23b is essential for fibronectin secretion, although the mechanism of Sec23-mediated cargo selection is unknown. Potentially, the cargo-specific function of Sec23 is mediated by differential binding to Sec24 paralogs. The divergent 18 amino acid loop that we have shown is important for secretion by Sec23a is located near the Sec24 binding site, giving credence to this hypothesis. It is possible that under *in vivo* conditions in chondrocytes, Sec23a has a greater affinity to Sec24d, which is then required for collagen secretion due to its cargo sorting function.

To test whether Sec23a has a greater affinity than Sec23b for Sec24d, we will perform competition assays in cultured human fibroblast, which secrete collagen and manifest phenotypes similar to zebrafish chondrocytes upon loss of Sec23a function (Boyadjiev et al., 2006). We will transfect cells with both SEC23 paralogs, perform pull-down experiments, and probe for endogenous SEC24D. The paralog with higher affinity should pull-down a larger portion of the limited endogenous SEC24D. We can then test whether the divergent 18 amino acid loop is important for this Sec24d interaction by using constructs with the divergent loops swapped as we did in fish.

If we find that Sec23a has a higher affinity for Sec24d than Sec23b, this would suggest that COPII paralogs have differential affinities not only for cargos, but also for each other, adding a greater level of complexity to the dynamic regulation of the COPII

coat. If Sec23a and Sec23b have similar affinities for Sec24d, this would suggest that a novel protein, such as a cargo adapter, binds Sec23a provides its cargo-specific function.

Elucidation of the role of *round* in protein trafficking

One of the mutants for which I identified a candidate gene, *round,* appears to be essential for protein secretion, likely in the post-Golgi. *round* is required for trafficking of both collagen and WGA-labeled proteins. The most likely candidate gene for *round* is *scarb2,* the role of which in the secretory pathway has not yet been elucidated. *scarb2* has, however, been implicated in Parkinson's disease, renal failure, and epilepsy (Hopfner et al., 2011, 2; Rubboli et al., 2011; Michelakakis et al., 2012), therefore understanding the cellular function of *round* may provide insights into the etiology and treatment of these diseases.

In closing, craniofacial and skeletal dysmorphologies account for the majority of birth defects and most of them are of unknown origin. The fact that random mutagenesis screens in zebrafish have yielded mutants that disrupt the transport machinery with high frequency, suggests that at least some of the birth defects of unknown origin are due to abnormal protein transport. Besides developmental defects, a host of human diseases, including arthritis, fibrosis leading to interstitial scar formation after organ injury, as well as aging, have been linked to deregulated collagen production. Therefore, better understanding of the regulatory and structural components of the intracellular transport machinery may lead to novel diagnostic tools and treatments for human diseases.

BIBLIOGRAPHY

Adams, D. S., Keller, R., and Koehl, M. A. (1990). The mechanics of notochord elongation, straightening and stiffening in the embryo of Xenopus laevis. *Development* 110, 115–130.

Adler, P., Kolde, R., Kull, M., Tkachenko, A., Peterson, H., Reimand, J., and Vilo, J. (2009). Mining for coexpression across hundreds of datasets using novel rank aggregation and visualization methods. *Genome Biology* 10, R139.

Alfandari, D., Cousin, H., Gaultier, A., Hoffstrom, B. G., and DeSimone, D. W. (2003). Integrin alpha5beta1 supports the migration of Xenopus cranial neural crest on fibronectin. *Dev. Biol.* 260, 449–464.

Allen, R., Schroeder, C., and Fok, A. (1989). Intracellular binding of wheat germ agglutinin by Golgi complexes, phagosomes, and lysosomes of Paramecium multimicronucleatum. *J. Histochem. Cytochem.* 37, 195–202.

Altan-Bonnet, N., Sougrat, R., and Lippincott-Schwartz, J. (2004). Molecular basis for Golgi maintenance and biogenesis. *Current Opinion in Cell Biology* 16, 364–372.

Appenzeller-Herzog, C. and Hauri, H.-P. (2006). The ER-Golgi intermediate compartment (ERGIC): in search of its identity and function. *J. Cell Sci.* 119, 2173–2183.

Aridor, M. and Hannan, L. A. (2002). Traffic Jams II: An Update of Diseases of Intracellular Transport. *Traffic* 3, 781–790.

Barlowe, C., Orci, L., Yeung, T., Hosobuchi, M., Hamamoto, S., Salama, N., Rexach, M. F., Ravazzola, M., Amherdt, M., and Schekman, R. (1994). COPII: a membrane coat formed by Sec proteins that drive vesicle budding from the endoplasmic reticulum. *Cell* 77, 895–907.

Barrallo-Gimeno, A., Holzschuh, J., Driever, W., and Knapik, E. W. (2004). Neural crest survival and differentiation in zebrafish depends on mont blanc/tfap2a gene function. *Development* 131, 1463–1477.

Bell, D. M., Leung, K. K., Wheatley, S. C., Ng, L. J., Zhou, S., Ling, K. W., Sham, M. H., Koopman, P., Tam, P. P., and Cheah, K. S. (1997). SOX9 directly regulates the type-II collagen gene. *Nat Genet* 16, 174–178.

Bianchi, P., Fermo, E., Vercellati, C., Boschetti, C., Barcellini, W., Iurlo, A., Marcello, A. P., Righetti, P. G., and Zanella, A. (2009). Congenital dyserythropoietic anemia type II (CDAII) is caused by mutations in the SEC23B gene. *Hum. Mutat.* 30, 1292–1298.

Bonfanti, L., Mironov, A. A., Martínez-Menárguez, J. A., Martella, O., Fusella, A., Baldassarre, M., Buccione, R., Geuze, H. J., and Luini, A. (1998). Procollagen Traverses the Golgi Stack without Leaving the Lumen of Cisternae: Evidence for Cisternal Maturation. *Cell* 95, 993–1003.

Bonifacino, J. S. and Glick, B. S. (2004). The mechanisms of vesicle budding and fusion. *Cell* 116, 153–166.

Boyadjiev, S. A., Fromme, J. C., Ben, J., Chong, S. S., Nauta, C., Hur, D. J., Zhang, G., Hamamoto, S., Schekman, R., Ravazzola, M., et al. (2006). Cranio-lenticulo-sutural dysplasia is caused by a SEC23A mutation leading to abnormal endoplasmic-reticulum-to-Golgi trafficking. *Nat. Genet.* 38, 1192–1197.

Bradley, K. M., Elmore, J. B., Breyer, J. P., Yaspan, B. L., Jessen, J. R., Knapik, E. W., and Smith, J. R. (2007). A major zebrafish polymorphism resource for genetic mapping. *Genome Biol.* 8, R55–R55.

Bruckner, P., Hörler, I., Mendler, M., Houze, Y., Winterhalter, K. H., Eich-Bender, S. G., and Spycher, M. A. (1989). Induction and prevention of chondrocyte hypertrophy in culture. *J. Cell Biol.* 109, 2537–2545.

Cai, H., Yu, S., Menon, S., Cai, Y., Lazarova, D., Fu, C., Reinisch, K., Hay, J. C., and Ferro-Novick, S. (2007). TRAPPI tethers COPII vesicles by binding the coat subunit Sec23. *Nature* 445, 941 – 4.

Campellone, K. G., Webb, N. J., Znameroski, E. A., and Welch, M. D. (2008). WHAMM Is an Arp2/3 Complex Activator That Binds Microtubules and Functions in ER to Golgi Transport. *Cell* 134, 148–161.

Canty, E. G. and Kadler, K. E. (2005). Procollagen trafficking, processing and fibrillogenesis. *J Cell Sci* 118, 1341–1353.

Chai, Y. and Maxson, R. E., Jr (2006). Recent advances in craniofacial morphogenesis. *Dev. Dyn.* 235, 2353–2375.

Dancourt, J. and Barlowe, C. (2010). Protein sorting receptors in the early secretory pathway. *Annu. Rev. Biochem* 79, 777–802.

DeLise, A. M., Fischer, L., and Tuan, R. S. (2000). Cellular interactions and signaling in cartilage development. *Osteoarthr. Cartil.* 8, 309–334.

Desban, N. and Duband, J. L. (1997). Avian neural crest cell migration on laminin: interaction of the alpha1beta1 integrin with distinct laminin-1 domains mediates different adhesive responses. *J. Cell. Sci.* 110 (Pt 21), 2729–2744.

DeSilva, T. M., Veglia, G., and Opella, S. J. (2005). Solution structures of the reduced and Cu(I) bound forms of the first metal binding sequence of ATP7A associated with Menkes disease. *Proteins* 61, 1038–1049.

Driever, W., Solnica-Krezel, L., Schier, A. F., Neuhauss, S. C., Malicki, J., Stemple, D. L., Stainier, D. Y., Zwartkruis, F., Abdelilah, S., Rangini, Z., et al. (1996). A genetic screen for mutations affecting embryogenesis in zebrafish. *Development* 123, 37–46.

Durán, I., Marí-Beffa, M., Santamaría, J. A., Becerra, J., and Santos-Ruiz, L. (2011). Actinotrichia collagens and their role in fin formation. *Dev. Biol.* 354, 160–172.

Espenshade, P. J., Li, W.-P., and Yabe, D. (2002). Sterols block binding of COPII proteins to SCAP, thereby controlling SCAP sorting in ER. *Proc. Natl. Acad. Sci. USA* 99, 11694–11699.

Fath, S., Mancias, J. D., Bi, X., and Goldberg, J. (2007). Structure and Organization of Coat Proteins in the COPII Cage. *Cell* 129, 1325–1336.

Ferg, M., Sanges, R., Gehrig, J., Kiss, J., Bauer, M., Lovas, A., Szabo, M., Yang, L., Straehle, U., Pankratz, M. J., et al. (2007). The TATA-binding protein regulates maternal mRNA degradation and differential zygotic transcription in zebrafish. *EMBO J* 26, 3945–3956.

Flint, M. H., Craig, A. S., Reilly, H. C., Gillard, G. C., and Parry, D. A. (1984). Collagen fibril diameters and glycosaminoglycan content of skins--indices of tissue maturity and function. *Connect. Tissue Res.* 13, 69–81.

Fraser, R. D., MacRae, T. P., and Suzuki, E. (1979). Chain conformation in the collagen molecule. *J. Mol. Biol.* 129, 463–481.

Fromme, J. C., Orci, L., and Schekman, R. (2008). Coordination of COPII vesicle trafficking by Sec23. *Trends in Cell Biology* 18, 330–336.

Fromme, J. C., Ravazzola, M., Hamamoto, S., Al-Balwi, M., Eyaid, W., Boyadjiev, S. A., Cosson, P., Schekman, R., and Orci, L. (2007). The genetic basis of a craniofacial disease provides insight into COPII coat assembly. *Dev. Cell.* 13, 623 – 34.

Fromme, J. C. and Schekman, R. (2005). COPII-coated vesicles: flexible enough for large cargo? *Current Opinion in Cell Biology* 17, 345–352.

Goldring, M. B. and Goldring, S. R. (2007). Osteoarthritis. *J. Cell. Physiol* 213, 626–634.

Goldring, M. B. and Marcu, K. B. (2009). Cartilage homeostasis in health and rheumatic diseases. *Arthritis Res. Ther* 11, 224.

Gould, D. B., Phalan, F. C., Breedveld, G. J., van Mil, S. E., Smith, R. S., Schimenti, J. C., Aguglia, U., van der Knaap, M. S., Heutink, P., and John, S. W. (2005). Mutations in Col4a1 cause perinatal cerebral hemorrhage and porencephaly. *Science* 308, 1167 – 71.

Gourdon, P., Liu, X.-Y., Skjørringe, T., Morth, J. P., Møller, L. B., Pedersen, B. P., and Nissen, P. (2011). Crystal structure of a copper-transporting PIB-type ATPase. *Nature* 475, 59–64.

Granero-Moltó, F., Sarmah, S., O'Rear, L., Spagnoli, A., Abrahamson, D., Saus, J., Hudson, B. G., and Knapik, E. W. (2008). Goodpasture Antigen-binding Protein and Its Spliced Variant, Ceramide Transfer Protein, Have Different Functions in the Modulation of Apoptosis during Zebrafish Development. *J Biol Chem* 283, 20495 –20504.

Gurkan, C., Koulov, A. V., and Balch, W. E. (2007). An evolutionary perspective on eukaryotic membrane trafficking. *Adv. Exp. Med. Biol.* 607, 73–83.

Harper, D. C., Theos, A. C., Herman, K. E., Tenza, D., Raposo, G., and Marks, M. S. (2008). Premelanosome amyloid-like fibrils are composed of only golgi-processed forms of Pmel17 that have been proteolytically processed in endosomes. *J. Biol. Chem* 283, 2307–2322.

Heinegård, D. and Saxne, T. (2011). The role of the cartilage matrix in osteoarthritis. *Nat Rev Rheumatol* 7, 50–56.

Hickok, N. J., Andrew R. Haas, and Tuan, R. S. (1998). Regulation of chondrocyte differentiation and maturation. *Microsc. Res. Tech.* 43, 174–190.

Hope, I. A. and Struhl, K. (1987). GCN4, a eukaryotic transcriptional activator protein, binds as a dimer to target DNA. *EMBO J.* 6, 2781–2784.

Hopfner, F., Schormair, B., Knauf, F., Berthele, A., Tölle, T. R., Baron, R., Maier, C., Treede, R.-D., Binder, A., Sommer, C., et al. (2011). Novel SCARB2 mutation in action myoclonus-renal failure syndrome and evaluation of SCARB2 mutations in isolated AMRF features. *BMC Neurol* 11, 134.

Huang, M., Weissman, J. T., Béraud-Dufour, S., Luan, P., Wang, C., Chen, W., Aridor, M., Wilson, I. A., and Balch, W. E. (2001). Crystal structure of Sar1-GDP at 1.7 Å resolution and the role of the NH2 terminus in ER export. *J. Cell Biol.* 155, 937–948.

Hynes, R. O. (2009). The extracellular matrix: not just pretty fibrils. *Science* 326, 1216–1219.

Jin, L., Pahuja, K. B., Wickliffe, K. E., Gorur, A., Baumgärtel, C., Schekman, R., and Rape, M. (2012). Ubiquitin-dependent regulation of COPII coat size and function. *Nature* 482, 495–500.

Jones, B., Jones, E. L., Bonney, S. A., Patel, H. N., Mensenkamp, A. R., Eichenbaum-Voline, S., Rudling, M., Myrdal, U., Annesi, G., Naik, S., et al. (2003). Mutations in a Sar1 GTPase of COPII vesicles are associated with lipid absorption disorders. *Nat Genet* 34, 29–31.

Kim, J., Thanabalasuriar, A., Chaworth-Musters, T., Fromme, J. C., Frey, E. A., Lario, P. I., Metalnikov, P., Rizg, K., Thomas, N. A., Lee, S. F., et al. (2007). The Bacterial Virulence Factor NleA Inhibits Cellular Protein Secretion by Disrupting Mammalian COPII Function. *Cell Host & Microbe* 2, 160–171.

Kimmel, C. B., Ballard, W. W., Kimmel, S. R., Ullmann, B., and Schilling, T. F. (1995). Stages of embryonic development of the zebrafish. *Dev. Dyn.* 203, 253–310.

Kimmel, C. B., Miller, C. T., and Keynes, R. J. (2001). Neural crest patterning and the evolution of the jaw. *J. Anat.* 199, 105–120.

Knapik, E. W. (2000). ENU mutagenesis in zebrafish--from genes to complex diseases. *Mamm. Genome* 11, 511–519.

Knapik, E. W., Goodman, A., Ekker, M., Chevrette, M., Delgado, J., Neuhauss, S., Shimoda, N., Driever, W., Fishman, M. C., and Jacob, H. J. (1998). A microsatellite genetic linkage map for zebrafish (Danio rerio). *Nat. Genet.* 18, 338–343.

Kondo, S., Saito, A., Hino, S., Murakami, T., Ogata, M., Kanemoto, S., Nara, S., Yamashita, A., Yoshinaga, K., Hara, H., et al. (2007). BBF2H7, a Novel Transmembrane bZIP Transcription Factor, Is a New Type of Endoplasmic Reticulum Stress Transducer. *Mol. Cell. Biol.* 27, 1716–1729.

Koteliansky, V. E., Glukhova, M. A., Bejanian, M. V., Smirnov, V. N., Filimonov, V. V., Zalite, O. M., and Venyaminov SYu (1981). A study of the structure of fibronectin. *Eur. J. Biochem* 119, 619–624.

Kuronita, T., Eskelinen, E.-L., Fujita, H., Saftig, P., Himeno, M., and Tanaka, Y. (2002). A role for the lysosomal membrane protein LGP85 in the biogenesis and maintenance of endosomal and lysosomal morphology. *J. Cell. Sci.* 115, 4117–4131.

Kwan, K. M., Fujimoto, E., Grabher, C., Mangum, B. D., Hardy, M. E., Campbell, D. S., Parant, J. M., Yost, H. J., Kanki, J. P., and Chien, C.-B. (2007). The Tol2kit: A multisite gateway-based construction kit forTol2 transposon transgenesis constructs. *Dev Dyn* 236, 3088–3099.

Lang, M. R., Lapierre, L. A., Frotscher, M., Goldenring, J. R., and Knapik, E. W. (2006). Secretory COPII coat component Sec23a is essential for craniofacial chondrocyte maturation. *Nat Genet* 38, 1198–1203.

Liu, D., Wang, W., **Melville, D. B**., Cha, Y. I., Yin, Z., Issaeva, N., Knapik, E. W., and Yarbrough, W. G. (2011). Tumor suppressor Lzap regulates cell cycle progression, doming, and zebrafish epiboly. *Dev Dyn* 240, 1613–1625.

Livak, K. J. and Schmittgen, T. D. (2001). Analysis of relative gene expression data using real-time quantitative PCR and the 2(-Delta Delta C(T)) Method. *Methods* 25, 402–408.

Logan, D. W., Burn, S. F., and Jackson, I. J. (2006). Regulation of pigmentation in zebrafish melanophores. *Pigment Cell Res.* 19, 206–213.

Löppönen, T., Körkkö, J., Lundan, T., Seppänen, U., Ignatius, J., and Kääriäinen, H. (2004). Childhood-onset osteoarthritis, tall stature, and sensorineural hearing loss associated with Arg75-Cys mutation in procollagen type II gene (COL2A1). *Arthritis Rheum* 51, 925–932.

Mancias, J. D. and Goldberg, J. (2008). Structural basis of cargo membrane protein discrimination by the human COPII coat machinery. *EMBO J.* 27, 2918–2928.

Marks, M. S. and Seabra, M. C. (2001). The melanosome: membrane dynamics in black and white. *Nat. Rev. Mol. Cell. Biol.* 2, 738–748.

Matsuoka, K., Orci, L., Amherdt, M., Bednarek, S. Y., Hamamoto, S., Schekman, R., and Yeung, T. (1998). COPII-coated vesicle formation reconstituted with purified coat proteins and chemically defined liposomes. *Cell* 93, 263–275.

McDowall, S., Argentaro, A., Ranganathan, S., Weller, P., Mertin, S., Mansour, S., Tolmie, J., and Harley, V. (1999). Functional and structural studies of wild type SOX9 and mutations causing campomelic dysplasia. *J. Biol. Chem.* 274, 24023–24030.

Melville, D. B. and Knapik, E. W. (2011). Traffic jams in fish bones: ER-to-Golgi protein transport during zebrafish development. *Cell Adh. Migr.* 5, (In press).

Melville, D. B., Montero-Balaguer, M., Levic, D. S., Bradley, K., Smith, J. R., Hatzopoulos, A. K., and Knapik, E. W. (2011). The feelgood mutation in zebrafish dysregulates COPII-dependent secretion of select extracellular matrix proteins in skeletal morphogenesis. *Dis Model Mech* 4, 763–76.

Mendelsohn, B. A., Yin, C., Johnson, S. L., Wilm, T. P., Solnica-Krezel, L., and Gitlin, J. D. (2006). Atp7a determines a hierarchy of copper metabolism essential for notochord development. *Cell Metab.* 4, 155–162.

Merte, J., Jensen, D., Wright, K., Sarsfield, S., Wang, Y., Schekman, R., and Ginty, D. D. (2010). Sec24b selectively sorts Vangl2 to regulate planar cell polarity during neural tube closure. *Nat. Cell Biol* 12, 41–46; sup pp 1–8.

Michelakakis, H., Xiromerisiou, G., Dardiotis, E., Bozi, M., Vassilatis, D., Kountra, P.-M., Patramani, G., Moraitou, M., Papadimitriou, D., Stamboulis, E., et al. (2012). Evidence of an association between the scavenger receptor class B member 2 gene and Parkinson's disease. *Mov. Disord.* 27, 400–405.

Miller, E. A. and Barlowe, C. (2010). Regulation of coat assembly--sorting things out at the ER. *Curr. Opin. Cell Biol* 22, 447–453.

Miller, E., Antonny, B., Hamamoto, S., and Schekman, R. (2002). Cargo selection into COPII vesicles is driven by the Sec24p subunit. *EMBO J* 21, 6105 – 13.

Mironov, A. A., Beznoussenko, G. V., Trucco, A., Lupetti, P., Smith, J. D., Geerts, W. J. C., Koster, A. J., Burger, K. N. J., Martone, M. E., Deerinck, T. J., et al. (2003). ER-to-Golgi Carriers Arise through Direct En Bloc Protrusion and Multistage Maturation of Specialized ER Exit Domains. *Developmental Cell* 5, 583–594.

Montero-Balaguer, M., Lang, M. R., Sachdev, S. W., Knappmeyer, C., Stewart, R. A., De La Guardia, A., Hatzopoulos, A. K., and Knapik, E. W. (2006). The mother superior mutation ablates foxd3 activity in neural crest progenitor cells and depletes neural crest derivatives in zebrafish. *Dev. Dyn.* 235, 3199–3212.

Müller, I. I., Knapik, E. W., and Hatzopoulos, A. K. (2006). Expression of the protein related to Dan and Cerberus gene--prdc--During eye, pharyngeal arch, somite, and swim bladder development in zebrafish. *Dev. Dyn.* 235, 2881–2888.

Nakano, A. and Luini, A. (2010). Passage through the Golgi. *Curr. Opin. Cell Biol.* 22, 471–478.

Neuhauss, S. C., Solnica-Krezel, L., Schier, A. F., Zwartkruis, F., Stemple, D. L., Malicki, J., Abdelilah, S., Stainier, D. Y., and Driever, W. (1996). Mutations affecting craniofacial development in zebrafish. *Development* 123, 357–367.

O'Donnell, J., Maddox, K., and Stagg, S. (2011). The structure of a COPII tubule. *J Struct Biol* 173, 358–364.

Ohisa, S., Inohaya, K., Takano, Y., and Kudo, A. (2010). sec24d encoding a component of COPII is essential for vertebra formation, revealed by the analysis of the medaka mutant, vbi. *Dev. Biol.* 342, 85–95.

Paccaud, J. P., Reith, W., Carpentier, J. L., Ravazzola, M., Amherdt, M., Schekman, R., and Orci, L. (1996). Cloning and functional characterization of mammalian homologues of the COPII component Sec23. *Mol Biol Cell* 7, 1535–1546.

Piecha, D., Muratoglu, S., Mörgelin, M., Hauser, N., Studer, D., Kiss, I., Paulsson, M., and Deák, F. (1999). Matrilin-2, a Large, Oligomeric Matrix Protein, Is Expressed by a Great Variety of Cells and Forms Fibrillar Networks. *Journal of Biological Chemistry* 274, 13353 –13361.

Postlethwait, J. H., Johnson, S. L., Midson, C. N., Talbot, W. S., Gates, M., Ballinger, E. W., Africa, D., Andrews, R., Carl, T., and Eisen, J. S. (1994). A genetic linkage map for the zebrafish. *Science* 264, 699–703.

Pulvirenti, T., Giannotta, M., Capestrano, M., Capitani, M., Pisanu, A., Polishchuk, R. S., Pietro, E. S., Beznoussenko, G. V., Mironov, A. A., Turacchio, G., et al. (2008). A traffic-activated Golgi-based signalling circuit coordinates the secretory pathway. *Nat Cell Biol* 10, 912–922.

Rauch, F. and Glorieux, F. H. (2004). Osteogenesis imperfecta. *The Lancet* 363, 1377–1385.

Riley, P. A., Sawyer, B., and Wolf, M. A. (1975). The melanocytotoxic action of 4-hydroxyanisole. *J. Invest. Dermatol.* 64, 86–89.

Routledge, K. E., Gupta, V., and Balch, W. E. (2010). Emergent properties of proteostasis-COPII coupled systems in human health and disease. *Mol. Membr. Biol* 27, 385–397.

Rubboli, G., Franceschetti, S., Berkovic, S. F., Canafoglia, L., Gambardella, A., Dibbens, L. M., Riguzzi, P., Campieri, C., Magaudda, A., Tassinari, C. A., et al. (2011). Clinical and neurophysiologic features of progressive myoclonus epilepsy without renal failure caused by SCARB2 mutations. *Epilepsia* 52, 2356–2363.

Sachdev, S. W., Dietz, U. H., Oshima, Y., Lang, M. R., Knapik, E. W., Hiraki, Y., and Shukunami, C. (2001). Sequence analysis of zebrafish chondromodulin-1 and expression profile in the notochord and chondrogenic regions during cartilage morphogenesis. *Mech. Dev.* 105, 157–162.

Saito, A., Hino, S., Murakami, T., Kanemoto, S., Kondo, S., Saitoh, M., Nishimura, R., Yoneda, T., Furuichi, T., Ikegawa, S., et al. (2009a). Regulation of endoplasmic reticulum stress response by a BBF2H7-mediated Sec23a pathway is essential for chondrogenesis. *Nat Cell Biol* 11, 1197–1204.

Saito, K., Chen, M., Bard, F., Chen, S., Zhou, H., Woodley, D., Polischuk, R., R, Schekman, y, and Malhotra, V. (2009b). TANGO1 Facilitates Cargo Loading at Endoplasmic Reticulum Exit Sites. *Cell* 136, 891–902.

Saito, K., Yamashiro, K., Ichikawa, Y., Erlmann, P., Kontani, K., Malhotra, V., and Katada, T. (2011). cTAGE5 mediates collagen secretion through interaction with TANGO1 at endoplasmic reticulum exit sites. *Mol. Biol. Cell* 22, 2301–2308.

Saitou, N. and Nei, M. (1987). The neighbor-joining method: a new method for reconstructing phylogenetic trees. *Mol. Biol. Evol.* 4, 406–425.

Sarmah, S., Barrallo-Gimeno, A., **Melville, D. B.**, Topczewski, J., Solnica-Krezel, L., and Knapik, E. W. (2010). Sec24D-Dependent Transport of Extracellular Matrix Proteins Is Required for Zebrafish Skeletal Morphogenesis. *PLoS One* 5, e10367.

Schonthaler, H. B., Lampert, J. M., von Lintig, J., Schwarz, H., Geisler, R., and Neuhauss, S. C. F. (2005). A mutation in the silver gene leads to defects in melanosome biogenesis and alterations in the visual system in the zebrafish mutant fading vision. *Dev. Biol* 284, 421–436.

Schwarz, K., Iolascon, A., Verissimo, F., Trede, N. S., Horsley, W., Chen, W., Paw, B. H., Hopfner, K.-P., Holzmann, K., Russo, R., et al. (2009). Mutations affecting the secretory COPII coat component SEC23B cause congenital dyserythropoietic anemia type II. *Nat. Genet.* 41, 936–940.

Scott, A. and Stemple, D. L. (2005). Zebrafish notochordal basement membrane: signaling and structure. *Curr Top Dev Biol* 65, 229–253.

Seidah, N. G., Mowla, S. J., Hamelin, J., Mamarbachi, A. M., Benjannet, S., Touré, B. B., Basak, A., Munzer, J. S., Marcinkiewicz, J., Zhong, M., et al. (1999). Mammalian subtilisin/kexin isozyme SKI-1: A widely expressed proprotein convertase with a unique cleavage specificity and cellular localization. *Proc. Natl. Acad. Sci. U.S.A* 96, 1321–1326.

Shimoda, N., Knapik, E. W., Ziniti, J., Sim, C., Yamada, E., Kaplan, S., Jackson, D., de Sauvage, F., Jacob, H., and Fishman, M. C. (1999). Zebrafish genetic map with 2000 microsatellite markers. *Genomics* 58, 219–232.

Stagg, S. M., Gurkan, C., Fowler, D. M., LaPointe, P., Foss, T. R., Potter, C. S., Carragher, B., and Balch, W. E. (2006). Structure of the Sec13/31 COPII coat cage. *Nature* 439, 234–238.

Stagg, S. M., LaPointe, P., Razvi, A., Gürkan, C., Potter, C. S., Carragher, B., and Balch, W. E. (2008). Structural Basis for Cargo Regulation of COPII Coat Assembly. *Cell* 134, 474–484.

Stankewich, M. C., Stabach, P. R., and Morrow, J. S. (2006). Human Sec31B: a family of new mammalian orthologues of yeast Sec31p that associate with the COPII coat. *J. Cell. Sci* 119, 958–969.

Stephens, D. J. and Pepperkok, R. (2002). Imaging of procollagen transport reveals COPI-dependent cargo sorting during ER-to-Golgi transport in mammalian cells. *J. Cell Sci.* 115, 1149–1160.

Storlazzi, C. T., Mertens, F., Nascimento, A., Isaksson, M., Wejde, J., Brosjo, O., Mandahl, N., and Panagopoulos, I. (2003). Fusion of the FUS and BBF2H7 genes in low grade fibromyxoid sarcoma. *Hum. Mol. Genet.* 12, 2349–2358.

Strachan, L. R. and Condic, M. L. (2008). Neural crest motility on fibronectin is regulated by integrin activation. *Exp. Cell Res.* 314, 441–452.

Sun, M., Mondal, K., Patel, V., Horner, V. L., Long, A. B., Cutler, D. J., Caspary, T., and Zwick, M. E. (2012). Multiplex Chromosomal Exome Sequencing Accelerates Identification of ENU-Induced Mutations in the Mouse. *G3 (Bethesda)* 2, 143–150.

Tabas, I. and Ron, D. (2011). Integrating the mechanisms of apoptosis induced by endoplasmic reticulum stress. *Nat. Cell Biol* 13, 184–190.

Tang, B. L., Kausalya, J., Low, D. Y., Lock, M. L., and Hong, W. (1999). A family of mammalian proteins homologous to yeast Sec24p. *Biochem. Biophys. Res. Commun* 258, 679–684.

Tautz, D. and Schlötterer (1994). Simple sequences. *Curr. Opin. Genet. Dev.* 4, 832–837.

Testaz, S., Delannet, M., and Duband, J. (1999). Adhesion and migration of avian neural crest cells on fibronectin require the cooperating activities of multiple integrins of the (beta)1 and (beta)3 families. *J. Cell. Sci.* 112 (Pt 24), 4715–4728.

Theos, A. C., Berson, J. F., Theos, S. C., Herman, K. E., Harper, D. C., Tenza, D., Sviderskaya, E. V., Lamoreux, M. L., Bennett, D. C., Raposo, G., et al. (2006). Dual loss of ER export and endocytic signals with altered melanosome morphology in the silver mutation of Pmel17. *Mol. Biol. Cell* 17, 3598–3612.

Theos, A. C., Truschel, S. T., Raposo, G., and Marks, M. S. (2005). The Silver locus product Pmel17/gp100/Silv/ME20: controversial in name and in function. *Pigment Cell Res* 18, 322–336.

Timpl, R. and Brown, J. C. (1996). Supramolecular assembly of basement membranes. *Bioessays* 18, 123–132.

Trojanowska, M., Carwile LeRoy, E., Eckes, B., and Krieg, T. (1998). Pathogenesis of fibrosis: type 1 collagen and the skin. *Journal of Molecular Medicine* 76, 266–274.

Vinson, C. R., Sigler, P. B., and McKnight, S. L. (1989). Scissors-grip model for DNA recognition by a family of leucine zipper proteins. *Science* 246, 911–916.

Wang, W.-D., **Melville, D. B.**, Montero-Balaguer, M., Hatzopoulos, A. K., and Knapik, E. W. (2011). Tfap2a and Foxd3 regulate early steps in the development of the neural crest progenitor population. *Dev. Biol.* 360, 173–185.

Ward, T. H., Polishchuk, R. S., Caplan, S., Hirschberg, K., and Lippincott-Schwartz, J. (2001). Maintenance of Golgi structure and function depends on the integrity of ER export. *J. Cell Biol.* 155, 557–570.

Watson, P., Forster, R., Palmer, K. J., Pepperkok, R., and Stephens, D. J. (2005). Coupling of ER exit to microtubules through direct interaction of COPII with dynactin. *Nat Cell Biol* 7, 48 – 55.

Wendeler, M. W., Paccaud, J.-P., and Hauri, H.-P. (2007). Role of Sec24 isoforms in selective export of membrane proteins from the endoplasmic reticulum. *EMBO Rep.* 8, 258–264.

Wilson, D. G., Phamluong, K., Li, L., Sun, M., Cao, T. C., Liu, P. S., Modrusan, Z., Sandoval, W. N., Rangell, L., Carano, R. A. D., et al. (2011). Global defects in collagen secretion in a Mia3/TANGO1 knockout mouse. *J. Cell Biol.* 193, 935–951.

Wood, A. and Thorogood, P. (1984). An analysis of in vivo cell migration during teleost fin morphogenesis. *J. Cell. Sci.* 66, 205–222.

Yan, Y.-L., Miller, C. T., Nissen, R., Singer, A., Liu, D., Kirn, A., Draper, B., Willoughby, J., Morcos, P. A., Amsterdam, A., et al. (2002). A zebrafish sox9 gene required for cartilage morphogenesis. *Development* 129, 5065–5079.

Yang, C.-T., Hindes, A. E., Hultman, K. A., and Johnson, S. L. (2007). Mutations in gfpt1 and skiv2l2 Cause Distinct Stage-Specific Defects in Larval Melanocyte Regeneration in Zebrafish. *PLoS Genet* 3, e88.

Zanetti, G., Pahuja, K. B., Studer, S., Shim, S., and Schekman, R. (2012). COPII and the regulation of protein sorting in mammals. *Nat Cell Biol* 14, 20–28.

Zeller, J. and Granato, M. (1999). The zebrafish diwanka gene controls an early step of motor growth cone migration. *Development* 126, 3461–3472.

Zheng, J., Wu, J., and Sun, Z. (2003). An approach to identify over-represented cis-elements in related sequences. *Nucleic Acids Res.* 31, 1995–2005.